

AD-A075 922

NATIONAL OCEANIC AND ATMOSPHERIC ADMINISTRATION BOUL--ETC F/G 1/5
A THUNDERSTORM GUST-FRONT DETECTION SYSTEM, PART I. SYSTEM OPER--ETC(I)
AUG 79 A J BEDARD, F H MERREM, D SIMMS DOT-FA76WAI-622

UNCLASSIFIED

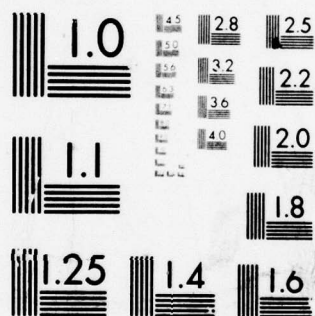
FAA-RD-79-55

NL

1 of 2

AD
A075922





MICROCOPY RESOLUTION TEST CHART
NATIONAL BUREAU OF STANDARDS-1963-A

REPORT NO. FAA-RD-79-55

LEVEL II

12

AD A 075922

A THUNDERSTORM GUST-FRONT DETECTION SYSTEM
PART I. SYSTEM OPERATION AND SIGNIFICANT CASE STUDIES
PART II. STATISTICAL RESULTS

A.J. Bedard Jr.,
F.H. Merrem,
D. Simms,
and M.M. Cairns



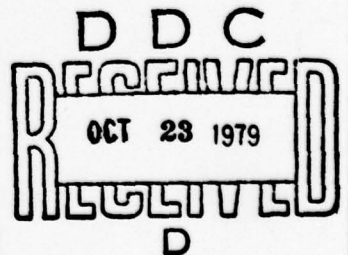
AUGUST 1979

SUMMARY REPORT

Document is available to the U.S. public through
the National Technical Information Service,
Springfield, Virginia 22161.

Prepared for

U.S. DEPARTMENT OF TRANSPORTATION
FEDERAL AVIATION ADMINISTRATION
Systems Research & Development Service
Washington, D.C. 20590



DDC FILE COPY

79 22 . 22 093

NOTICE

This document is disseminated under the sponsorship of the Department of Transportation in the interest of information exchange. The United States Government assumes no liability for its contents or use thereof.

1. Report No. 18 FAA-RD-79-55	2. Government Accession No.	3. Recipient's Catalog No.	
4. Title and Subtitle 6 A Thunderstorm Gust-Front Detection System Part I. System Operation and Significant Case Studies. Part II. Statistical Results.	5. Report Date 11 August 1979		
6. Performing Organization Code		7. Author(s) 10 A. J. Bedard, Jr., F. H. Merrem, D. Simms, M.M. Cairns	
8. Performing Organization Report No. 12 147		9. Performing Organization Name and Address Wave Propagation Laboratory National Oceanic and Atmospheric Administration 325 Broadway Boulder, Colorado 80302	
10. Work Unit No. (TRAIS)		11. Contract or Grant No. 15 DOT-FA76 WAI-622	
12. Sponsoring Agency Name and Address U.S. Department of Transportation Federal Aviation Administration Washington, D.C. 20590		13. Type of Report and Period Covered Summary Report Oct 1976 to Apr 1979	
14. Sponsoring Agency Code FAA/ARD-450		15. Supplementary Notes Prepared under Interagency Agreement No. DOT-FA76 WAI-622 Task V managed by the Aviation Weather Branch, ARD-450	
16. Abstract The Dulles International Airport wind and wind shear detection system recorded more than 160 events from November 1976 through March 1978. Eighty-two percent of 113 significant events occurred in conjunction with thunderstorms, squall-lines and frontal passages. The chief source of false alarms for anemometers was boundary layer disturbances representing 10% of the total; while gravity shear waves related to the 500-mb winds caused the most false alarms for pressure sensors (4% of the total). Using complementary arrays of wind and pressure sensors, total system false alarms can be greatly reduced. These data demonstrate the importance of stable surface layers in determining how well surface temperature and wind measurements represent flow at higher levels and explain underestimates of system severity. Moreover, because we demonstrate the value of wind vector information and since temperature is a scalar quantity, there seems little operational value in using temperature sensors as part of a detection system. Conversely, pressure sensors will not reliably detect relatively thin outflows (100-200 M thick) occurring at a distance from downflows having small dimensions. Again, the wind and pressure sensors combine to provide a total system offering good reliability for detection of thunderstorm outflows. The results suggest an array configuration (composed of wind and pressure jump sensors) for use in airport warning systems. This configuration extending about 10 km from the airport provides a warning for thunderstorm gust-fronts. The data set offers wide possibilities for further exploitation including case study comparisons with numerical models, case study comparisons with weather radar data, and summaries of shear data and Doppler sounder profiles for use by those computing aircraft response and those designing remote sensing systems.			
17. Key Words Wind Shear, Gust Front, Density Current, Atmospheric Pressure Jumps, Aircraft Safety, Anemometers, Surface		18. Distribution Statement Document is available to the U.S. public through the National Technical Information Service, Springfield, Virginia 22151	
19. Security Classif. (of this report) Unclassified	20. Security Classif. (of this page) Unclassified	21. No. of Pages 145	22. Price

METRIC CONVERSION FACTORS

Approximate Conversions to Metric Measures

Symbol	When You Know	Multiply by	To Find	Symbol
LENGTH				
in	inches	2.5	centimeters	cm
ft	feet	30	centimeters	cm
yd	yards	0.9	meters	m
mi	miles	1.6	kilometers	km
AREA				
in ²	square inches	6.5	square centimeters	cm ²
ft ²	square feet	0.09	square meters	m ²
yd ²	square yards	0.8	square meters	m ²
mi ²	square miles	2.6	square kilometers	km ²
	acres	0.4	hectares	ha
MASS (weight)				
oz	ounces	28	grams	g
lb	pounds	0.45	kilograms	kg
	short tons (2000 lb)	0.9	tonnes	t
VOLUME				
teaspoon	teaspoons	5	milliliters	ml
fl oz	fluid ounces	15	milliliters	ml
c	cup	30	milliliters	ml
pt	pints	0.24	liters	l
qt	quarts	0.47	liters	l
gal	gallons	0.95	liters	l
ft ³	cubic feet	3.8	cubic meters	m ³
yd ³	cubic yards	0.03	cubic meters	m ³
		0.76		
TEMPERATURE (exact)				
°F	Fahrenheit temperature	5/9 (after subtracting 32)	Celsius temperature	°C

*1 in = 2.54 (exactly). For other exact conversions and more detailed tables, see NBS Spec. Publ. 286, Units of Weights and Measures, Price \$2.25, SO Catalog No. C13.10.286.

Approximate Conversions from Metric Measures

Symbol	When You Know	Multiply by	To Find	Symbol
LENGTH				
mm	millimeters	0.04	inches	in
cm	centimeters	0.4	inches	in
m	meters	3.3	feet	ft
km	kilometers	1.1	yards	yd
		0.6	miles	mi
AREA				
cm ²	square centimeters	0.16	square inches	in ²
m ²	square meters	1.2	square yards	yd ²
km ²	square kilometers	0.4	square miles	mi ²
ha	hectares (10,000 m ²)	2.5	acres	
MASS (weight)				
g	grams	0.035	ounces	oz
kg	kilograms	2.2	pounds	lb
t	tonnes (1000 kg)	1.1	short tons	
VOLUME				
ml	milliliters	0.03	fluid ounces	fl oz
l	liters	2.1	pints	pt
l	liters	1.06	quarts	qt
m ³	cubic meters	0.26	gallons	gal
m ³	cubic meters	35	cubic feet	ft ³
		1.3	cubic yards	yd ³

TEMPERATURE (exact)

°C	Celsius temperature	9/5 (then add 32)	Fahrenheit temperature	°F
-40				-40
-30				-22
0				32
32				90
40				104
60				140
80				176
100				212
120				248
140				284
160				320
180				356
200				392
212				400

ACKNOWLEDGMENTS

The work reported here was funded under a joint agreement between the Federal Aviation Administration and the Wave Propagation Laboratory of NOAA. We are grateful for the support, guidance, and assistance of many individuals within the FAA; these include Messrs. R. Colao and J. Sower as well as F. Coons and G. Tinsley. We also wish to acknowledge WPL/ERL support at a critical juncture. The large amount of work in providing leased lines for the 120 sensor locations plus over 20 power drops in a rural area succeeded because of the efforts of a number of individuals. Among these we especially acknowledge the efforts of Continental Telephone of Virginia, H. Pultz and J. D. Harris; the Chesapeake and Potomac Telephone Co., G. A. Cox, D. Vineyard, A. H. deButts, and J. V. Rodier; The Tri-County Electric Cooperative, B. M. Schafer, R. M. Fleming, and J. W. Fiske; The Virginia Electric and Power Co., C. H. Smith, Jr., and R. Hurt. A number of people from WPL worked on the fabrication and installation of this system. Among these were E. Cole, W. Cartwright, C. Ramzy, T. Kohrs, J. Murashige, J. W. Turner, D. Simms, D. Sipple, and M. Watts. Among those WPL workers contributing to the development of analysis software were F. H. Merrem, Jr., D. Simms, D. W. Lewis, and D. C. Sorensen. Finally, we are grateful to the National Weather Service, Test and Evaluation Division, at Sterling, Va., for providing a building for our central recording site and assisting with our field operation. We thank in particular R. Strickler, K. Davis, M. Cummings, and R. Stone. Dick Bollinger and Gene Hollingworth insured we obtained reliable and timely data for analysis. The monostatic acoustic radar operated independently of this experiment by the Equipment Development Laboratory of NOAA's Weather Service. We thank M. Sanders for providing monostatic acoustic radar data. As a separate program (also with FAA support) workers of the Wave Propagation Laboratory designed and deployed the acoustic/microwave radar. We thank D. Beran, P. Mandics, M. Hardesty and R. Strauch for providing these data. We also thank D. Beran for his help and advice during all phases of this work. Finally, we acknowledge Professor T. T. Fujita who also provided encouragement and valuable advice in these efforts. Portions of Part I of this report appeared in the paper by Bedard and Hooke (1978).

TABLE OF CONTENTS

	Page
A Thunderstorm Gust-Front Detection System	
Part I System Operation and Significant Case Studies	
Acknowledgments	iii
List of Figures	x
List of Tables	xvi
1. Introduction	1
1.1 Background	1
1.2 History of Operation and Instrumentation	7
2. Analysis	12
2.1 Analysis Philosophy	12
2.2 Analysis Programs	13
3. Noteworthy Case Studies	13
3.1 20 July 1977 - Spatially uniform and readily interpretable surface wind surges accompanying a gust-front cold-air outflow.	15
3.2 25 July 1977 - A gust-front change in wind direction with no accompanying change in speed.	18
3.3 7 August 1977 - A gust-front showing the impulsive nature common to many wind-speed surges caused by thunderstorms.	19
3.4 2 May 1977 - A gust-front associated with large and continuous changes in wind azimuth and speed.	21
3.5 10 June 1977 - A gust-front showing considerable spatial irregularity in winds but not in surface pressure.	23
3.6 8 August 1977 - A gust-front showing spatial complexity in both the surface-wind and pressure fields.	26
3.7 8 July 1977 - Large amplitude pressure changes caused by gravity waves.	27

TABLE OF CONTENTS (continued)

	Page
3.8 27 September 1977 - A gust-front showing only minor temperature and anemometer disturbances at the surface.	29
3.9 18 May 1977 - Comparison calculations of direction and speed of motion of a gust front using data from Po and dP arrays.	32
3.10 7 August 1977 - Gust front showing evidence of non-uniform motion.	36
3.11 17 November 1977 - Comparison illustrating a limitation of conventional weather radar for tracking discontinuities.	36
3.12 17 June 1977 - An aircraft flight path shown in relation to approach zone meteorology.	40
3.13 26 June 1978 - A thunderstorm showing evidence of an intense down-flow.	48
 4. Sensor Operation	 52
4.1 Causes of dP sensor response	52
4.1.1 Thunderstorm gust fronts and down-flows	55
4.1.2 Cold fronts	55
4.1.3 Gravity waves	56
4.1.4 Gravity-shear waves	56
4.1.5 Local winds	56
4.1.6 Aircraft weight transfer	57
4.1.7 Aircraft wake vortices	59
4.1.8 Aircraft jet blast effect	59
4.1.9 Vehicle wakes	60
4.1.10 Thunder and sonic booms	60
 5. Sensor Siting	 61
5.1 Extremes of site locations	61
5.2 Possibility of local terrain effects	61
5.3 Building locations	63
5.4 Practical limitations	63

TABLE OF CONTENTS (continued)

	Page
6. Spacing Considerations	64
6.1 Required spatial resolution	64
6.2 Required time resolution	64
6.3 Practical constraints	64
7. Anemometers versus pressure sensors relative strengths and weaknesses	65
7.1 Relative arrival times of pressure temperature and wind disturbances.	65
7.2 A comparison between anemometers and pressure sensors.	66
8. Instrumentation problem areas and their solutions	67
8.1 dP Detector temperature sensitivity	67
8.2 Noise on telephone lines	68
8.3 Absolute pressure sensor problems	69
8.4 Plugged inlets	70
8.5 Vandalism	70
8.6 Lightning damage	71
8.7 Anemometer problems	71
8.8 Power failures	72
8.9 System stability	73
8.10 Central recording station problems	74
9. System Maintenance	74
9.1 Calibration	74
9.2 Alternate calibration methods	75
9.3 Tests after bad weather	75
10. Outlook for the Future and Concluding Remarks	76

vii

Accession For	
NTIS GRA&I	<input checked="" type="checkbox"/>
DDC TAB	<input type="checkbox"/>
Unannounced	<input type="checkbox"/>
Justification	
By _____	
Distribution/	
Availability Codes	
Dist.	Avail and/or special
A	

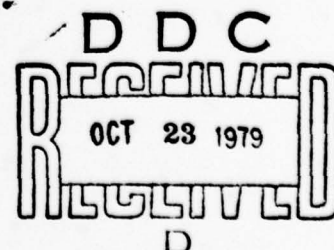


TABLE OF CONTENTS (continued)

	Page
Part II: Statistical Results	
11. Introduction and Summary	78
12. Histograms showing frequency of various types of events as a function of month-of-year	81
12.1 Thunderstorms, Squall-Lines and Fronts	81
12.2 Boundary Layer Effects	82
12.3 Gravity-Shear Waves	83
12.4 Gravity Waves	84
12.5 High Winds	84
13. Statistics of observations related to thunderstorms, squall-lines and fronts	86
13.1 Surface Wind Observations	86
13.2 Surface Pressure Observations	88
13.3 Doppler Acoustic/Microwave Radar Observations	88
13.4 Surface Temperature Observations	92
13.5 Weather Radar Observations	94
13.6 Implications for the Design of Detection Systems	96
14. Statistics of observations related to boundary layer effects	102
14.1 Sample Case Study Illustrating a Boundary Layer Disturbance	102
14.2 Measurement Statistics of Boundary Layer Disturbances	104
14.3 Implications for the Design of Detection Systems	106
15. Statistics of observations related to gravity-shear waves	107
15.1 Sample Case Study Illustrating a Gravity-Shear Wave Disturbance	107
15.2 Measurement Statistics of Gravity-Shear Wave Disturbances	107
15.3 Implications for the Design of Detection Systems	107

TABLE OF CONTENTS (continued)

	Page
16. Observations related to gravity waves	110
16.1 Case Study Comparing Surface Observations	110
16.2 Implications for the Design of Detection Systems	110
17. Observations related to high winds	110
17.1 Implications for the Design of Detection Systems	110
18. Special Topics	112
18.1 Comparisons Between Daytime and Nighttime Events	112
18.2 Effects of Thunderstorm Outflows on Subsequent Outflows	112
18.3 Height of "nose" of Outflow	112
18.4 Maximum Height of Outflow	112
18.5 The Widths of Transition Regions at the Leading Edges of Gust-Fronts	115
18.6 Froude Number and Reynolds Number Determinations for Gust-Fronts	117
19. Possibilities for additional use of these data sets	122
20. Concluding Remarks	122
Appendix I	124
References	126

LIST OF FIGURES

Figure		Page
1.1	Dulles airport array of pressure jump detectors.	3
1.2	Dulles airport array of anemometers.	3
1.3	Dulles airport array of absolute pressure sensors.	4
1.4	System block diagram.	8
1.5	Operating history of acoustic/microwave radar, dP array, and standard barograph.	8
1.6	Operating history of anemometer array (1977).	12
3.1	Example of wind surge for the case of 20 July 1977.	16
3.2	Absolute pressure data for the case of 20 July 1977.	17
3.3	Surface wind vectors before and at the peak of the disturbance of 20 July 1977.	18
3.4	Case of 25 July 1977 showing an abrupt change in wind vector with little surface wind speed disturbance.	19
3.5	Surface wind vectors before and after the direction shift on 25 July 1977.	20
3.6	Example of anemometer data on 7 August 1977 illustrating the impulsive nature of gust-fronts.	20
3.7	Surface wind vectors before and at the peak of the first disturbance on 7 August 1977.	22
3.8	Surface wind vectors before and at the peak of the second disturbance on 7 August 1977.	22
3.9	Example of anemometer data on 2 May 1977 illustrating the large changes in wind direction that can accompany the disturbed portion of a gust surge.	23
3.10	Absolute pressure data for the case of 10 June 1977.	24
3.11	Example of anemometer data on 10 June 1977 for A1.	24
3.12	Example of anemometer data on 10 June 1977 for A2.	25
3.13	Pressure jump detector array data for the case of 8 August 1977 illustrating a spatially complex event.	27
3.14	Absolute pressure data for a gravity-wave event.	28

LIST OF FIGURES (continued)

Figure		Page
3.15	Wind profiles associated with thunderstorm gust front of 27 September 1977; the outflow structure vividly shown by a monostatic acoustic sounder. The increase of winds aloft (about 10 m s^{-1}) had little influence at the surface, permitting the monostatic sounder to detect the event.	30
3.16	Surface measurements associated with gust-front of 27 September 1977. A significant pressure jump occurs associated with the leading edge of the outflow; while only a minor wind surge ($< 3 \text{ m s}^{-1}$) accompanies the event.	31
3.17	Absolute pressure determinations of the propagation speed and azimuth for the gust-front of 27 September 1977.	32
3.18	Inferred 3-dimensional structure of the density current from four viewpoints.	33
3.19	Summary figure illustrating a complex density current flowing from a source region on a stable layer. This figure combines an artist's conception with actual data from the 27 Sept. 1977 case study.	33
3.20	Basis for calculations of direction and speed of motion of a gust front using data from dP array for event of 18 May 1977.	34
3.21	Absolute pressure determinations of propagation speed and azimuth for the gust front of 18 May 1977.	35
3.22	Gust front showing evidence of non-uniform motion on 7 August 1977.	37
3.23	Anemometer data on 17 November 1977.	38
3.24	Doppler sounder profiles on 17 November 1977.	39
3.25	Weather radar data with a 10 km-square identifying the site of the Dulles International Airport array.	41

LIST OF FIGURES (continued)

Figure		Page
3.26	The pressure disturbance of 17 November 1977 together with an artist's view illustrating some mechanisms responsible for the pressure field.	41
3.27	Flight path of PI33 relative to Dulles International Airport.	42
3.28	Weather radar data near the time of the encounter with a 10-km square identifying the site of the Dulles International Airport array.	44
3.29	Anemometer data on 17 June 1977.	45
3.30	Temperature and rainrate data on 17 June 1977.	46
3.31	Doppler sounder profiles on 17 June 1977.	47
3.32	Weather radar data showing the thunderstorm cell relative to the 10-km square identifying the site of the Dulles International Airport array.	49
3.33	Composite indicating the location of various sensors relative to the total rainfall contours, tree damage, and hail observations.	49
3.34	Anemometer data on 26 June 1978.	50
3.35	Pressure data on 26 June 1978.	51
3.36	Numerical simulation of pressure field beneath a thunderstorm downflow (after Teske and Lewellan, 1978).	51
4.1	Sporadic nature of wind-induced dP triggers on 22 March 1977.	58
5.1	Examples of sensor siting.	62
8.1	dP detector threshold variation with temperature.	68
8.2	Typical anemometer location.	73
10.1	Possible array configuration for the detection of large-scale coherent events.	77
12.1.	Histogram showing the number of events related to thunderstorms, squall-lines or frontal passages as a function of month-of-the-year.	82
12.2.	Histogram showing the number of events related to boundary layer effects as a function of month-of-the-year.	83

LIST OF FIGURES (continued)

Figure		Page
12.3.	Histogram showing the number of events related to gravity/shear waves and the 500 mb winds as a function of month-of-the-year.	84
12.4.	Histogram showing the number of events related to gravity waves as a function of month-of-the-year.	85
12.5.	Histogram showing the number of events related to high winds as a function of month-of-the-year.	85
13.1.	Plot of surface wind speed change as a function of surface wind vector change.	86
13.2.	Plot of peak surface wind as a function of surface wind vector change.	87
13.3a.	Pressure change (dP) as a function of rise time (τ) for all events.	89
13.3b.	Pressure change (dP) as a function of rise time (τ) for events showing a surface wind vector change exceeding 15 knots.	89
13.4.	Relative arrival times of pressure and wind disturbances.	90
13.5a.	Doppler acoustic/microwave radar wind direction in degrees as a function of surface wind direction in degrees.	91
13.5b.	Doppler acoustic/microwave radar vector change in m s^{-1} as a function of surface wind vector change.	91
13.6a.	Doppler acoustic/microwave wind direction in degrees as a function of pressure disturbance direction in degrees.	93
13.6b.	Doppler acoustic/microwave vector change in m s^{-1} as a function of pressure disturbance speed.	93
13.7a.	Surface wind vector change as a function of surface temperature change.	95
13.7b.	Plot of the ratio of the Doppler sounder wind vector change $d\vec{U}_d$ to the surface wind vector change $d\vec{U}$ as a function of the surface temperature change.	95
13.8a.	Direction of surface wind as a function of weather radar echo direction in degrees.	97
13.8b.	Direction of pressure disturbances as a function of weather radar echo in degrees.	97

LIST OF FIGURES (continued)

Figure		Page
13.8c.	Direction of Doppler acoustic/microwave radar wind as a function of weather radar echo in degrees.	98
13.9a.	Surface wind vector change as a function of speed of motion of radar echo in m s^{-1} .	98
13.9b.	Speed of pressure disturbance as a function of speed of motion of radar echo in m s^{-1} .	99
13.9c.	Doppler acoustic/microwave radar wind vector change as a function of speed of motion of radar echo in m s^{-1} .	99
13.10a.	Vertical shear in s^{-1} determined from Doppler acoustic/microwave radar as a function of layer thickness in meters for thunderstorm squall-line and frontal-related events.	101
13.10b.	The ratio of vertical shear S_1 associated with the discontinuity to the vertical shear S_2 prior to the discontinuity as a function of the horizontal wind vector change.	101
14.1.	Sample case study illustrating a boundary layer disturbance.	103
14.2.	Surface wind vector change in kts as a function of surface temperature change in $^{\circ}\text{C}$.	105
14.3.	Histogram showing the number of boundary layer disturbances as a function of time of day.	105
14.4.	Vertical shear in s^{-1} determined from Doppler acoustic/microwave radar as a function of layer thickness in meters for events related to boundary-layer disturbances.	106
15.1.	Case study illustrating a gravity-shear wave disturbance.	108
15.2.	Horizontal trace velocity of pressure disturbance as a function of 500-mb wind speed.	109
15.3.	Azimuth of pressure disturbance as a function of 500-mb wind direction.	109
16.1.	Case study illustrating a gravity wave disturbance.	111
18.1.	Histogram showing the percentage of gust-fronts as a function of height.	114
18.2.	Gust front height in kilometers as a function of propagation speed.	114
18.3.	Gust front height in kilometers as a function of temperature drop across the front in $^{\circ}\text{C}$.	116

LIST OF FIGURES (continued)

Figure		Page
18.4.	Histogram of the widths of gust-front transition regions.	116
18.5.	Transition region width as a function of propagation speed.	118
18.6.	Histogram of the Froude number for gust-fronts.	118
18.7.	Froude number as a function of temperature drop in $^{\circ}\text{C}$.	120
18.8.	Gust front height as a function of Froude number.	120
18.9.	Froude number as a function of propagation speed.	121
18.10.	Froude number as a function of Reynolds number.	121

LIST OF TABLES

Table		Page
1.1	Key Recommendations and Results.	5
1.2	Significant Problem Areas.	6
1.3	Instrumentation Functions and Characteristics.	9
2.1	Data Sources.	14
11.1	Summary of Key Conclusions.	80
13.1	Key Results from Observations of Disturbances Caused by Thunderstorms, Squall-Lines and Fronts.	100

PART I SYSTEM OPERATION AND SIGNIFICANT CASE STUDIES

1. INTRODUCTION

1.1 Background

In response to an FAA urgent need for low-level wind-shear information at air terminals, the Wave Propagation Laboratory (WPL) of NOAA with FAA support developed and installed an experimental thunderstorm gust front detection system near Dulles International Airport. Dangerous wind shear can normally be classified in two ways: either as extending over large areas, as it does when associated with warm frontal passages, or as being highly localized, as it is when resulting from thunderstorm downbursts (as described by Fujita and Byers, 1977) or gust fronts (extensively documented by Goff, 1976, Greene, et al., 1977 and the references therein). The Dulles system consisted of two major elements -- a hybrid acoustic-microwave-radar system for providing a detailed height profile of the wind directly above the sensor (and hence providing a useful picture when the shear condition is widespread) and a dense surface array of pressure jump detectors for detecting the development and motion of the more localized features. This system in its dual and complementary aspects has been described recently in companion papers appearing in the American Meteorological Society's Bulletin (Hardesty, et al., 1977; Bedard, et al., 1977). In addition, the design of the pressure jump detectors themselves has been described by Bedard and Meade (1977); Bedard and Cairns (1977) and Bedard and Beran (1977) give further information.

While it is generally agreed that surface arrays of in situ sensors are useful for tracking the progress of thunderstorm gust fronts, there remains some unofficial but nonetheless spirited controversy concerning which kind of surface sensor should be optimum for gust-front detection. More precisely, the question is whether we should monitor gust-front-associated changes in wind speed and direction or focus on the related pressure changes. Proponents of the former argue that it is wind velocity itself that is most relevant to aviation and hence wind velocity that ought to be measured, whereas proponents of the latter point out that the surface-pressure changes are better indications of conditions aloft, where the plane is, because they measure changes in the integrated air mass above the sensor. Questions

also remain concerning the optimum geometry and spatial density of the sensor arrays, false alarm rate, and miss rate of the system, etc. Data are required to resolve these issues, and the Dulles system was designed and operated with such a goal in mind. In addition to approximately 120 pressure-jump (dP) sensors (Bedard and Meade, 1977) deployed, the system also included ten anemometers, twelve absolute pressure sensors, and two temperature sensors (Figures 1.1, 1.2, and 1.3 show the positioning of these instruments relative to the Dulles runways). Thus the Dulles system provided a means for detecting cold-air outflows from thunderstorms, measuring the spatial structure of their surface properties, and relating these to the resulting wind shear and the local meteorology. This complex of instruments operated for a long enough period to document some of the advantages and shortcomings of the various monitoring approaches. Our report highlights these approaches by presenting data from selected events. The results suggest (perhaps unsurprisingly) the advantages of hybrid systems (including both wind and pressure sensors) for operational use.

Data sets obtained from the Dulles airport wind and wind-shear measuring system, are presented together with interpretations emphasizing the significance of these data for the wind-shear detection problem. The report appears in two parts. Part I highlights case studies that illustrate properties of gust fronts and thunderstorm down flows important for the design of surface arrays for wind-shear detection. In addition, Part I reviews the history of the system, describing the operation, equipment problems encountered, and proposed solutions.

Part II concentrates upon documentation of the data sets obtained. The system detected over 100 events so that Part II of the report represents a significant data base, including weak as well as strong gust front events. Part II develops the statistics for this data base, including, for example, plots of propagation speed as a function of the maximum gust surge, peak pressure and wind maximum in the lower 500 meters of the atmosphere.

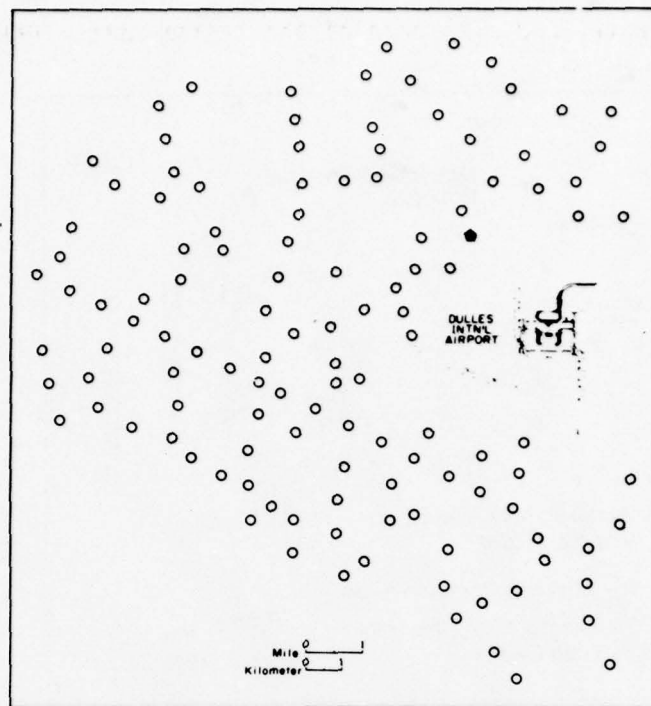


Figure 1.1. Dulles airport array of pressure jump detectors.

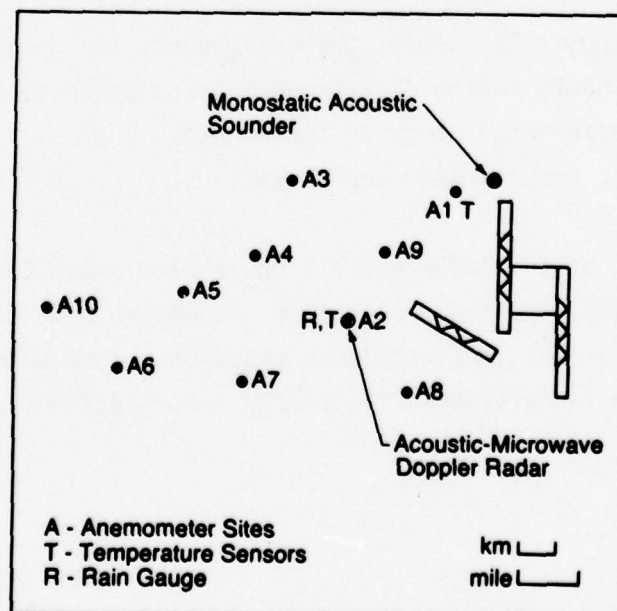


Figure 1.2. Dulles airport array of anemometers.

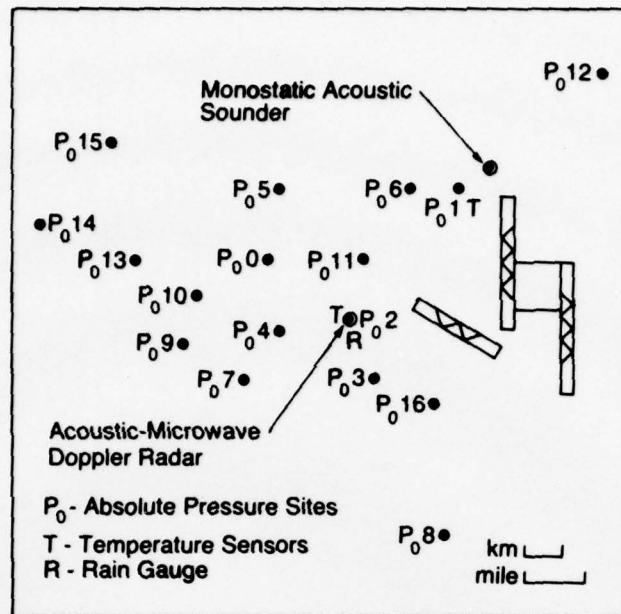


Figure 1.3. Dulles airport array of absolute pressure sensors.

The scope of this report is broad, providing bases for designing surface arrays as well as for understanding data presentations which concentrate on the statistics and/or meso-meteorology of the events. Table 1.1 highlights significant conclusions, results and recommendations.

Portions of Part I of this report dwell on problem areas involving surface arrays, their deployment and operation. However, none of the problems identified prevent the use of the techniques described. The chief problems and their solutions are identified in Table 1.2, later sections provide specific details.

Table 1.1 Key Recommendations and Results

1. Approach thunderstorm wind-shear as a dual problem and develop detection methods for both the thunderstorm gust front and downflow regions.
2. Combinations of pressure jump detectors and wind sensors should constitute reliable thunderstorm wind-shear warning systems for both large-scale and smaller scale events.
3. Use 2-km spacings for arrays designed to detect large scale, coherent gust fronts (Section 10).
4. Set up an array configuration designed to detect spatially concentrated outflows. Do theoretical and experimental evaluations of the pressure fields from various sources (e.g., aircraft weight transfer).
5. Continue to apply meso-analysis to existing and future data sets (Fujita's analysis of the 18 May 1977 Dulles events is an example of the value of such efforts).
6. Update future systems with the following improvements:
 - a. Provide additional lightning protection
 - b. install modified dP sensors,
 - c. install new oscillator designs for high-loss telephone lines,
7. Do not consider the Dulles style dense array approach as a practical warning system, chiefly because of the massive logistics problem it presents (e.g., to merely visit all the dP sites you must drive a distance exceeding a Washington, DC to New York trip).
8. Measure and/or document the pressure fields related to wing tip vortices, aircraft weight transfer, and jet blast prior to deployment near runways.
9. On future systems use a remote calibration capability and/or an interrogate type of data transfer to increase reliability and ease of maintenance.
10. Recommend testing of array (whether it consists of dP detectors, wind sensors or combinations) following severe storms. Most problems were storm-related.
11. Add lightning protection to anemometer towers.
12. Absolute pressure sensors are not required for operational detection systems (unless alternate needs require e.g., gravity-shear wave detection).
13. Additional laboratory testing of selected sensors from the array to verify long-term reliability is desirable.
14. The use of a local display and portable two-way radio can ease maintenance of large array installations.
15. Recommend further work to understand the relative contributions of various mechanisms to the pressure field (e.g., how accurate a representation is the pressure nose of the maximum vertical downflow speed?).

Table 1.2 Significant Problem Areas

Problem Area	Operational Impact	Solution
1. dP temperature sensitivity	Threshold for detection depends upon thermal changes	Improve current design with longer thermal time constant
2. Lightning damage	<ul style="list-style-type: none"> a. Doppler sounder did not operate through some events b. Some dP sensors were damaged c. Anemometer outages 	<ul style="list-style-type: none"> a. Add additional protection b. Add local lightning grounds where missing c. Add lightning protection
3. Wind gust dP triggers	Could constitute a source of false alarms	Process data to require trigger duration of several seconds
4. Data line noise	Could constitute a source of false alarms	New oscillator design providing higher signal level
5. Plugged Po and dP inlets	Pressure sensor response reduced	New inlet adaptor eliminating need for removal of porous cylinder
6. Local power failures	Loss of data during key intervals	Battery back-up for all system elements

1.2 History of Operation and Instrumentation

Figure 1.1 shows the array of pressure jump (dP) detectors in relation to Dulles airport. Figures 1.2 and 1.3 detail the locations of anemometers and absolute pressure (Po) sensors in relation to Dulles airport and the Doppler acoustic/microwave radar and a monostatic acoustic sounder. A monostatic acoustic sounder operated independently of this experiment and is described in a paper by Parry and Sanders (1972). The Dulles system is described in papers by Hardesty et al. (1977) and Bedard et al. (1977), with the original concept first appearing in a paper by Beran et al. (1976). This section describes some details of the instrumentation and also shows when the various system elements operated and which time periods had the most types and numbers of operating sensors.

Figure 1.4 is a system block diagram showing the data flow and also indicating the method of powering the system — where a battery bank and charges provide back-up in case of local power failures. Table 1.3 defines the functions and characteristics of the major system components. The names in parentheses next to the underlined primary component name indicate alternate names used. The acoustic/microwave radar is described separately by Hardesty et al. (1977).

The local display shown in an element of Figure 1.4 consisted of a large map of the dP array with a light at each sensor location displaying its status. Such a local display is invaluable for maintaining the system as is a reliable portable two-way radio link. The remote display had the capability of reconstructing the local display at a distant location using a conventional telephone circuit. On several instances during the initial operation, the status of the Dulles system was monitored at Boulder, Colorado over a telephone circuit.

Figure 1.5 compares the operating times of the acoustic/microwave radar, dP array, Po array and recording drum barograph. The number of Po sensors increased from 1 in March to 12 in August of 1977. An FM discriminator

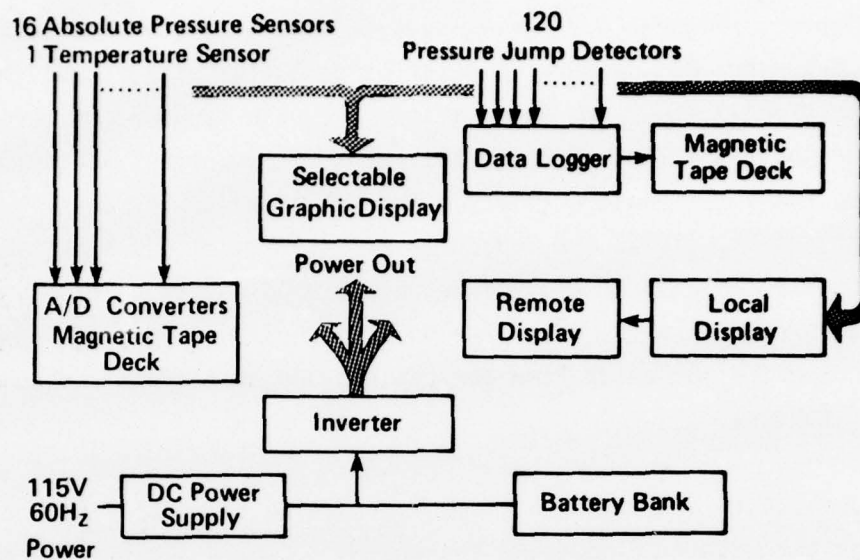


Figure 1.4. System block diagram.

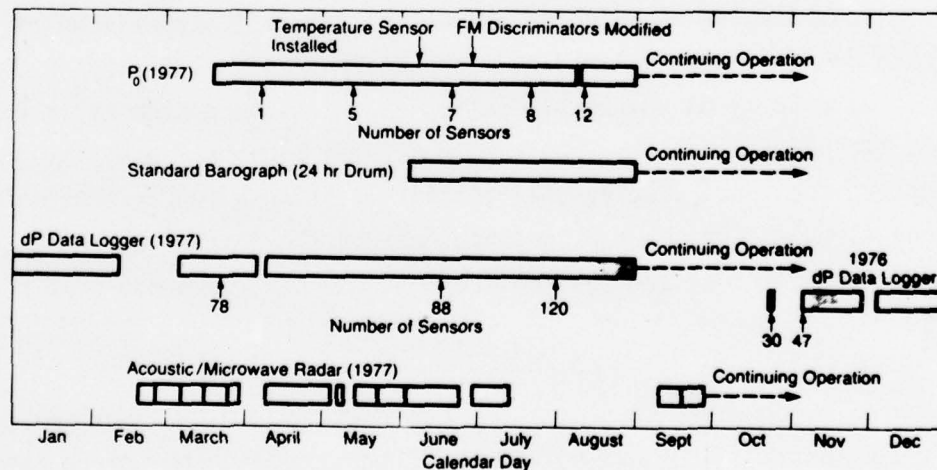


Figure 1.5. Operating history of acoustic/microwave radar, dP array, and standard barograph.

Table 1.3. Instrumentation Functions and Characteristics

Instrument	Function	Characteristics	Manufacturer
dP dector (pressure jump detector, dP/dt sensor, P, P dot sensor)	Provide a yes-no indication of the existence of a pressure jump meeting preset threshold requirement. (e.g. pressure jumps greater than 1 mb occurring in less than 10 minutes)	a) pressure switch threshold: .5 mb b) high pass filter: RC (3 minutes) c) output: fixed audio tone when triggered d) power requirements: internal battery e) reference (Bedard and Meade, 1977)	WPL
Po sensor (absolute pressure detector, microbarometer)	Provide a continuous recording of atmospheric pressure.	a) resolution: less than .1 mb b) range: ± 50 mb about the local mean pressure c) frequency response: DC to 1 Hz d) output: FM tone e) power requirements: 115V, 60 Hz	Pressure Sensor - EX410 Ball Engineering Co. 2140 Kohler Boulder, CO 80303 Voltage controlled oscillator and packaging - WPL
<u>Anemometers</u>	Provide continuous data on wind speed and wind direction.	a) height: 7 meter towers b) wind speed: 0-100 mph (± 5 mph) (normally used) 0-50 mph (± 2.5 mph) c) wind direction: 0-540° (± 1.50) d) output: stripchart recording e) power: 115V, 60 Hz with internal battery backup	Wind Mark III System Climatronics Corp 1324 Motor Parkway Hauppauge, NY 11787
Temperature sensor at recording site	Provide a continuous recording of local temperature.	a) range: -30° to $+100^{\circ}$ C b) accuracy: ± 0.5 C c) power: 115V, 60 Hz d) output: analog voltage	Thermivolt temperature probe type 705 - (Yellow Springs Instrument Co.) Gill naturally ventilated radiation shield - (R. M. Young Co. Type 43103) Interface electronics and packaging - WPL
Temperature sensor at sounder site	Provide a continuous recording of local temperature.	a) range: -30° to $+50^{\circ}$ C b) accuracy: ± 1.5 C c) output recorded with acoustic/ microwave radar data	YSI #44303 linearized thermistor

Table - continued

Instrument	Function	Characteristics	Manufacturer
Rain gauge at sounder site	Provide record of precipitation	a) accuracy: 0.5% (at 0.5 in/hour) b) output: momentary switch closure for each 0.25 mm of precipitation. Output recorded with acoustic/micro-wave radar data	Weather measure heated snowgauge Model P511E
Data logger (dP recorder)	Scan array of DP sensors once per second and send data to tape recorder	Provides time, site coding and an internal alarm. Standard output is array status every 10 minutes. Will record array status once per second as long as a dP detector is triggered	Easterline Angus PD2064 Programmable Data System Kennedy 9 track 1600/360 tape recorder
Po recorder	Digitize and record Po data and one temperature sensor	Scans and records data from all Po sensors and one temperature sensor once every 4.8 seconds	Monitor Labs 9100P Data System (modified) Pertec Formatter

modification in June 1977 resulted in more accurate Po data being recorded (Section 8.3). The standard (24-hr) drum barograph operated from early June 1977 as a "quick look" guide for significant events. Those magnetic tapes containing the times of large pressure disturbances found on the barograph were processed first.

The dP data logger operated from December 1976 to December 1977 without problems. Although the data logger had a bad ROM during the first month of operation, we had no other problem until December 1977 when the data logger malfunctioned (November, 1977). The other gaps in operation were due to general system maintenance or to problems with the magnetic tape deck. In general, the logging/recording part of the operation was quite reliable. The numbers below the bar indicating data logger operation show the numbers of dP detectors installed, aligned, and calibrated as a function of time. This number rose from 47 in November 1976 to 120 in late July 1977. Sensor checking was difficult since it took approximately 3 days to calibrate the entire dP array (Section 9.1). Problems with phone lines (due to lightning) were the chief source of outages. One conclusion is that a better means of verifying operation is a necessity for dense and extended arrays. A remote calibration capability, or an interrogate type of data transfer system are possible solutions.

One unfortunate occurrence during the acoustic/microwave radar operation was a major outage suffered from mid-July through mid-September, 1977. This was due to lightning and emphasized the need for both complete lightning protection and power backup for systems designed for the detection of thunderstorm effects.

The anemometer array history (Figure 1.6) shows a spotty operation. Most of the anemometers operated well through key portions of the test interval, with full-time maintenance. The anemometers were plagued by electronic and mechanical failures, as well as by problems caused by leakages in the enclosures. It seems that the addition of lightning rods would have reduced lightning damage. These problems, discussed in more detail in a later section,

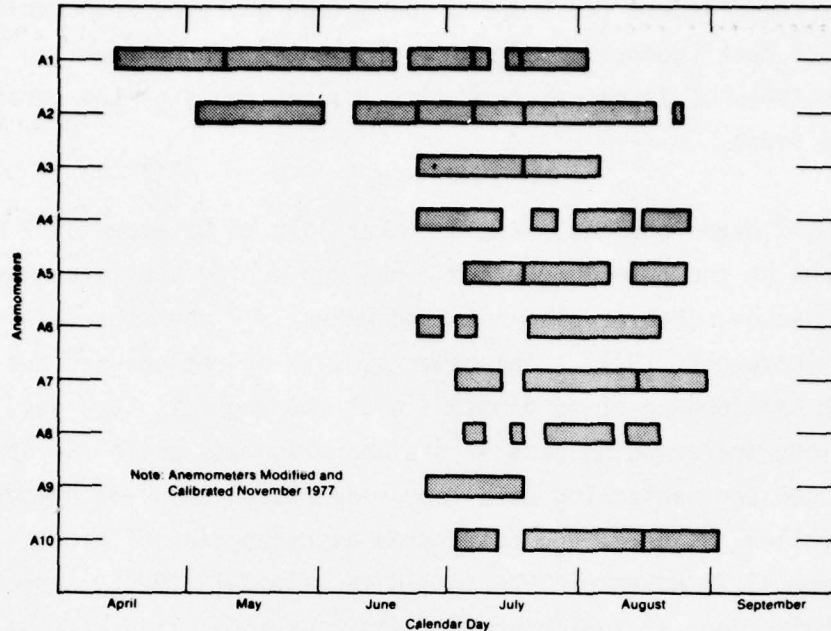


Figure 1.6. Operating history of anemometer array (1977).

suggest that a more reliable approach would have been to telemeter the anemometer data back to the central recording site rather than to record graphically at each anemometer site. Fortunately, we recorded many events with most of the major elements of the Dulles system in operation. Case studies illustrating the value and breadth of these data appear in Section 3.

2. ANALYSIS

2.1 Analysis Philosophy

The data sets from several of the different sensor types are considered separately (e.g., analyze the anemometer data looking for wind surges or sudden vector shifts (typically greater than 10 kts) without using pressure data as a guide). All the dP data tapes were printed out, flagging all sensor triggers, creating special data cartridges of dP events for more complete

analysis. Standard barograph records were quite useful for quick identification of those absolute pressure data sections to be given priority analysis. No routine analysis was made of all absolute pressure data, acoustic/microwave Doppler data, or temperature data; rather, the analysis used event times defined from either the standard barograph, dP array, anemometer array, monostatic sounder, or local weather reports. Because of the large number of events, more detailed analyses was performed of events which either provide guidance for the design of detection systems or illustrate important properties of shear producing weather systems. Table 2.1 lists the meteorological data sources used in interpreting the data sets obtained during this experiment.

2.2 Analysis Programs

All the analyses were performed on an after-the-fact basis at NOAA's Wave Propagation Laboratory in Boulder, Colorado. Appendix 1 lists the programs developed and applied to these extensive data sets. First level of analysis of the Po and dP digital tapes made use of a main computer (CDC 6600) capable of handling the large quantities of data. Through a high-speed data line to this computer we control the processing and editing of tapes from a terminal to generate files containing data sets essential to Po and dP analysis. These files are then transferred via the high-speed data line to the WPL terminal and stored on data cartridges. A second level of processing is done "off-line", using a Tektronix 4051 graphics system and working with pre-processed data cartridges. Methods were developed for display of anemometer and temperature data from Dulles airport.

3. NOTEWORTHY CASE STUDIES

From the available Dulles data more than 100 events have been identified, including gust fronts and other phenomena that range from intense squall lines to the very weakest wind gusts. These events manifest themselves through wind surges, pressure rises recorded by the pressure sensors, pressure jumps sufficient

Table 2.1 Data Sources

- a. Surface Weather Observations for Dulles International Airport, Forms 10A and 10B.
- b. Standard Barograph Records.
- c. Anemometer Records.
- d. Controller's Logs, Dulles International Airport.
- e. Weather Radar Covering Dulles International Airport (usually Patuxent River Naval Air Station).
- f. Metropolitan Climatological Summaries National Capital Area.
- g. Rawinsonde, Sterling, Virginia.
- h. National Weather Service, Radar Summaries.
- i. Surface Weather Maps and 500 mb Contours.

to trigger the jump detectors, large wind-shear recorded by the acoustic-sounder system, and combinations of the above. The case studies selected show the diversity inherent in the data set. All are either related to gust fronts (through association with thunderstorms reported by the National Weather Service or on radar) or illustrate some property important for use in detection systems. The case studies appear in the sections that follow.

- 3.1 20 July 1977 — Spatially uniform and readily interpretable surface wind surges accompanying a gust-front cold-air outflow.
 - 3.2 25 July 1977 — a gust-front change in wind direction with no accompanying change in speed.
 - 3.3 7 August 1977 — a gust front showing the impulsive nature common to many wind-speed surges caused by thunderstorms.
 - 3.4 2 May 1977 — a gust front associated with large and continuous changes in wind azimuth and speed.
 - 3.5 10 June 1977 — a gust-front showing considerable spatial irregularity in winds but not in surface pressure.
 - 3.6 8 August 1977 — a gust front showing spatial complexity in both the surface-wind and pressure fields.
 - 3.7 8 July 1977 — large-amplitude pressure changes caused by gravity waves.
 - 3.8 27 September 1977 — A gust-front showing only minor temperature and anemometer disturbances at the surface.
 - 3.9 18 May 1977 — Comparison calculations of direction and speed of motion of a gust front using data from P_0 and dP arrays.
 - 3.10 7 August 1977 — Gust-front showing evidence of non-uniform motion.
 - 3.11 17 November 1977 — Comparison illustrating a limitation of conventional weather radar for tracking discontinuities.
 - 3.12 17 June 1977 — An aircraft flight path shown in relation to approach zone meteorology.
 - 3.13 26 June 1978 — A thunderstorm showing evidence of an intense down-flow.
- 3.1 20 July 1977 — Spatially uniform and readily interpretable surface wind surges accompanying a gust-front cold-air outflow.

On 20 July 1977, nocturnal thunderstorms occurred to the north of the Dulles system causing a gust surge in the wind to pass over the site at about 0400 EDT (Figure 3.1). Figure 3.2 presents the pressure data for the absolute pressure sensor near the anemometer A1 location, which indicates

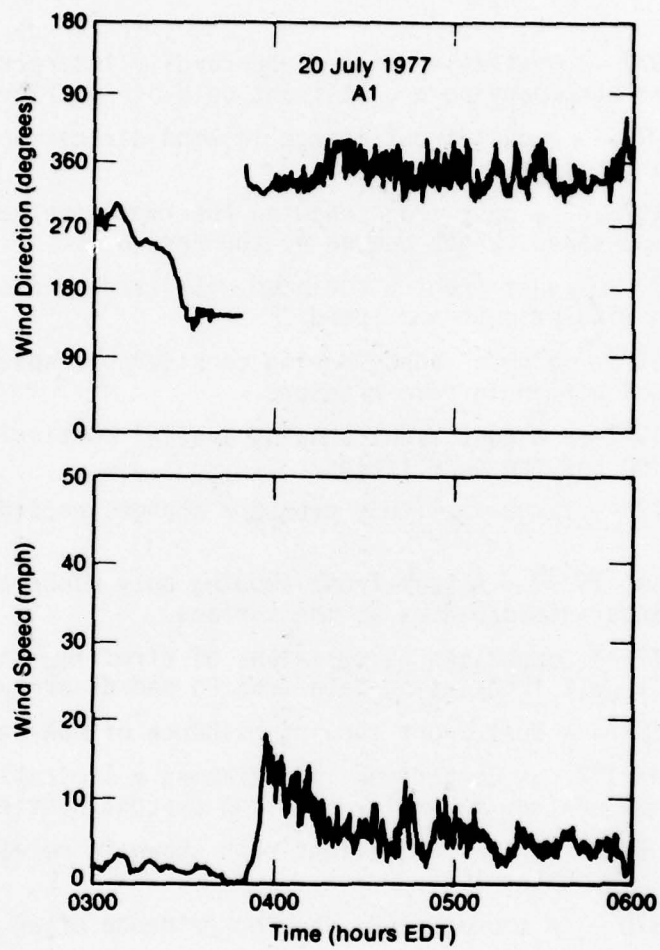


Figure 3.1. Example of wind surge for the case of 20 July 1977.

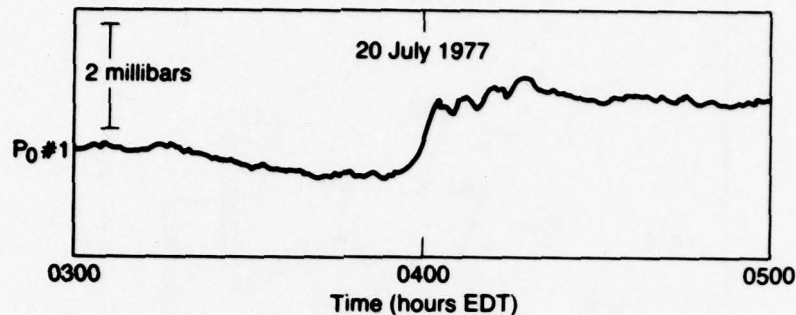


Figure 3.2. Absolute pressure data for the case of 20 July 1977.

that the gust surge and pressure rise arrived essentially simultaneously. For this event, the pressure rise was about 1.4 millibars and was constant across the array of pressure sensors to within 0.15 millibar as it moved with a nearly uniform propagation speed of about 8 m s^{-1} from the north. Figure 3.3 depicts the maxima for the wind surges observed by all of the (operating) anemometers. The solid-line vector at the lower left of the figure defines the wind speed scale for all the maximum winds associated with the event. (In corresponding figures for the case studies to follow, a dashed line vector also appears at the lower left of the figure, defining the wind-speed scale for the winds measured just prior to the onset of the event. However, for this case the winds prior to the event are essentially calm and hence are not shown.) There is very little spatial variability revealed in either the pressure or anemometer data for this event. Unfortunately, from the standpoint of airport operation, such unique events, which show relatively uniform surface effects and easily interpreted azimuth variations, do not appear to be the rule. The cases that follow indicate that the detection problem is frequently more complex.

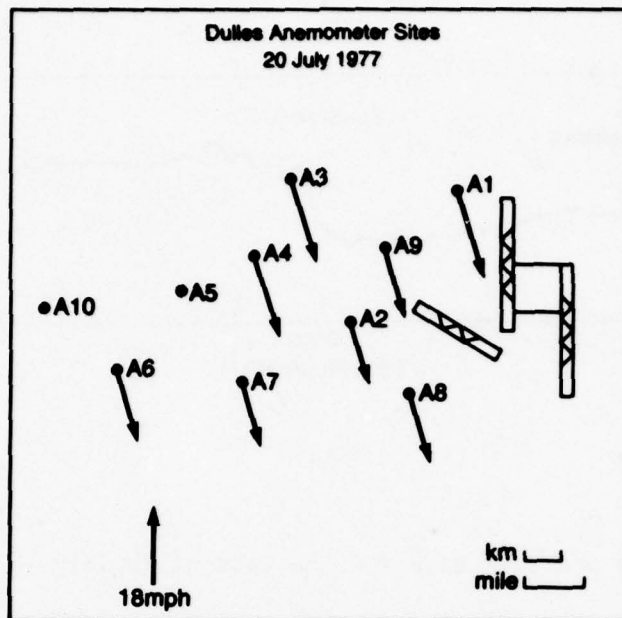


Figure 3.3. Surface wind vectors before and at the peak of the disturbance of 20 July 1977.

3.2 25 July 1977 — A gust-front change in wind direction with no accompanying change in speed.

On 25 July 1977, the Dulles area experienced thundershower activity with cloud tops reaching 7 km (23,000 ft). Shortly before 1800 EDT, a disturbance from storms northwest of the site propagated across the array at a speed of 13 m s^{-1} , producing a pressure rise of about 0.9 mb over a 450-second period. This event was particularly noteworthy because the gust front produced a change in wind direction with little corresponding change in the wind speed itself. As indicated in Figure 3.4, the event is clearly evident in the wind direction data but not immediately discernible in the wind speed; the average change in the wind vector amounted to some 4.7 m s^{-1} . This case does suggest the importance of measuring the wind vector rather than the wind speed, a point considered in more detail in Part II of this report. The 25 July 1977

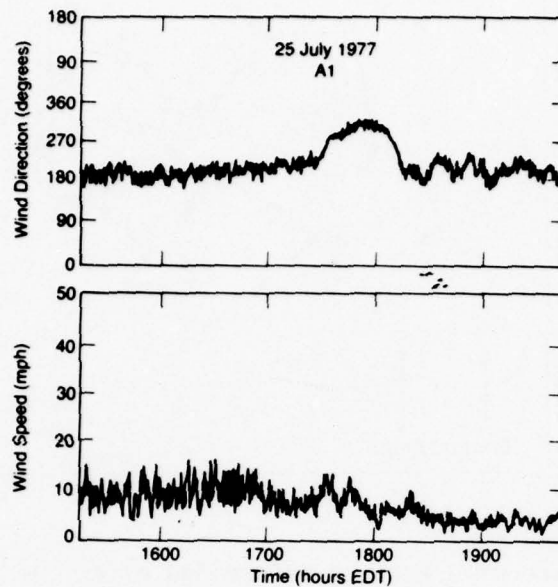


Figure 3.4. Case of 25 July 1977 showing an abrupt change in wind vector with little surface wind speed disturbance.

case also illustrates considerable spatial and temporal variability in the wind. Figure 3.5, which shows wind vectors before and during the event, reveals large differences in the wind behavior from site to site; for example, the difference between the anemometer readings during the event at sites A6 and A3 amounts to a factor of three. The corresponding spatial variations in pressure are relatively minor amounting to no more than a factor of 30%. This point is considered in more detail in the discussion of the cases in sections 3.5 and 3.6.

3.3 7 August 1977 — A gust-front showing the impulsive nature common to many wind-speed surges caused by thunderstorms.

Two events of 7 August 1977 provide examples of impulsive wind surges caused by thunderstorm outflows. Figure 3.6 shows the wind speed and direction data for one of the anemometers (A9) and indicates the two events.

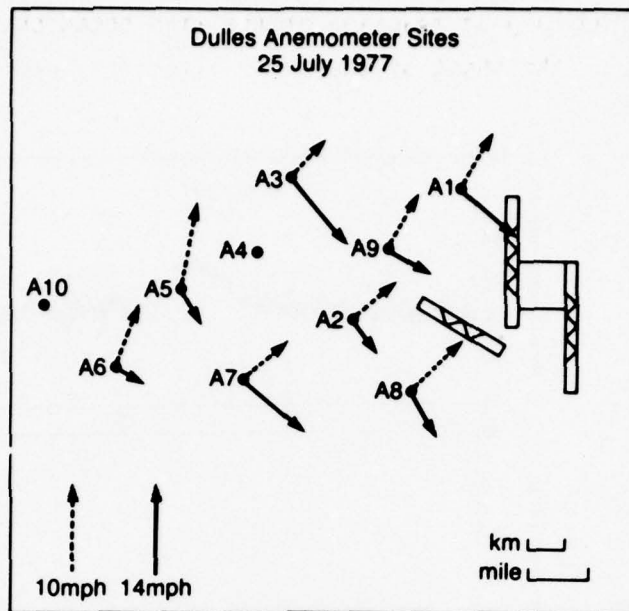


Figure 3.5. Surface wind vectors before and after the direction shift on 25 July 1977.

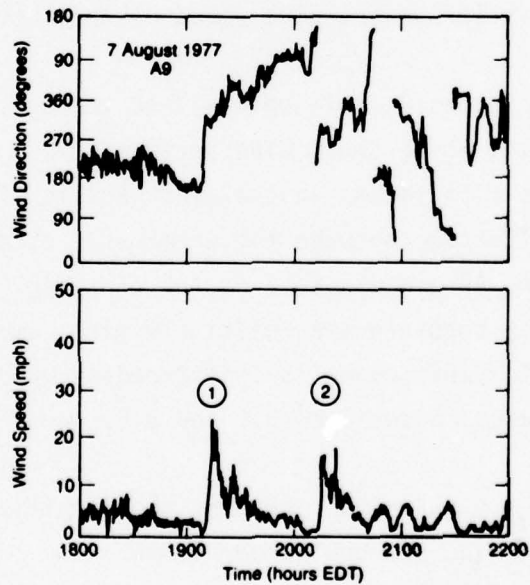


Figure 3.6. Example of anemometer data on 7 August 1977 illustrating the impulsive nature of gust-fronts.

In both cases the largest fraction of the wind speed change occurs in well under 10 minutes, the onset of the surge being more rapid than the following decay. The relatively short duration of the peak winds compared with the duration of the events themselves suggests that the gust front is most violent in a relatively small region (e.g., 2 km) near the leading edge. Some change in wind azimuth also occurs during the events. Figures 3.7 and 3.8 show the corresponding wind-vector summaries from the anemometer array. Although there is some spatial variability in the surface peak-wind surges, the vector maxima are all within a factor of two of one another. A pressure jump of 1.1 mb was recorded on a standard barograph near the A1 site with rise times of 7 minutes and 2 minutes for the first and second events, respectively. Unfortunately, a lightning strike caused the loss of the absolute pressure sensor array data. The pressure-jump-detector array did not respond to the slower rise time of the first event, but it did trigger on the second event and revealed that the speed of the gust front changed considerably as it propagated over the site. When it entered the array, the gust front was moving with a 20 m s^{-1} motion from the northwest; by the time it was exiting, however, its speed had been reduced to 5 m s^{-1} . This is statistically unusual; by far the majority of such disturbances are observed to propagate with nearly uniform speed across the array. Section 3.10 provides more detail concerning propagative speed calculations.

3.4 2 May 1977 — A gust-front associated with large and continuous changes in wind azimuth and speed.

On 2 May 1977, an abrupt wind surge occurred, with wind speed increasing by more than 10 m s^{-1} within 5 minutes (Figure 3.9), in a fashion analogous to that of the events in section 3.3. During the event, wind direction changed dramatically and continuously from 270° clockwise through north to 20° . Even after passage of the gust front itself, the wind kept changing continuously in time, eventually coming from due east and finally from the southeast before the winds died down. Interestingly, the event was detected only by the northeast sector of the array, making velocity determinations more difficult. However, indications from the acoustic sounder data were that the gust-front was propagating from the northwest. This type of event needs relatively densely spaced

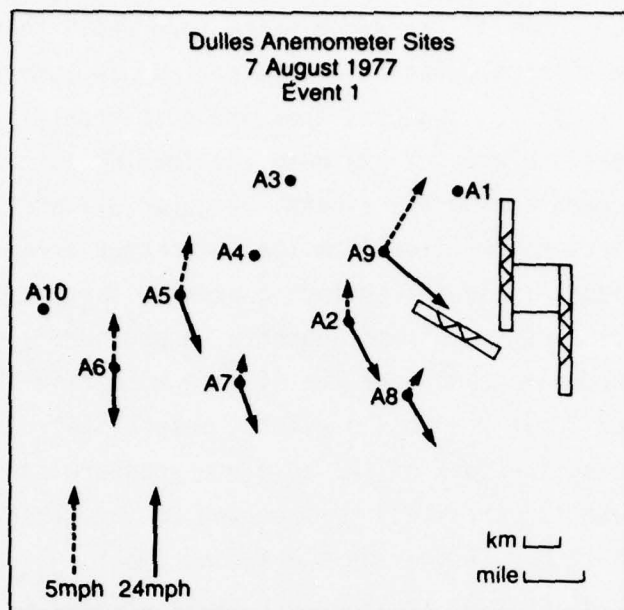


Figure 3.7. Surface wind vectors before and at the peak of the first disturbance on 7 August 1977.

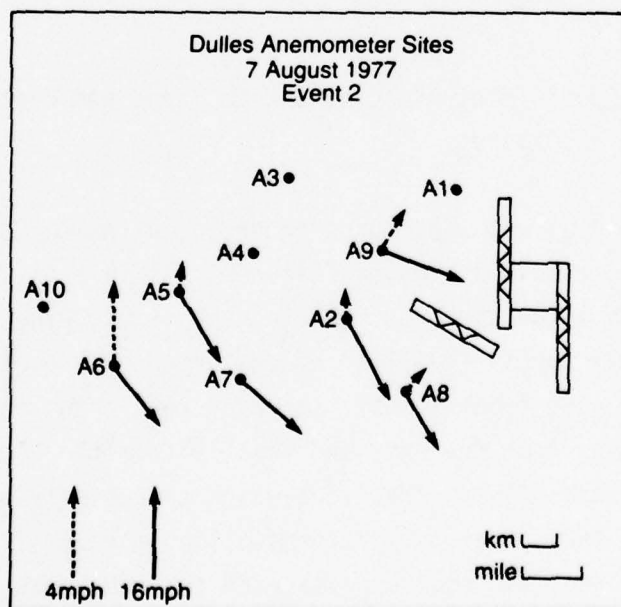


Figure 3.8. Surface wind vectors before and at the peak of the second disturbance on 7 August 1977.

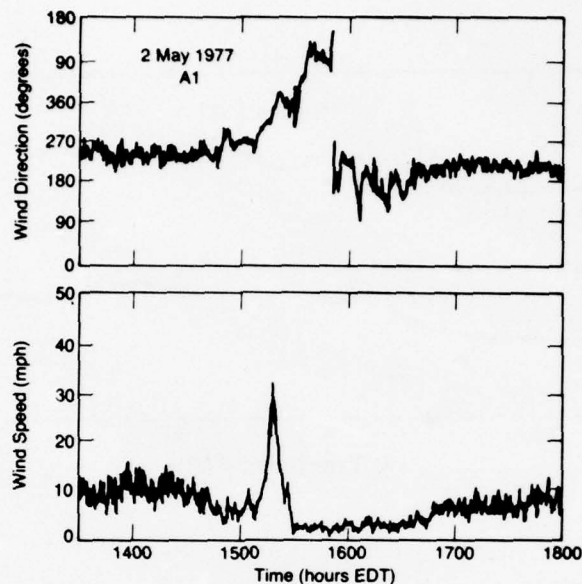


Figure 3.9. Example of anemometer data on 2 May 1977 illustrating the large changes in wind direction that can accompany the disturbed portion of a gust surge.

multiple sensors to provide accurate estimates of the shape of the front and its propagation. Such complex shifts will tend to occur most frequently near the center of thunderstorm downflows.

3.5 10 June 1977 — A gust front showing considerable spatial irregularity in winds but not in surface pressure.

On 10 June 1977, the Dulles area experienced rain with cloud tops at the 7 km level in the late afternoon and early evening. During this time, the system data showed a pressure jump propagating from the north at just under 11 m s^{-1} ; the pressure increase amounted to 2 mb over 500 seconds, as shown in Figure 3.10, for the P_{01} and P_{02} sites. Figures 3.11 and 3.12 show the corresponding wind traces from the collocated anemometers. At site A1

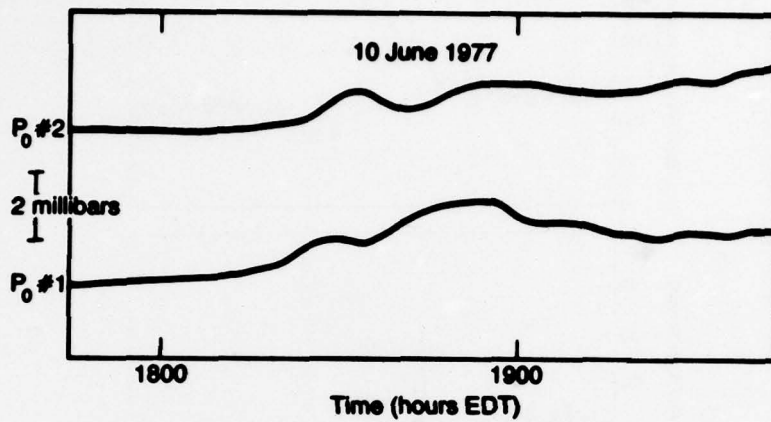


Figure 3.10. Absolute pressure data for the case of 10 June 1977.

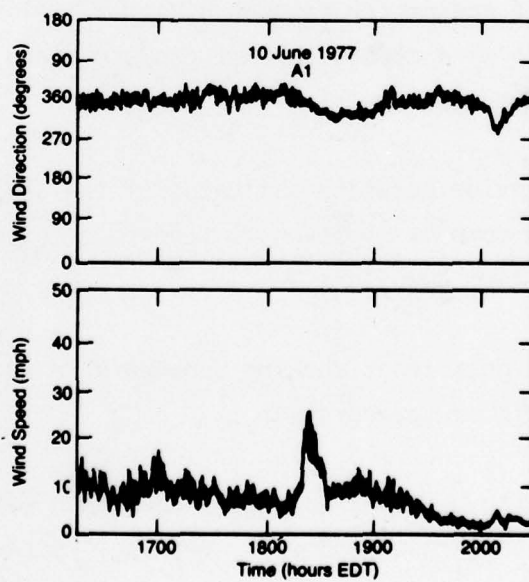


Figure 3.11. Example of anemometer data on 10 June 1977 for A1.

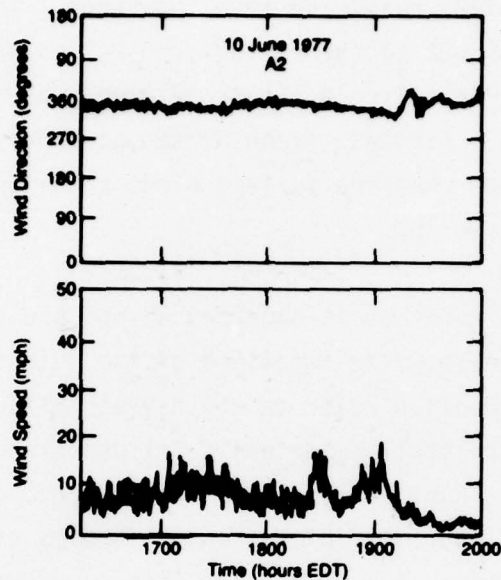


Figure 3.12. Example of anemometer data on 10 June 1977 for A2.

only a single wind surge with a 12 m s^{-1} maximum is evident, occurring at about 1820 EDT. At A2 a smaller initial surge (8 m s^{-1}), occurring at about 1830 EDT is followed by yet another surge (9 m s^{-1}). During both events, wind-direction changes are small. In a case like this, a larger number of wind sensors in a surface array is required to provide an unambiguous picture of the low-level airflow; a few sensors might give a quite misleading picture of the event. It should also be noted that the apparent discrepancy between the anemometry data and the pressure-sensor system can be resolved if we recall that the wind sensor measures the local wind while the pressure sensor measures the total mass of the air above it (if we ignore inertial effects). Because the two instruments are sensing different height regions of the atmosphere, we may quite naturally expect them to show different results on occasion.

3.6 8 August 1977 — A gust front showing spatial complexity in both the surface-wind and pressure fields.

In the afternoon and early evening of 8 August 1977 severe storms hit the Dulles area causing 1-1/2" rains and leveling trees. These storms began to the south and then broke out to the north. The Dulles array data show that three pressure jumps occurred during a 1-hour interval, the third and largest amounting to about 2 mb in 5 minutes. Each of the pressure jumps showed surface wind changes during a period when the surface winds remained generally disturbed and exhibited significant veering.

Figure 3.13 shows the event as it appeared on the pressure jump detectors. Solid circles on the figure show the locations of the detectors, whereas the numbers above the sensor location refer to the key at left, giving the time interval during which the respective sensors first detected the gust-front-associated pressure rise. Thus, for example, designator 2 (D2) refers to the time interval between 1915 and 1918 EDT, at which time D3 is set. (The sites that apparently did not respond were, in fact, either unconnected at this time (western segment) or had phone-line problems (south-west) because of lightning damage.) Thus the progression of the numbers indicates the progress of the pressure jumps. The initial disturbance propagated from the southwest at 10 m s^{-1} , producing a small surge in surface wind. A subsequent "burst" of triggers developed to the north, as indicated by designator 3, in an area shaded for emphasis. Although analysis of this event is in its preliminary stages, it would appear that a "downburst" of the type described by Fujita and Caracena (1977) could have caused the pattern. Thus, this case again indicates the importance of using dense enough arrays to detect and interpret complex situations.

It might be noted parenthetically that in addition to the pressure-jump detectors, the acoustic sounder installation and a large number of anemometers and pressure sensors were knocked out by lightning. This points up the critical need for "hardening" the system by providing auxiliary power sources, etc., to keep the system operational under such adverse but important conditions.

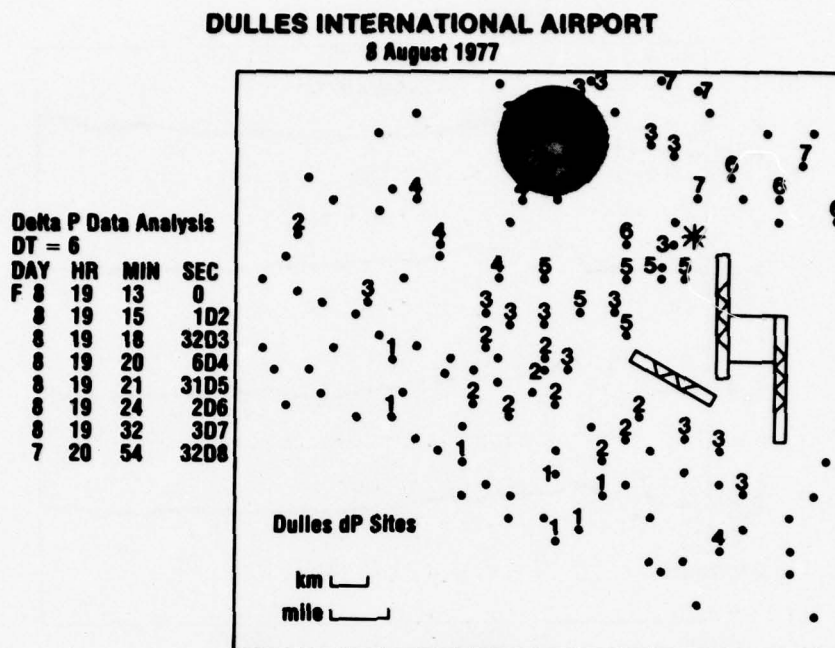


Figure 3.13. Pressure jump detector array data for the case of 8 August 1977 illustrating a spatially complex event.

3.7 8 July 1977 — Large amplitude pressure changes caused by gravity waves.

During the night of 8 July 1977, a wave-like pressure disturbance, with a 400-second period, propagated across the array from the north with a phase speed of about 8 m s^{-1} (Figure 3.14). The weather radar summary showed no echoes in the region when this occurred and was unable to relate this disturbance (which did cause pressure-jump detector triggers) to any surface weather feature. The most probable explanation is that the event was due to a gravity wave of the type reviewed by Gossard and Hooke (1975) and routinely detected by acoustic echo sounders (e.g., Hooke et al., 1972; Beran et al., 1973). Indeed, the Sterling, Va. monostatic sounder records indicate an inversion of about 350-m depth with 200-m perturbations at the time of the event. Further support to the wavelike nature of the disturbance is given by the validity of the impedance relation (Gossard and Munk, 1954;

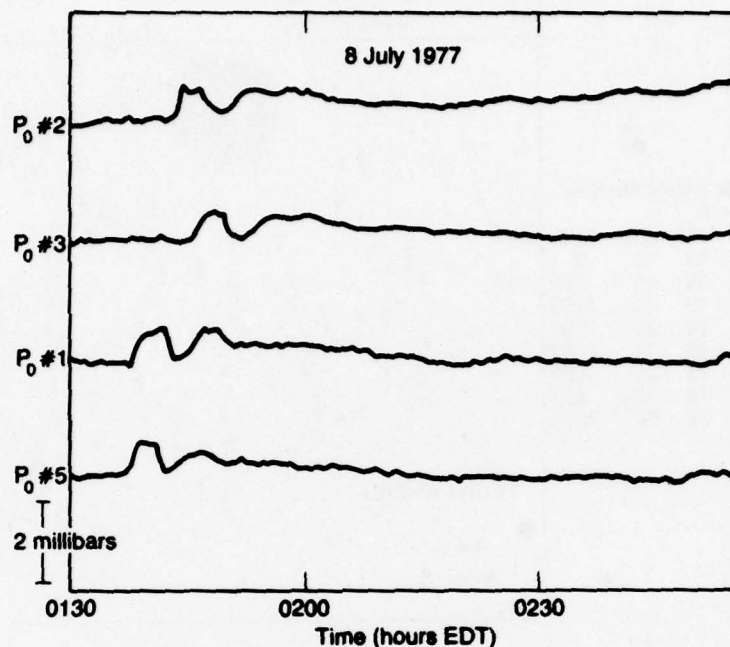


Figure 3.14. Absolute pressure data for a gravity-wave event.

Kjelaas et al., 1975) applied to this case, which relates the phase speed, c , to the ratio of the pressure and velocity perturbations (dp and du , respectively) through the formula

$$c = \frac{dp}{\rho_0 du},$$

where ρ_0 is the background atmospheric density. The measured and computed values of the induced velocity perturbations are 9.3 m s^{-1} and 8.4 m s^{-1} respectively. It should be noted that while this event was not associated with a gust front per se, it did produce updrafts and downdrafts of the order of $\pm 1 \text{ m s}^{-1}$ near the ground, which could be hazardous to aircraft especially if there were many cycles which excited an aircraft or control resonance (e.g., Chimonas and Bedard, 1979). Further, even the horizontal wind field vector changes themselves (9 m s^{-1} accompanied by wind direction shifts of 180°) could be dangerous. It is therefore doubtful whether such events should be considered false alarms.

3.8 27 September 1977 - A gust-front showing only minor temperature and anemometer disturbances at the surface.

Bedard and Sanders (1978) document this event in some detail and have produced several figures which illustrate how ground-based inversions influence surface measurements. The monostatic sounder clearly shows the structure of a density current with the flow measured by a Doppler sounder (Fig. 3.15). There is an inversion evident prior to the disturbance near 2100 and after the disturbed period (2200). This is a case where a ground-based inversion apparently reduced the effects of the density current at the surface. (Additional examples of weak surface interaction appear in the report by Greene et al., 1977.) The low surface winds permitted the monostatic sounder to detect the event with a good signal-to-noise ratio. Since we can infer the height of the current and know the speed of motion of the discontinuity from the Po array, we can construct the 3-dimensional flow for the system.

Surface measurements compared with the monostatic sounder data (Figure 3.16) illustrate that outflows aloft can occur with little or no surface temperature and wind speed disturbances. The upper level flow surge, in excess of 10 m s^{-1} , produced only a small surface wind increase. No temperature drop (but rather a temperature rise probably caused by mixing the boundary layer) accompanied the leading edge of the disturbance near 2100. The three anemometers operating for this event — A2, A8 and the airport center field anemometer all showed similar traces.

Figure 3.17 illustrates the Po data for four of the site locations. The computed speed of motion is 12.8 m s^{-1} from an azimuth of 339° . The mean rise time and pressure peak are 352 seconds and .64 millibar, respectively. This event was slightly below the detection level for dP sensors and none responded. Slight decreases in threshold level and increases in sensor time constant would be required to reliably detect events with these characteristics. It is important to note that there is evidence that over half of the events detected with dP sensors at O'Hare airport during 1977 show weak interaction with the surface. The problem of surface inversions preventing strong

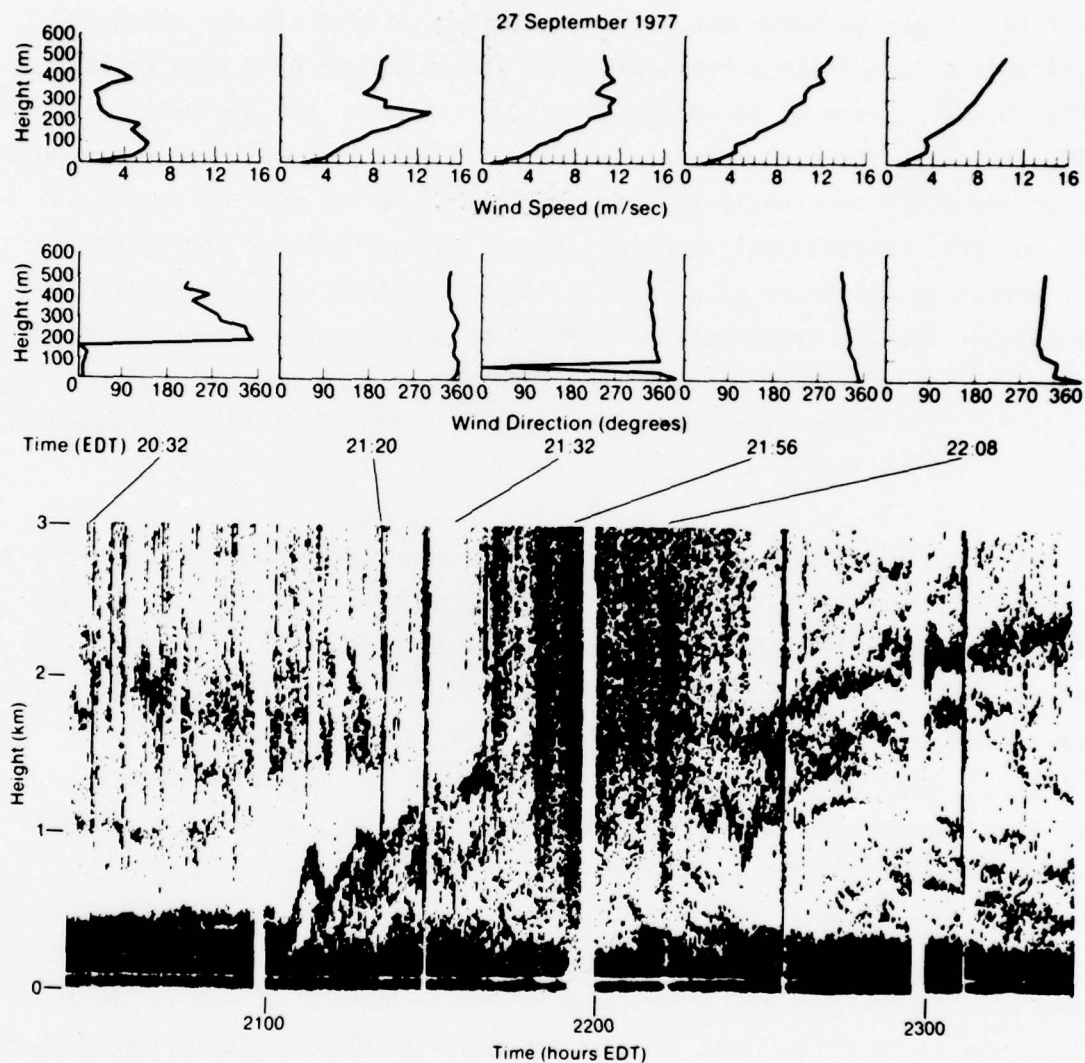


Figure 3.15. Wind profiles associated with thunderstorm gust front of 27 September 1977; the outflow structure vividly shown by a monostatic acoustic sounder. The increase of winds aloft (about 10 m s^{-1}) had little influence at the surface, permitting the monostatic sounder to detect the event.

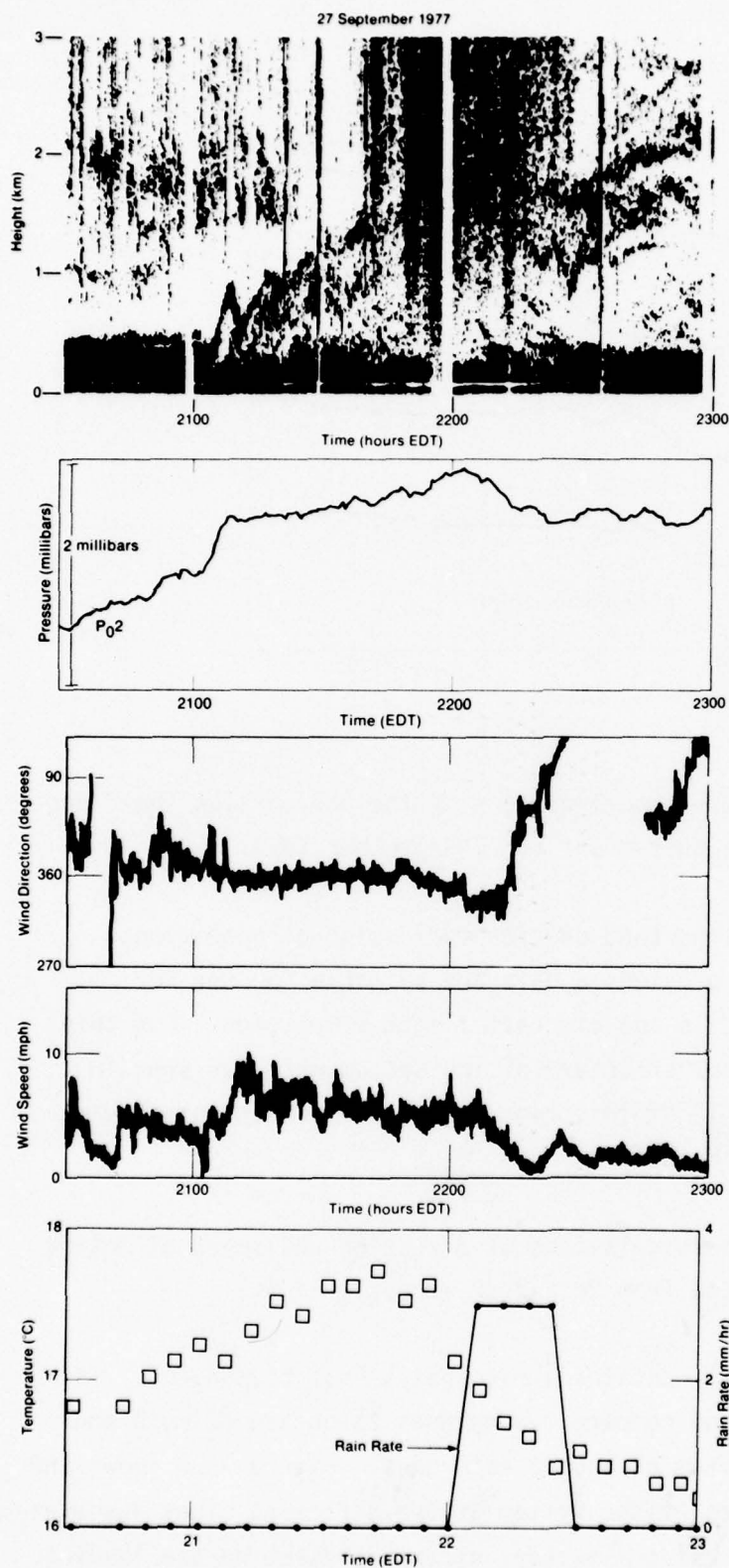


Figure 3.16.

Surface measurements associated with gust-front of 27 September 1977. A significant pressure jump occurs associated with the leading edge of the outflow; while only a minor wind surge ($< 3 \text{ m s}^{-1}$) accompanies the event.

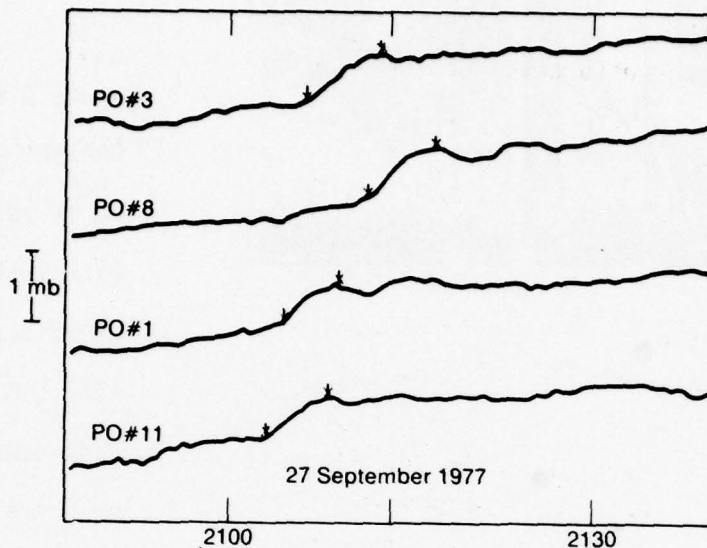


Figure 3.17. Absolute pressure determinations of the propagation speed and azimuth for the gust-front of 27 September 1977.

low-level interaction is an important one for the design of operational warning systems. This event provides a data set suitable for use for comparison with numerical models and aircraft flight simulation. For this case we infer the 3-dimensional structure of the system which we show in Figures 3.18 and 3.19. Part II of this report treats observations showing weak surface effects in more detail.

3.9 18 May 1977 - Comparison calculations of direction and speed of motion of a gust-front using data from Po and dP arrays.

A report by Fujita (1978) contains a mesoanalysis of this event. This example is used to describe and compare two methods to obtain azimuth and speed of motion information from dP and Po data sets. Figure 3.20 shows the estimates of the leading edges of the system at the different times designated A, B, C, or D. For dP data, using a marker, sites representing the leading

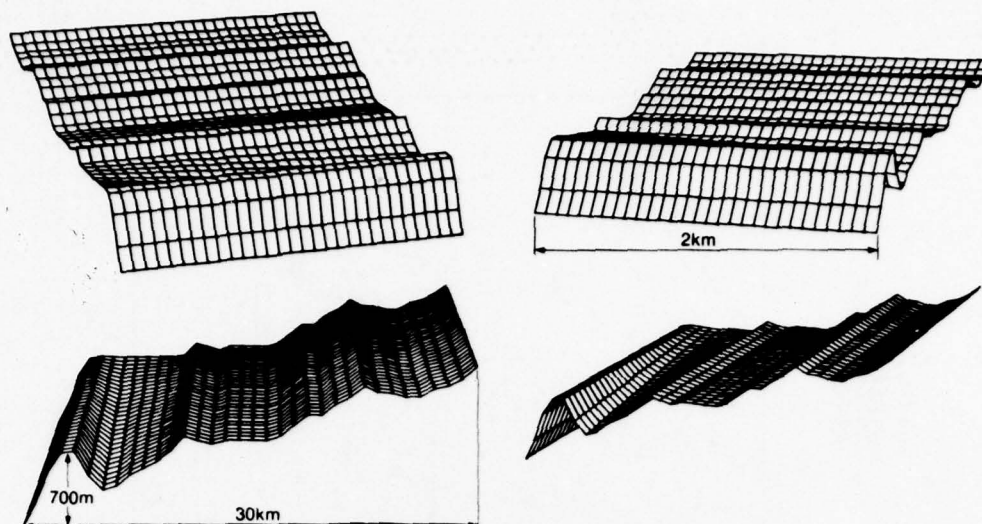


Figure 3.18. Inferred 3-dimensional structure of the density current from four viewpoints.

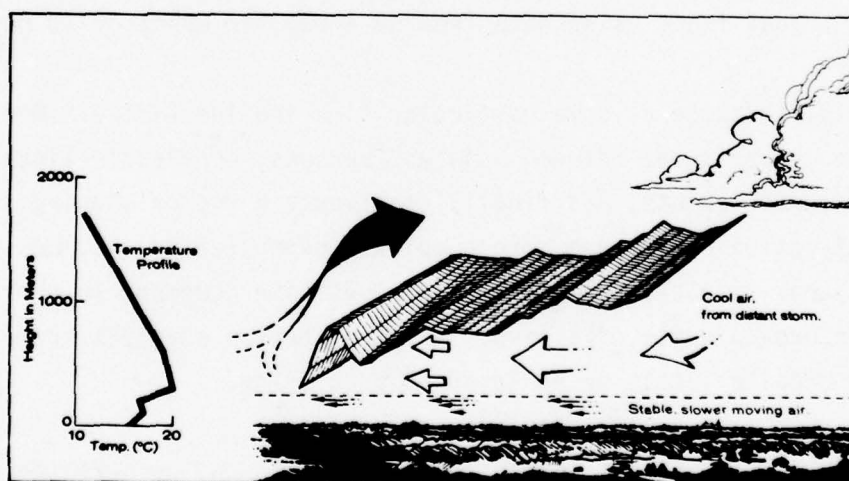


Figure 3.19. Summary figure illustrating a complex density current flowing from a source region on a stable layer. This figure combines an artist's conception with actual data from the 27 Sept. 1977 case study.

Times (EDT)
 A - 1827 14"
 B - 1829 14"
 C - 1834 58"
 D - 1837 16"

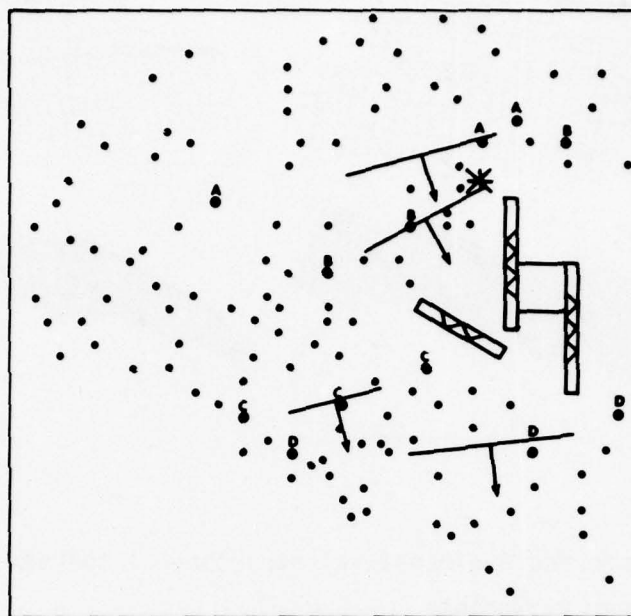


Figure 3.20. Basis for calculations of direction and speed of motion of a gust front using data from dP array for event of 18 May 1977.

edge of the disturbance at some particular time are identified. One algorithm computes the center point between adjacent sensors, constructs lines, connects the various center points, and finally constructs a vector showing the direction of motion. Although more complex (and objective) methods could be applied, this simple method, which involves some judgment in choice of sensors, has proven quite effective. A later section suggests array configurations which require little or no advanced processing.

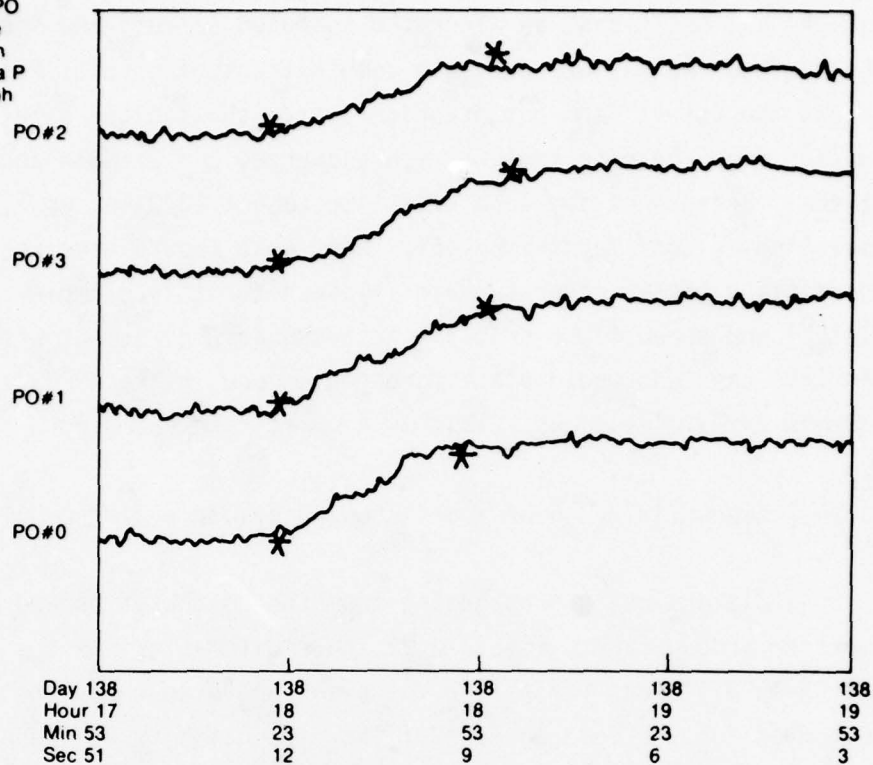
Since the times for the line estimates were known, as were the distances between them, speeds of motion for the various possible combinations were computed. A speed of motion of 13 m s^{-1} from an average direction of 344° was obtained.

Figure 3.21 indicates the absolute pressure data for four of the Po sites. A marker was used to identify the start of the pressure rise and the same portion of the peak for each sensor (each point is marked with an asterisk). Using the time differences between the arrival of some feature

For Specified PO
Please Indicate
Minimum, Then
Maximum Delta P
Points on Graph

PO# 0
PO# 1
PO# 3
PO# 2

7.14 mb



NW - PO# 0 Time 0 Sec
NE - PO# 1 Time 195 Sec
SE - PO# 3 Time 437 Sec
SW - PO# 2 Time 305 Sec

Scan # 1: az 320.154 Vel 10.592
Scan # 2: az 318.750 Vel 11.307
Scan # 3: az 301.622 Vel 10.761
Scan # 4: az 323.430 Vel 13.211

Average : az 315.989 Vel 11.381

Rise Time - Min to Max:

PO# 0 1093 Seconds
PO# 1 1266 Seconds
PO# 3 1334 Seconds
PO# 2 1411 Seconds

Change in Pressure:

PO# 0 0.84 Millibar
PO# 1 0.92 Millibar
PO# 3 1.11 Millibar
PO# 2 0.97 Millibar

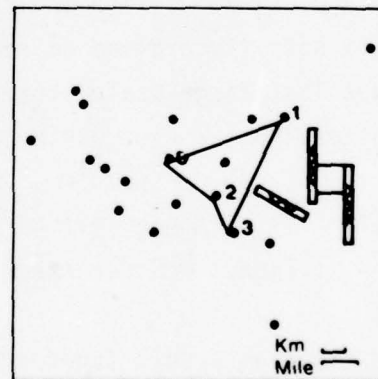


Figure 3.21. Absolute pressure determinations of propagation speed and azimuth for the gust front of 18 May 1977.

at the various sites, an algorithm computed azimuth and speed of motion based upon the various possible combinations of sites. Figure 3.21 also shows the output from our graphics system showing the site locations together with the rise time, pressure change, and azimuth and speed calculations. Because of the long rise time (about 2000 seconds), the time resolution is poor for this event. Most gust fronts have shorter rise times permitting better accuracy than is shown for this example. The azimuth (315°) and speed (10 m s^{-1}) are in reasonable agreement with the dP data. In this case one would place more confidence in the dP data because of the larger array dimensions. This is a worst-case example.

3.10 7 August 1977 - Gust front showing evidence of non-uniform motion.

A discontinuity propagating from the northwest showed evidence of non-uniform propagation. Figure 3.22 shows with asterisks the sensors triggered at three different times into the event and also shows the simulated front computed for the leading edge of the discontinuity at these times. Between lines 1 and 2 the computed propagation speed was 14 m s^{-1} , while between lines 2 and 3 the speed was 6 m s^{-1} (less than half). Thus far, this is the only event identified indicating such changes in motion. The O'Hare airport data sets (Bedard and Cairns, 1977) and other Dulles system events indicate that most large-scale, coherent density currents propagate at approximately uniform speeds over distances in excess of 10 km.

3.11 17 November 1977 - Comparison illustrating a limitation of conventional weather radar for tracking discontinuities.

During a cold front approach on 17 November 1977, both the surface anemometers (Figure 3.23) and the Doppler sounder (Figure 3.24) measured vector changes in the horizontal wind in excess of 10 ms^{-1} . This wind shift occurred with a temperature drop of 8°C and a pressure jump of 1.4 mb having

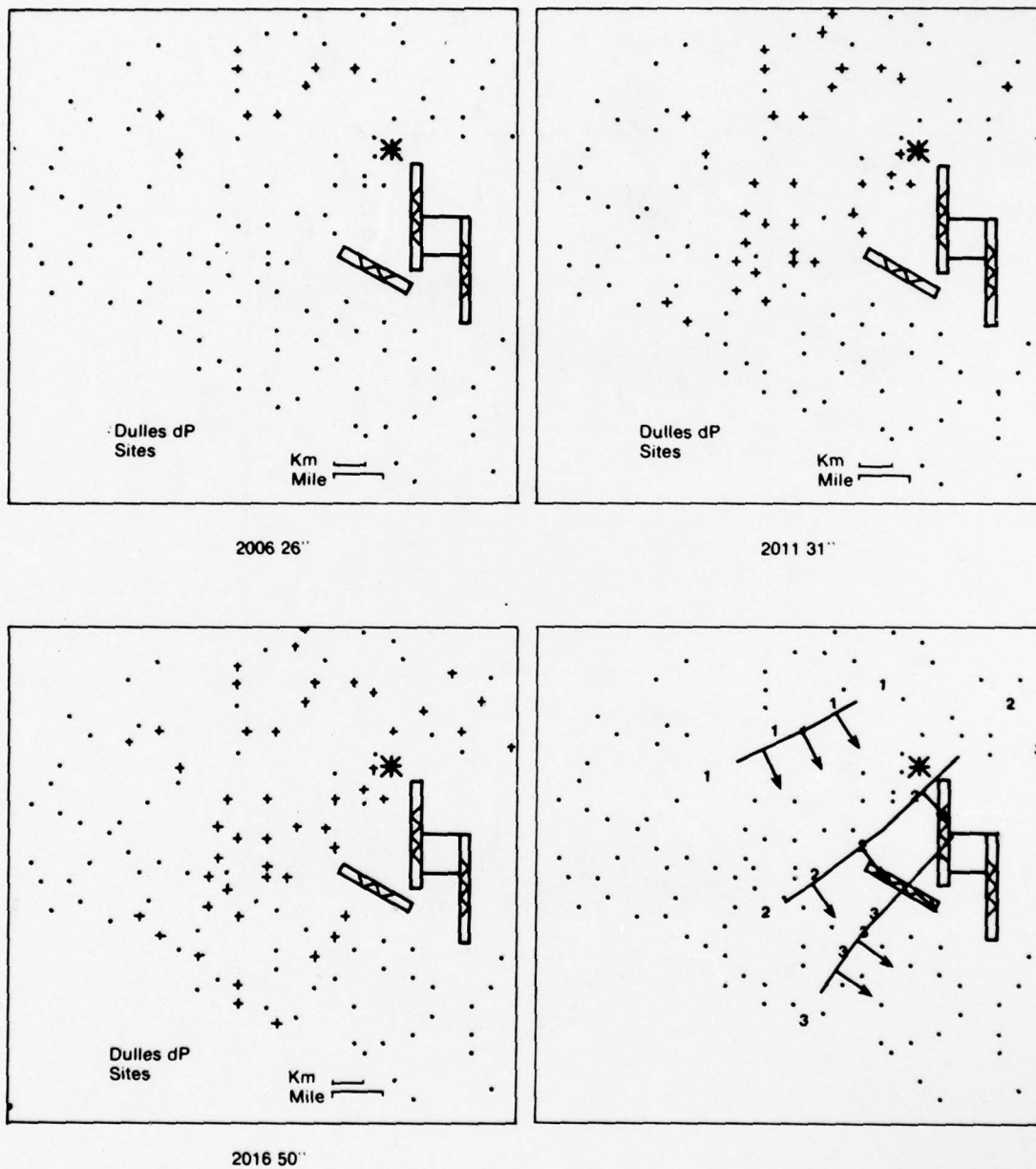


Figure 3.22. Gust front showing evidence of non-uniform motion on 7 August 1977.

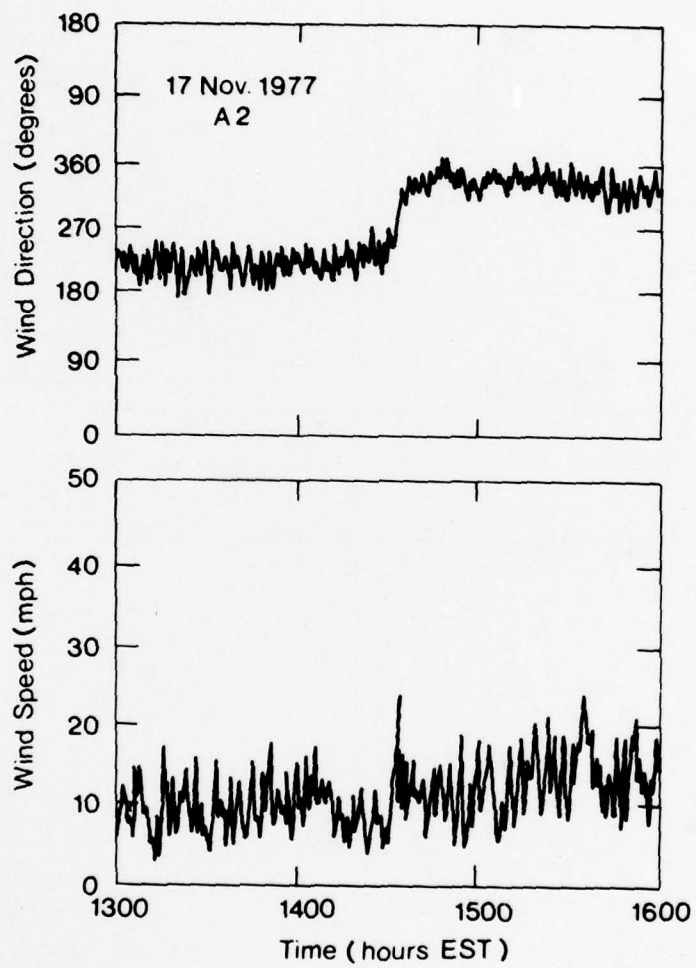
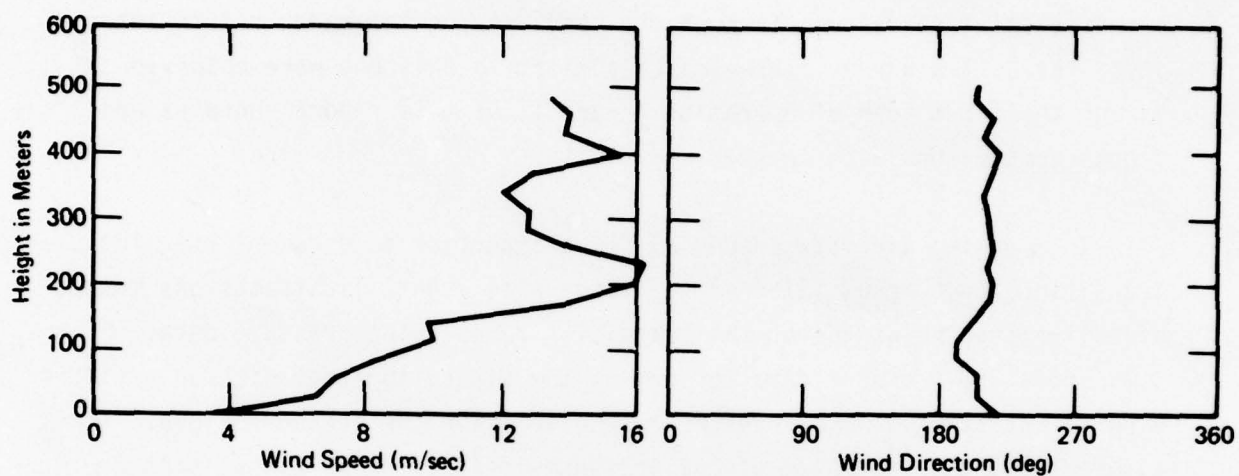
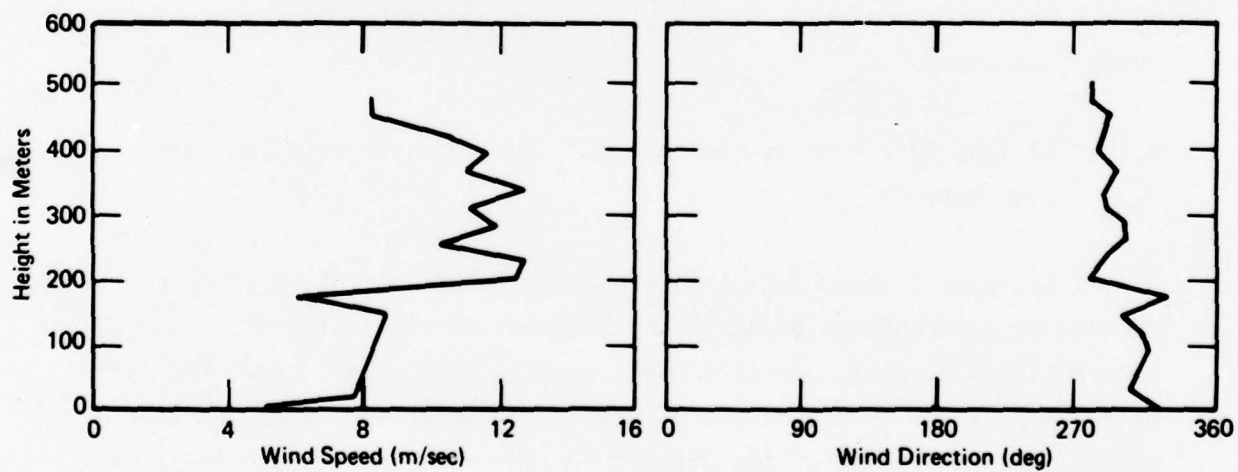


Figure 3.23. Anemometer data on 17 November 1977.



17 November 1977 1419 EST



17 November 1977 1455 EST

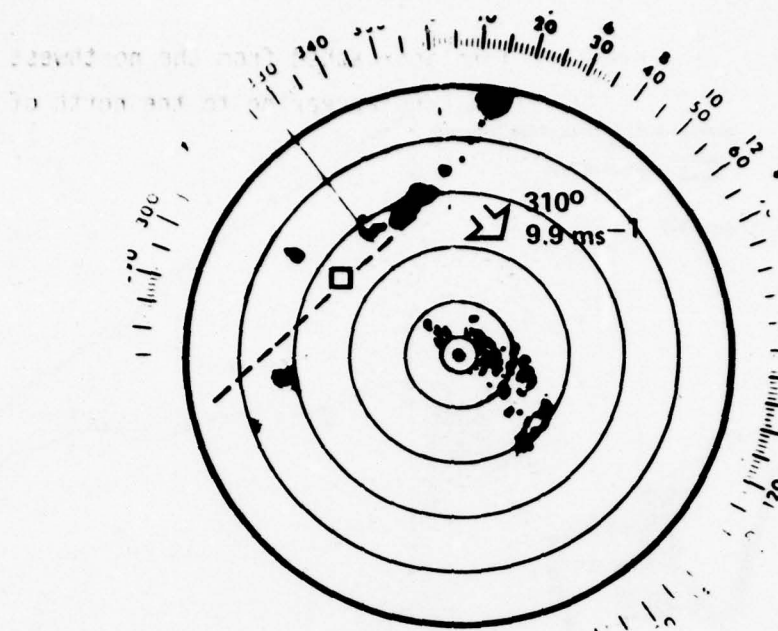
Figure 3.24. Doppler sounder profiles on 17 November 1977.

a rise time of 320 s. The pressure jump approached from the northwest with a speed of 15 m s^{-1} . A radar line echo appearing to the north of the Dulles array also propagated from the northwest at about 10 m s^{-1} . Figure 3.25 (the Dulles array location relative to the radar return at the time of arrival of the discontinuity) shows the disturbance at Dulles occurred in a clear-air region of the radar return, at a time when the extension of line passing through the long axis of the radar return intersects the Dulles array. Three cases similar to this one were observed during the first year of operation. Part II of this report contains additional comparisons with weather-radar data.

In modeling aircraft response, it is important to document the widths of transition zones across discontinuities. This event illustrates one method of estimating the widths of the transition zones using pressure data. Figure 3.26 shows the pressure data for one of the sites, together with an artist's view illustrating some mechanisms responsible for the pressure field. It is assumed that the rise-time of the pressure field is proportional to the width of the transition zone. Knowing the propagation speed of the pressure jump, the width of the transition can be computed, which for this case was estimated as 4.8 km. Caracena and Kuhn (1978) provide some data concerning widths of transition zones.

3.12 17 June 1977 - An aircraft flight path shown in relation to approach zone meteorology.

A National Transportation Safety Board (NTSB) report of 22 July 1977 documented a turbulence encounter by Piedmont Airlines Flight 33 into Dulles International Airport. An attachment to this NTSB report shows the flight path and altitude as a function of time. The superimposed key portion of this path on a view of the airport — indicates where the flight lost 400 feet of altitude in 12 seconds (Figure 3.27). The indicated time is approximate (accurate to within two minutes). However, abstracts concerning the flight from the NTSB report appear below and these make more accurate note of the time-history of events.



17 NOV. 1977
1925 EST

Figure 3.25. Weather radar data with a 10 km-square identifying the site of the Dulles International Airport array.

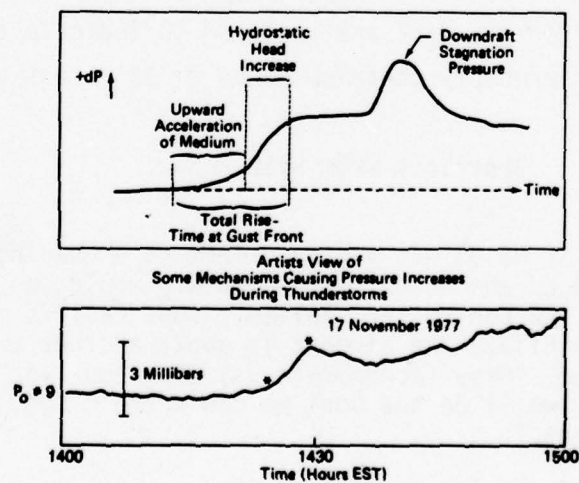


Figure 3.26. The pressure disturbance of 17 November 1977 together with an artist's view illustrating some mechanisms responsible for the pressure field.

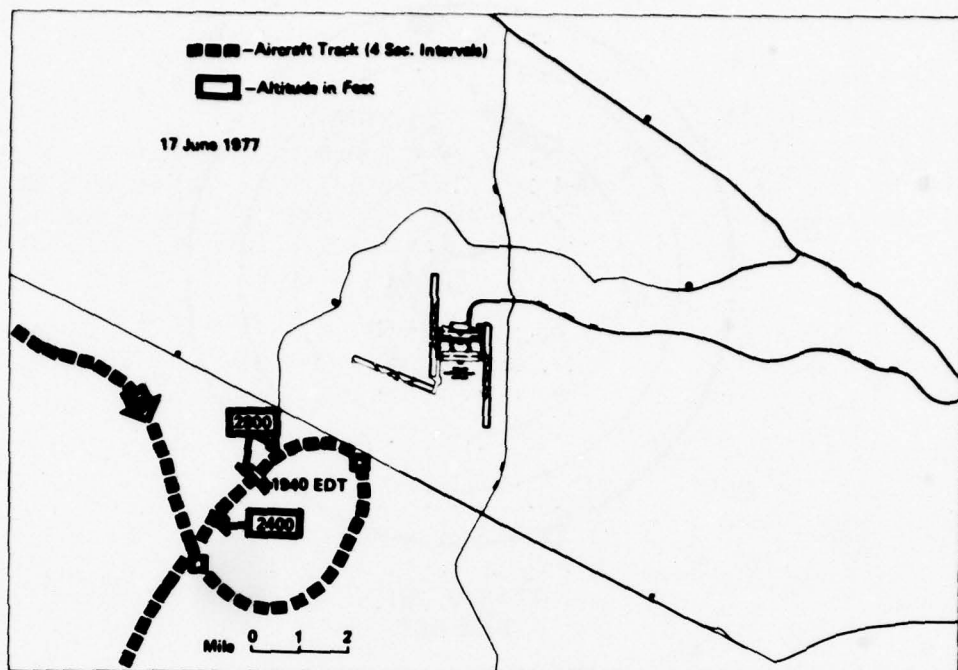


Figure 3.27. Flight path of PI33 relative to Dulles International Airport.

The purposes of this case study are to show the value of re-constructed flight paths for after-the-fact analyses and to indicate the portions of a thunderstorm that probably contributed to PI 33's loss of altitude.

Abstracts from NTSB report

At 1935:45, PI 33 was vectored left to a heading of 120° . The crew acknowledged and asked "... which way would you say it (weather) was moving?" The controller replied, "that cell is moving due south it's gonna annihilate the airport in about another twenty minutes." PI 33 responded, "Okay (accomodate us) when you can." The controller then advised, "we'll do the best we can there's two guys ahead of you on one right."

At 1936:19, PI 33 was advised, "... now plan a visual approach to runway one left, I think I can get you in quicker that way." The crew replied, "roger." PI 33 was vectored right to a heading of 170° . About 1 minute later the flight was given a left turn to a heading of 090° for

a left base leg to runway 1 left. The crew acknowledged "zero nine zero," and the controller responded promptly with the following advisory:

"and we are now in the midst of a thunderstorm, I can hear it over head."

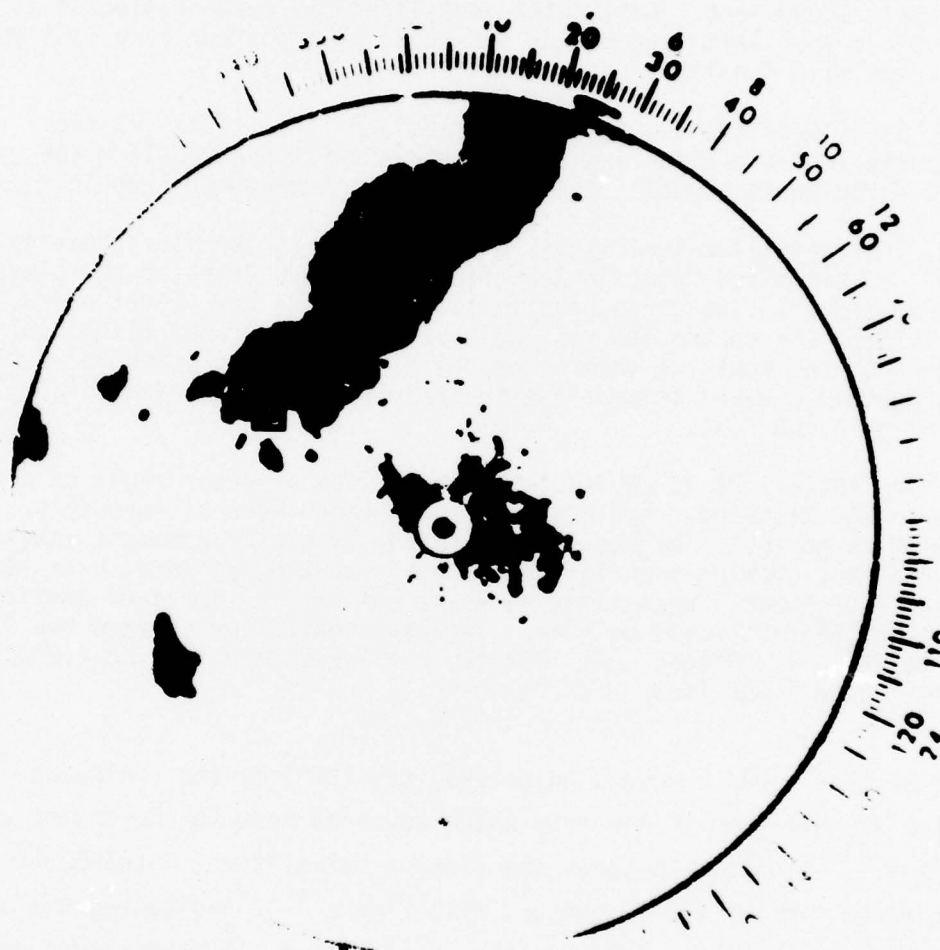
At 1938:15, PI 33 stated, "Okay we'll take a look at it." A lower altitude was requested and PI 33 was cleared to descend and maintain 1,600 feet. At 1938:44 the flight was further cleared to, "continue your left turn now on a heading of zero four zero, put you on a two mile final."

At 1939:30 the AR-2 controller advised PI 33 that "... the airports twelve o'clock and about -uh - about two and half miles, you have anything in sight?" The crew replied, "uh-we can't do it."

The controller immediately cleared PI 33 to turn left heading 300°, to climb and maintain 2000 feet. The crew repeated the clearance and stated, "... we gonna have to turn back outa here right quick." At 1939:50 the controller replied that he would get the flight on around to the south as soon as he could. About 20 seconds later PI 33 was further cleared to continue the left turn to a heading of 235° and climb to 4,000 feet.

At 1941:12 PI 33 advised, "... we'd like a vector right on down to -uh-to-uh- Richmond, that's pretty rough back there if anybody's trying to go in." The controller stated, "yes sir, nobody's making approaches. Now-uh-turn left heading of -uh-two one zero, be a vector to -uh- Richmond. What altitude would you like?" The crew advised that 10,000 feet would be fine. The AR-2 controller cleared the flight to maintain 7,000 feet. At 1942:12, PI 33 reported leaving 4,000 feet climbing to 7,000 feet.

The weather radar showed a bulge (Fujita, 1978) moving southward toward the airport from a line echo which advanced from the northwest at about 9 m s^{-1} . Figure 3.28 shows the radar echo relative to the Dulles array near the time of the encounter, with Figure 3.29 indicating the abrupt shift of surface winds accompanying the thunderstorm. A temperature drop of over 4°C occurred 10 minutes before the rainrate maximum of 20 mm per hr (Figure 3.30). The total temperature drop exceeded 8°C before lightning caused loss of data. Although array data was lost because of local power failures, recording barographs indicated a pressure jump in excess of 1.3 millibars. Comparing the vertical wind profiles before and after the passage of the gust front (Figure 3.31), a maximum in the thunderstorm outflow occurred below 300 meters.



**17 JUNE 1977
1940 EDT**

Figure 3.28. Weather radar data near the time of the encounter with a 10-km square identifying the site of the Dulles International Airport array.

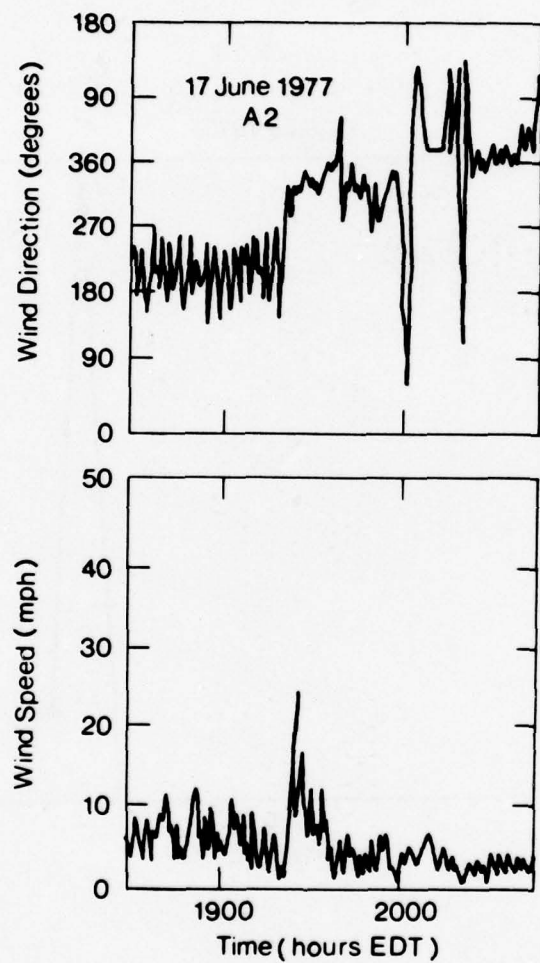


Figure 3.29. Anemometer data on 17 June 1977.

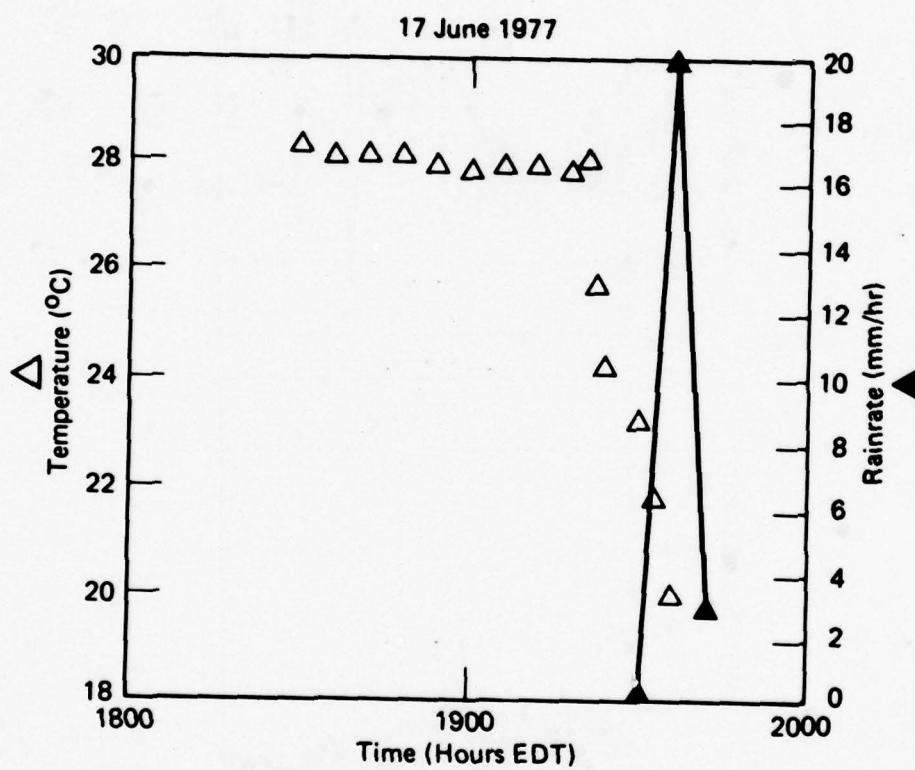
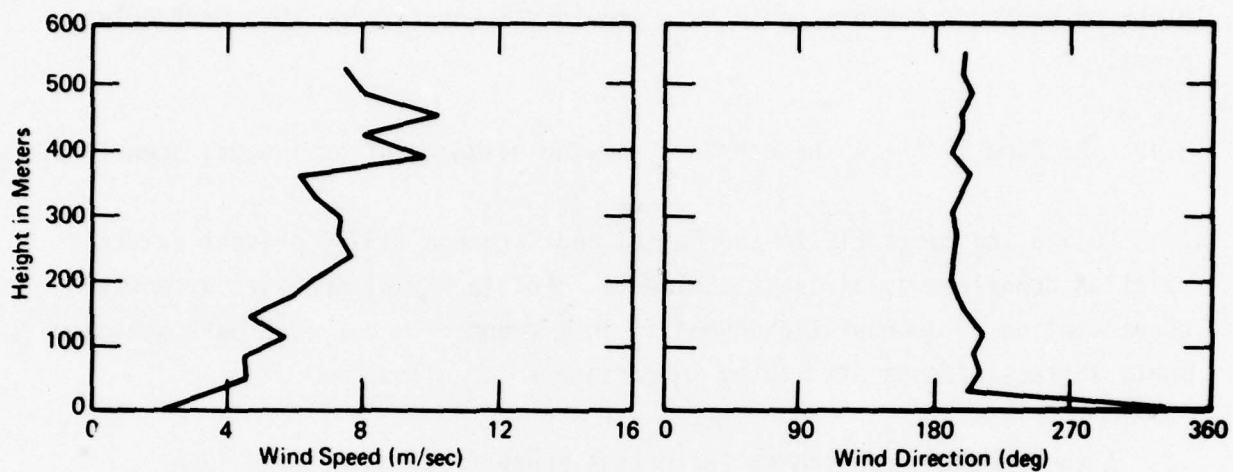
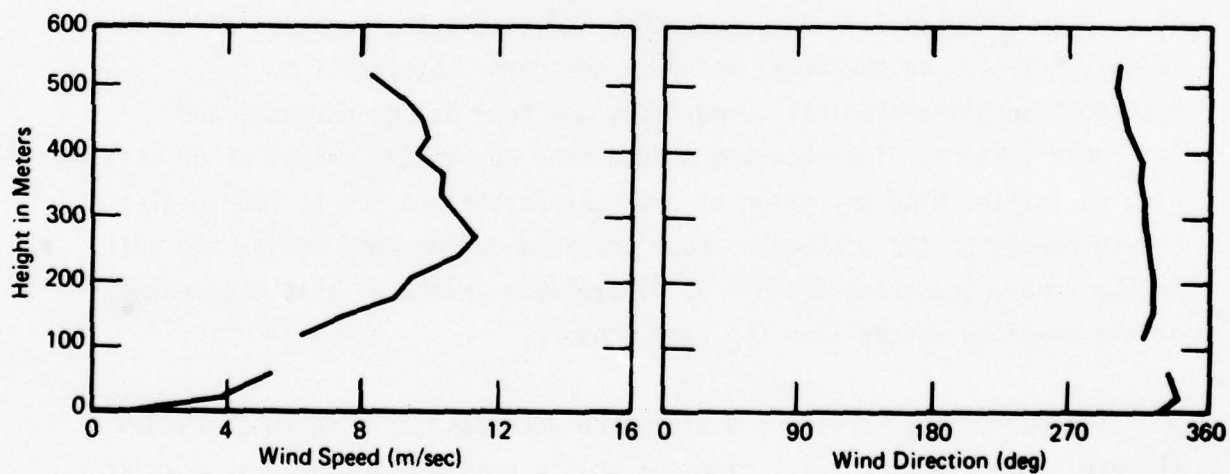


Figure 3.30. Temperature and rainrate data on 17 June 1977.



17 June 1977 1924 EST



17 June 1977 1942 EST

Figure 3.31. Doppler sounder profiles on 17 June 1977.

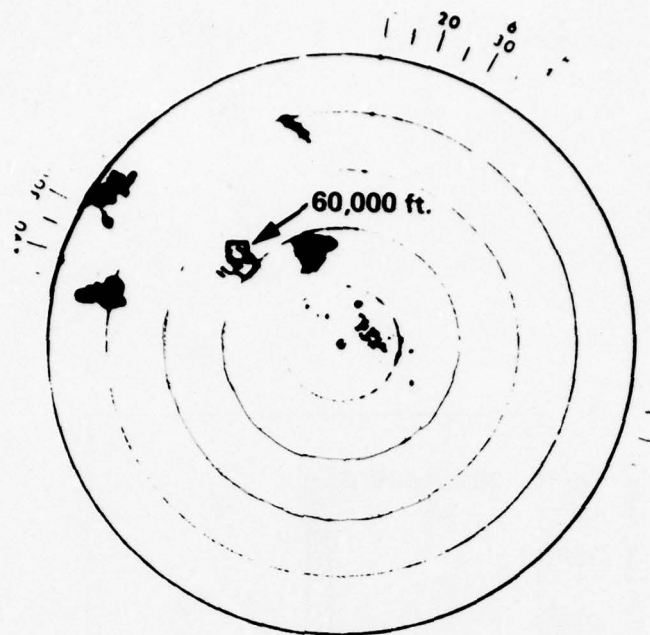
One might have expected to encounter inflow to the thunderstorm by turning the aircraft south at higher altitudes, thus increasing performance. Instead, the aircraft lost 400 feet in 12 seconds (a downward movement of 10 m s^{-1}). The rainrate maximum, the fact that the aircraft was higher (727 m) than the outflow maximum (300 m), and the position of the radar echo (extending to the south of the airport) provide evidence that PI 33 encountered a downdraft. Arrays of surface anemometers, thermometers or pressure sensors could have provided a warning for this particular event.

3.13 26 June 1978 - A thunderstorm showing evidence of an intense down-flow.

Fujita and Byers (1977) and Fujita and Caracena (1977) present evidence relating downflows to aircraft accidents. Fujita (1978) provides extensive documentation on downburst phenomena. This event from our 1978 data set documents surface effects attributed to an intense downflow.

A thunderstorm approached the Dulles array from NNW 26 June 1978, passing over the airport with cloud tops of 60,000 feet (Figure 3.32). The storm appeared on the weather radar as an isolated echo approximately 10 km wide. Figure 3.33 is a composite indicating the location of various sensors relative to the total rainfall contours (obtained from the Metropolitan Climatological Summaries), the tree damage pattern, and hail observations. The observed sudden wind surges (in excess of 60 kts) with an initial wind direction of 360° varied through 90° to 180° . Although damage to the anemometer cups occurred during this event, the null in the wind speed trace (Figure 3.34) probably indicates that the center of the downflow passed near the wind sensor.

The exceptional pressure disturbance accompanying this thunderstorm (Figure 3.35) shows a small rise (.7 mb) in pressure followed by a small drop (.7 mb) preceeding a pressure nose in excess of 5 mb with a duration of less than 15 minutes. If the pressure nose is interpreted as the stagnation pressure resulting from dynamic effects alone, then vertical downflow



26 JUNE 1978
2010 EDT

Figure 3.32. Weather radar data showing the thunderstorm cell relative to the 10-km square identifying the site of the Dulles International Airport array.

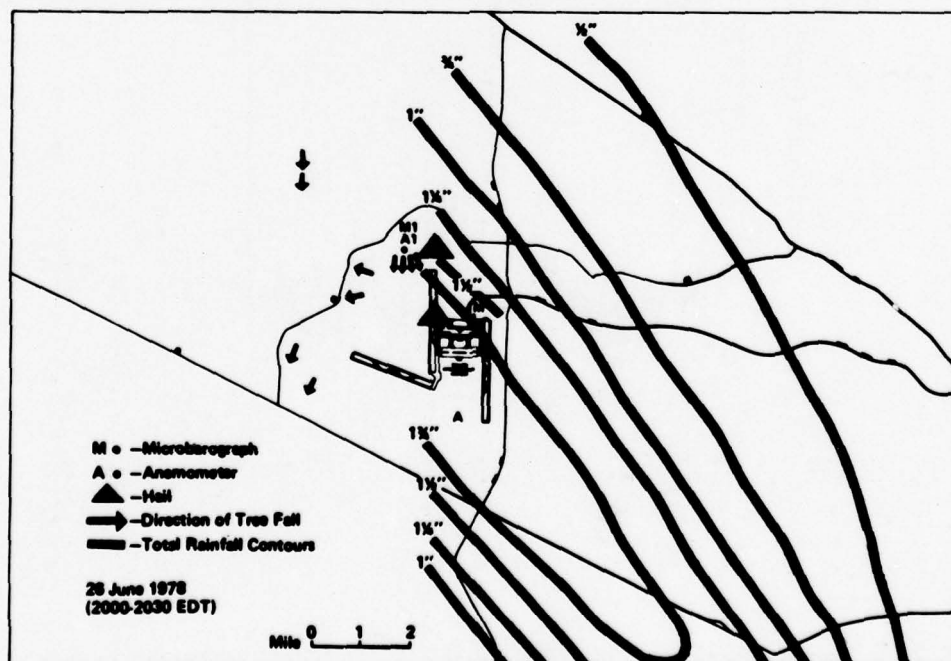


Figure 3.33. Composite indicating the location of various sensors relative to the total rainfall contours, tree damage, and hail observations.

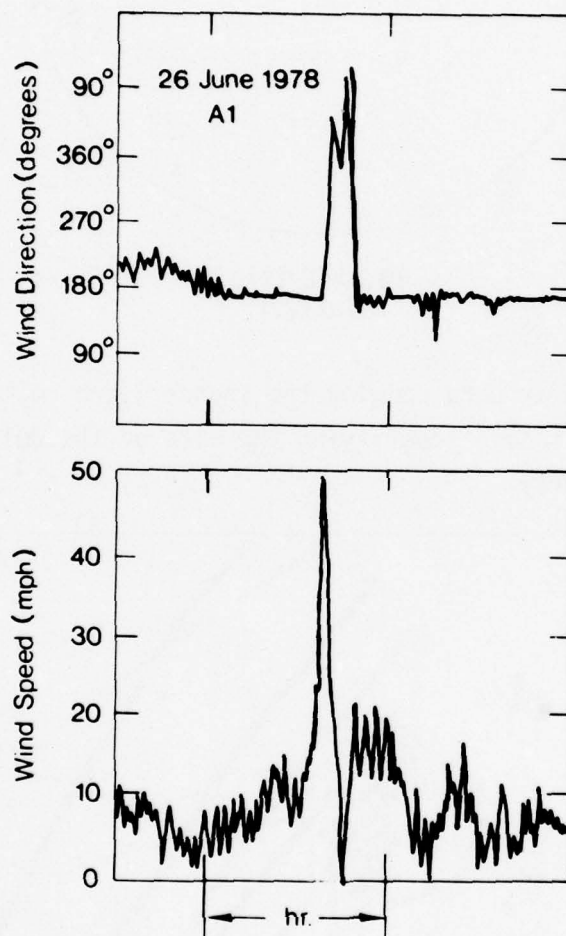


Figure 3.34. Anemometer data on 26 June 1978.

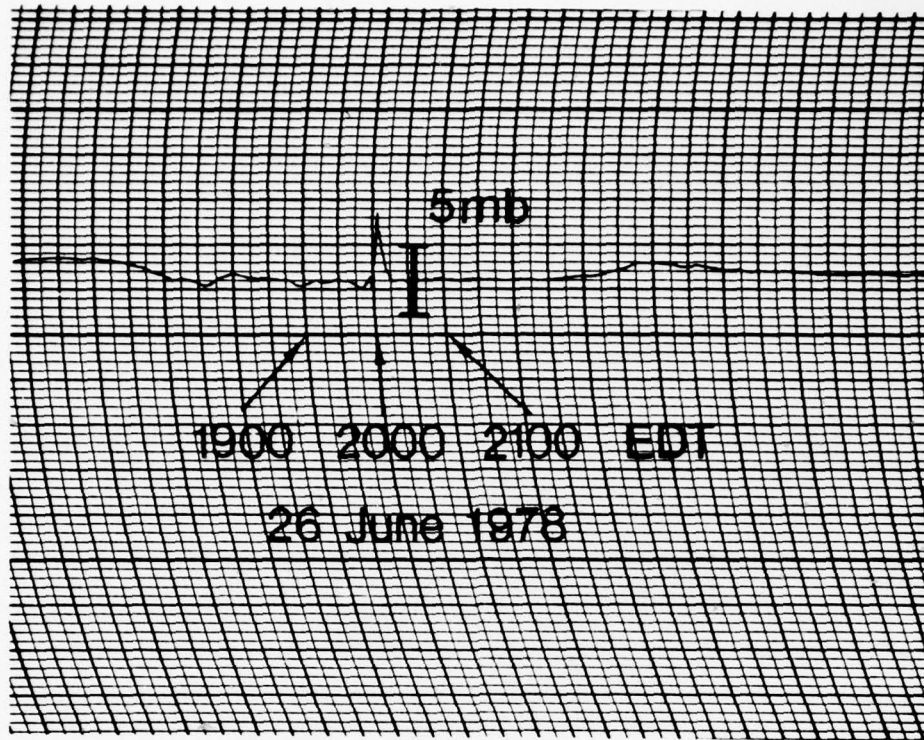


Figure 3.35 Pressure data on 26 June 1978.

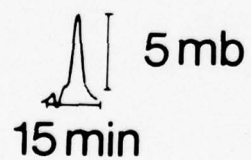


Figure 3.36 Numerical simulation of pressure field beneath a thunderstorm downflow (after Teske and Lewellan, 1978).

speeds in excess of 30 m s^{-1} can be predicted. The pressure trace is quite similar to the numerical results of Teske and Lewellen (1978). Figure 3.36 is derived from Figure 6 of their paper, where they assume downflow speeds of 23 m s^{-1} .

The literature contains a number of observations of large pressure noses indicating that this observation is not unique — e.g., Faust (1947), Caracena (1978).

This case study as well as those in Sections 3.6 and 3.12 indicate the significance of thunderstorm downflows to aircraft operations. Later sections of this report discuss differences in detection philosophy for thunderstorm downflows and outflows.

4. SENSOR OPERATION

This section reviews causes of dP sensor response (both natural and manmade) and outlines considerations important to the use of dP sensors in dense arrays. Practical details involved with the operation of such a dense array of sensors are great. Keeping track of the siting, phone line routing, documentation of sensor locations and characteristics, and maintenance of the instrumentation combine into an impressive logistics problem.

4.1 Causes of dP Sensor Response.

Various causes of dP sensor response listed and defined below vary in their practical importance. A discussion of each appears in sections that follow. Part II of this report provides additional information concerning the first five mechanisms.

4.1.1 Thunderstorm Gust Fronts and Down-flows.

Thunderstorm Gust Front - The leading edge of the cold air spreading outward near the earth's surface from a thunderstorm.

Thunderstorm Down-flow - The descending column of cool air within a thunderstorm (usually accompanied by a rain shaft) which feeds the near-surface divergence causing the gust-front.

4.1.2 Cold Fronts.

Cold Front - The leading edge of a mesoscale or larger mass of air, cooler than its surrounding airmass, and moving so that the colder air replaces the warmer air.

4.1.3 Gravity Waves.

Gravity Waves - Waves propagating on ground-based inversions (similar to waves propagating on the surface of the ocean). These are called gravity waves because the earth's gravitational field provides the restoring force allowing them to propagate.

4.1.4 Gravity-Shear Waves.

Gravity-Shear Waves - Waves depending upon both gravity and shear in the medium for their existence and propagation characteristics. Cases of aircraft turbulence have been attributed to gravity-shear waves propagating at jet stream altitudes.

4.1.5 Local Winds.

Local Winds - By local winds we mean air flowing in the immediate vicinity of a sensor. Since for our purposes we wish to measure the static pressure field, deviations caused by local Bernoulli pressures are a source of error.

4.1.6 Aircraft Weight Transfer.

Aircraft Weight Transfer - By aircraft weight transfer we mean the weight of an aircraft distributed on the earth's surface as a pattern of increased pressure. This total weight transfer will occur independent of the altitude of the aircraft, although wider distribution occurs at higher altitudes.

4.1.7 Aircraft Wake Vortices.

Aircraft Wake Vortices - Two counter-rotating vortices that leave the wing-tips of an aircraft when lift is being generated.

4.1.8 Aircraft Jet Blast Effects.

Aircraft Jet Blast Effects - Sensor response resulting either from the high temperature or large air velocity changes caused by flows behind a jet engine.

4.1.9 Vehicle Wakes.

Vehicle Wakes - A large vehicle moving at high speeds can generate strong flows in its lee — similar to the vortices behind an aircraft.

4.1.10 Thunder and Sonic Booms.

Thunder and Sonic Booms - Acoustical transients, usually in the form of an "N" wave, causing sudden increases in pressure capable of triggering dP detectors. While the thunderclap results from the sudden compression of air in a lightning channel, the sonic boom occurs from an object in supersonic flight.

4.1.1 Thunderstorm gust-fronts and down-flows.

For the vicinity of O'Hare airport, pressure changes directly related to thunderstorms accounted for more short-period pressure disturbances than any other mechanism (Bedard and Cairns, 1977). The O'Hare statistical study that covers the years 1968-1972 shows that, during the months from May through September, thunderstorms accounted for 60% of the pressure disturbances. However, there are multiple mechanisms contributing to the thunderstorm-pressure-field. Figure 3.22 illustrates two of these mechanisms. The pressure rise after 2100 occurs with the leading edge of the density current and can result from both acceleration of air at the leading edge and the increased weight of the cooler air above the sensor. The pressure rise at 2200 is interpreted as a source region of descending cooler air and rain in an advecting cell. Quite large pressure increases can occur due to the stagnation pressures beneath downflows, as well as to the increased weight of the column of air in these regions (Section 3.13). There is a need to understand the relative contributions of these mechanisms to the resultant pressure field.

4.1.2 Cold Fronts

Frequently prefrontal squall-lines precede cold fronts and are shear-producing systems accompanied by pressure jumps (Bedard and Cairns, 1977; Greene et al., 1977). The frontal interface of cold fronts tends to be quite broad (many kilometers), in comparison with gust-front interfaces (often less than 2 km). Caracena and Kuhn (1978) provide statistics on the widths of these transition regions. Also, the speed of motion tends to be slower. As a result, the pressure rise can be much more gradual (10's of minutes) compared with the more rapid rise related to gust-front passages. The Dulles system provides data comparing the vertical wind profiles to the surface pressure changes related to cold fronts. False alarms due to the detection of longer term pressure rises related to cold fronts does not seem to present a problem.

4.1.3 Gravity Waves

The one gravity-wave event detected by the Dulles dP array (Section 3.7) seems quite unusual. There were a number of cases detected by the absolute pressure sensors with equivalent amplitudes. However, the periods were long enough (e.g., 20 minutes) so that the dP detector high-pass filter suppressed the response. The combination of large amplitude and short wave periods made the event of 8 July 1977 unique. Also, there is evidence that the flows induced near the surface constituted an aircraft hazard.

Figure 3.2 shows an example of a pressure jump on 20 July 77 showing oscillations at the peak (after about 0400). These oscillations are probably gravity waves propagating on the upper surface of the gust-front density discontinuity. Such oscillations could cause some anomalous triggering, but because of their relatively small amplitudes would not interfere with the detection of the event or with its analysis. It is concluded that gravity waves are not a significant source of false alarms.

4.1.4 Gravity-Shear Waves

Gravity-shear waves related to upper level jet-streams are another cause of significant pressure disturbances capable of triggering dP detectors (Bedard and Cairns, 1977; Greene et al., 1977). The Dulles dP array detected several gravity-shear wave events. The propagation speeds tend to be quite large ($30\text{--}50\text{ m s}^{-1}$) and surface wind speed changes are correspondingly low. The lack of large wind speed disturbances and the fact that they usually occur in the absence of adverse weather offer means of identifying triggers caused by gravity-shear waves. Nevertheless at certain times of the year (usually the winter months) at jet stream latitudes, gravity-shear waves could be a troublesome source of false alarms.

4.1.5 Local Winds

Changes in local winds can produce large pressure changes. For example, a speed change from 20 m s^{-1} to 10 m s^{-1} involves a pressure increase of

almost 2 millibars. Based upon wind tunnel testing estimates, the use of a cylindrical porous sensor inlet (Section 8.4) reduces the dynamic "local" pressures by about a factor of 5. This suggests that the dP sensors are relatively insensitive to wind changes. However, it is another matter to insure that the dP sensors do not respond to wind changes in a real, turbulent atmosphere. Field experience suggests that although dP sensors can respond to unusually gusty and severe local winds, the incidences are quite infrequent. On 22 March 1977, the Dulles array indicated sporadic dP triggers during a period of gusty winds (Figure 4.1). Since the duration of these triggers was quite short (usually 1 sec) they could be identified on the basis of duration. It is a simple matter to add logic either at the sensor or at the central recording location which requires a trigger to be longer than some interval to be recorded. Figure 4.1 shows the total number of network triggers with durations of 1, 2, and 4 seconds during half hour intervals centered at the times plotted. The upper graph is the mean wind and the center graph is an estimate of the fluctuating wind field for this interval, using the airport anemometer as a reference. One sensor, notable in terms of the number and duration of triggers, had an exposed location (Section 5.2). We observed few such instances (4) on the Dulles array. The wind gusts for a severe thunderstorm gust-front could cause multiple on-off indications for marginally triggered sensors. In retrospect, the temperature effects identified for dP sensors could have prevented or caused wind induced triggers depending upon the thermal history and local winds.

Probably the worst case is when winds are steady at some high speed and then suddenly decrease. At Boulder, Colorado, during down-slope wind events, sudden changes in mean wind speed occur and the pressures induced can be large. On at least two occasions this mechanism caused dP triggers of tens of seconds durations.

4.1.6 Aircraft Weight Transfer

The aircraft weight appears at the ground as an increase in pressure. Bedard and Cook (1968) measured this pressure increase as a function of

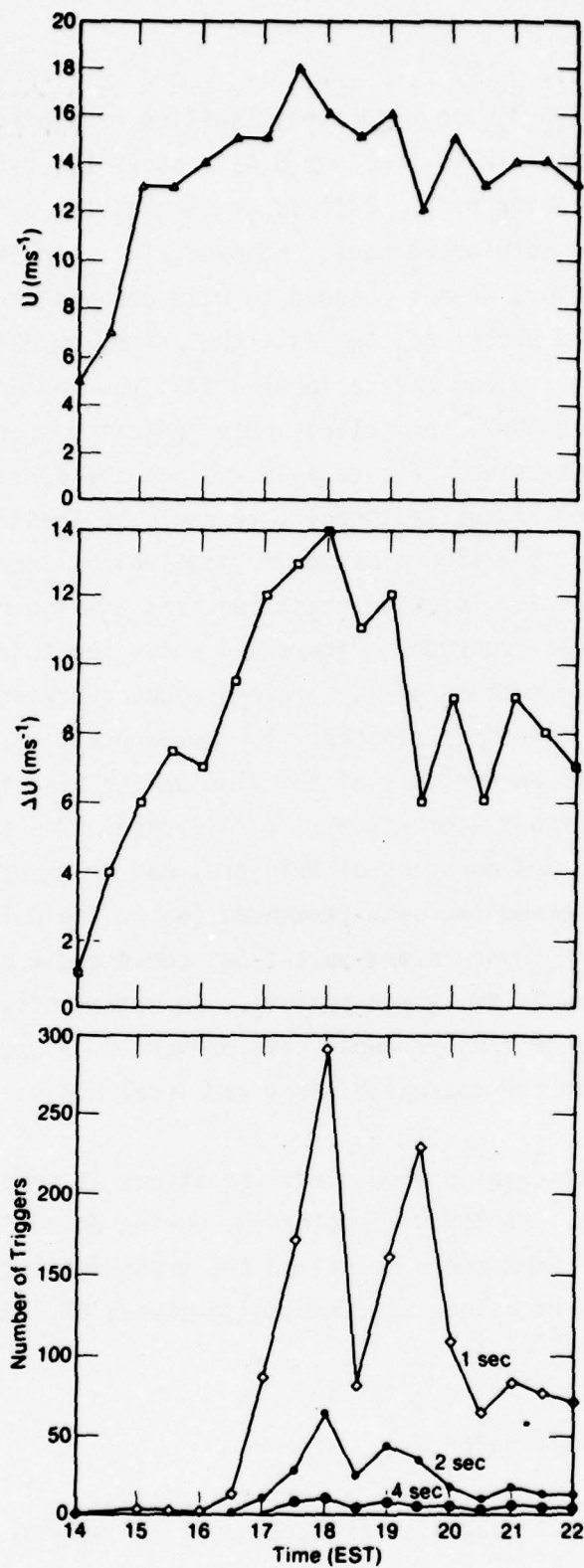


Figure 4.1. Sporadic nature of wind-induced dP triggers on 22 March 1977.

altitude for several different aircraft. For example, a CH21B helicopter at 100 feet produces a pressure increase of about .1 mb. For a C5A at 300 feet the theory of Prandtl and Tietjens (1934) predicts a .5 mb pressure increase. For sensors displaced from beneath the aircraft a distance equal to the aircraft altitude (or at least one wing span distance at altitudes below about 100 feet), these effects should not cause false triggers. Because the pressure varies inversely with the square of the distance from the aircraft, the pressure increase tends to be concentrated directly beneath the aircraft and falls off rapidly with aircraft altitude. Thus it is wise to avoid locating dP sensors under glide paths where the aircraft altitude is below 100 feet. False triggers produced by this mechanism could have durations of several seconds depending upon the weight, speed, and height of the particular aircraft. Only the very heaviest aircraft such as the C5A presents a significant source of possible false alarms. Actually, for large numbers of dP sensors the effect of aircraft weight transfer offers a possible method of performing tests by using a helicopter flying over sites at low levels.

4.1.7 Aircraft Wake Vortices

Limited measurements of wake vortices (Hallock, 1972) and theoretical calculations indicate that significant pressure changes can occur (tenths of millibars). We would not expect wake vortices to cause anomalous dP triggers, but rather to cause sporadic triggering of sensors already marginally triggered by other mechanisms. We recommend experimental measurements of the pressure field for wake vortices, prior to "near runway" installation of dP detectors.

4.1.8 Aircraft Jet Blast Effects.

Sensors deployed in the vicinity of runways could encounter jet blasts, resulting in two possible effects. First, the local flows could produce negative pressures relative to the surrounding, undisturbed air. Initially, this would increase the threshold for +dP changes. If the jet flow remains constant for some time (several minutes), a capillary leak would equalize the pressure across the switch and the dP sensor threshold would return to its

normal setting. If the jet is then removed, the local pressure would increase again to the undisturbed value and +dP triggers of long duration (tens of seconds) could occur.

A second possible effect related to aircraft jets is a threshold change due to a large temperature change. If large temperature changes occur between the medium and the jet temperature near the sensor, these can induce threshold shifts (as indicated in section 8.1). Prior to dP installations in the vicinity of runways (e.g., Figure 10.2), field testing of dP sensors subjected to aircraft jet blasts can determine the magnitude of the problem.

4.1.9 Vehicle Wakes

Sensors positioned near high-speed roads (particularly those used by large trucks) encounter significant pressure perturbations. Pressure sensors near a high-speed road, although connected to a noise reducing space filter (Bedard, 1977), revealed the pressure disturbance. A positive pressure disturbance occurred initially followed by a larger negative pressure disturbance. No data concerning the absolute magnitude of these wakes is available, but measurements indicate that they are of short duration (< 5 sec). It seems prudent to choose locations displaced back as far as possible from high-speed roads. More measurements are required to establish the absolute magnitudes of these "noise" sources.

4.1.10 Thunder and Sonic Booms.

The pressure wave from a close lightning strike will probably be an N-wave and could cause dP triggers. However, the duration will be short (< 1 sec). There are no documented instances of thunder-caused dP triggers.

Sonic booms will also involve N-wave pressure signatures although of longer duration. The criterion of long-duration triggers suggested to suppress wind noise will also eliminate thunder and sonic boom induced triggers.

5. SENSOR SITING

5.1 Extremes of Site Locations.

The site locations for dP detectors at Dulles include installation on the sides of buildings and on telephone poles in locations varying from hilltops to shaded areas covered with poison ivy. Some sensors are near high-speed roads while others are in backyards. Figure 5.1 shows two extremes of site locations.

5.2 Possibility of Local Terrain Effects.

There is no evidence of sensors that would not operate due to local terrain effects. However, it is reasonable to expect that wind induced triggers (Section 4.1.5) increase for more exposed locations. For the example shown in Figure 4.1 the sensor showing the most triggers was situated in a completely exposed location near the knob of a hill (Figure 5.1a). Conversely the two sensors mounted on the sides of buildings showed no triggers during this interval. Although triggers due to local winds can easily be suppressed by defining significant triggers as those occurring for more than 5 seconds, it does seem prudent, when given the opportunity, to locate dP detectors in less exposed locations. Also, times in which wind-induced triggers occur for long periods are invariably during conditions when thunderstorms are not present. Even for exposed locations, techniques are available (e.g., the pressure summator described by Bedard, 1977) to reduce further the local wind problem, but extra methods are not necessary. As mentioned in (Section 4.1.5), the pressures related to local winds behind the gust front probably cause sporadic triggers after the initial detection of the pressure jump itself. The chance

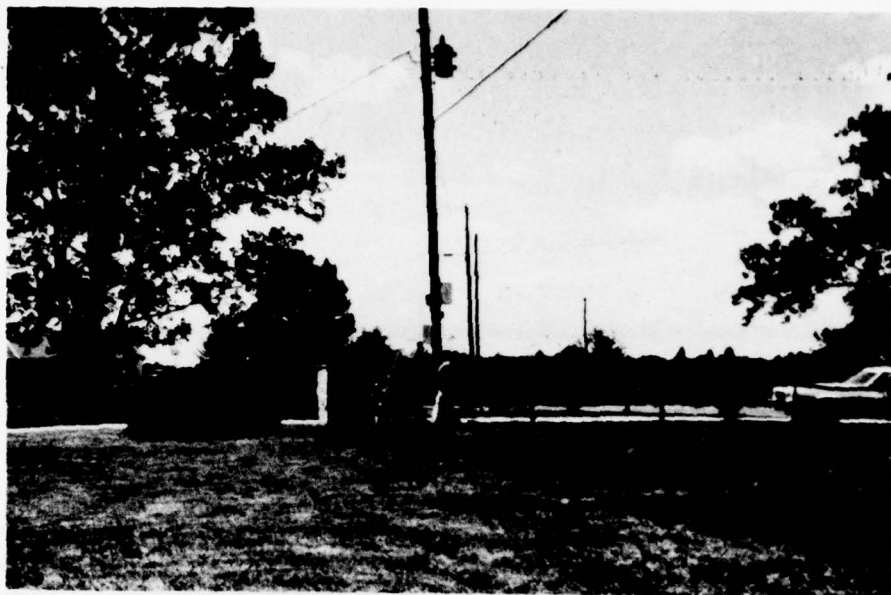


Figure 5.1. Examples of sensor siting.

for this increases because the temperature drop increases the sensitivity of the dP sensor used in the Dulles system.

7 9A3142

5.3 Building Locations.

One advantage of dP sensors is the fact that they can be installed inside most buildings without special precautions (e.g., routing the sensor inlet to the outside atmosphere). Bedard and Meade (1977) point out that building ventilation systems should insure that the time constant for building "low-pass-filter-effects" is much shorter than the rise time of atmospheric pressure jumps (typically 5 minutes). Building installations are not susceptible to wind-gusts. Large capacity air conditioning systems can cause a problem in that they produce a pressure differential between the inside and outside of the building. Some buildings, so equipped, could encounter large (> 1 mb) pressure changes when outside doors are opened or closed. An outside vent for the sensor input is the solution to this problem. Five sensors in the O'Hare system (Bedard and Cairns, 1977) operated satisfactorily within buildings.

5.4 Practical Limitations.

With dense arrays made up of many elements (the Dulles array consisted of over 120 dP sensors), ease of access becomes an important consideration. A number of the sites hidden in poison ivy and at the end of a gauntlet of ticks are difficult to maintain. Several sites require those servicing sensors to watch carefully for bulls or large dogs prior to carrying equipment through a field full of "meadow muffins." Thus, attention to the ease of maintenance is probably the prime consideration. The dP sensors at Dulles (except two) were mounted on telephone poles. Although most of these were near roads, it was difficult to find a convenient place to park safely. Attention to these practical details can make the difference between a successful and unsuccessful installation. Telephone poles are quite logical points, especially if telephone lines are used to transfer data.

6. SPACING CONSIDERATIONS

6.1 Required Spatial Resolution

The dual nature of the thunderstorm wind-shear problem (referred to in section 4.1.1) requires two scales of spatial resolution. The largest scale for the detection of coherent gust fronts requires spacings on the order of 1 to 3 km. The spacing should be larger than the scale of instabilities on the leading edge of the discontinuity (> 1 km) and smaller than the scale of disturbance itself. Pressure jumps detected by an experiment at Chicago's O'Hare airport propagated with approximately uniform motion for distances of over 10 km. For reliable detection and tracking of smaller-scale transient features (e.g., spatially concentrated downflow regions), smaller spacings (of hundreds of meters) seem necessary. Based upon preliminary experimental and theoretical information such near-configurations seem feasible as far as wake vortex and aircraft weight effects are concerned. However the influence of engine jets upon sensor operation remains to be determined. Avoiding runway areas where jet blasts from turning aircraft could strike a sensor is one solution to this problem.

6.2 Required Time Resolution.

Typical propagation speeds for thunderstorm gust fronts range from 10 to 20 m s^{-1} or, in terms of time differences for 1-km spacings, 100 to 50 seconds. Because of sensor variability (e.g., caused by temperature effects, manufacturing tolerances or local siting effects) or spatial variability of gust fronts, errors of 10 seconds could occur for large events and greater errors of tens of seconds could occur for marginal events. Such problems could be the source of anomalous triggers measured during some dP events. dP spacings of 2 km (100 to 200 seconds expected propagation times) are recommended for the detection of coherent gust fronts. For the spatially concentrated transient systems, time resolution becomes much less important because such detection systems will be in the immediate vicinity of runway locations, providing "nowcasts."

6.3 Practical Constraints

One of the greatest problems is that of maintaining large sensor arrays with elements separated by many kilometers. A conservative estimate of the distance involved was 240 miles in making a visit to all of the Dulles dP sites (over 120 sensors with about 1-km spacings).

This assumed that none of the sites were missed, which would require additional mileage. In fact, because many sensors become hidden by foliage and are difficult to see from the road, the actual mileage required for maintenance is considerably larger. Marking roadside locations with special paint can ease the maintenance process. As mentioned previously, ease of access and maintenance should be an important consideration in the site selection process. The rural nature of the area west of Dulles limited the selections and prevented a more logical choice of sites. "Close in" dense arrays near runways could be much more easily maintained.

7. ANEMOMETERS VERSUS PRESSURE SENSORS: RELATIVE STRENGTHS AND WEAKNESSES

7.1 Relative Arrival Times of Pressure, Temperature, and Wind Disturbances.

Bedard and Beran (1977) reviewed past measurements treating the relative arrival times of pressure, temperature and wind disturbances. However, more statistics are needed concerning the temporal relationships. (Bedard and Cairns, 1977) present data taken near O'Hare International airport during the summer of 1976, depicting the time differences between the arrival of the peak of the pressure and the peak of the wind disturbances. Using propagation speeds determined from the pressure sensor array, equivalent distances were computed for each of the time differences. In 8 out of 11 cases the pressure disturbance arrived coincident with or several minutes prior to the arrival of the surface wind surge. In the two cases in which the wind surge occurred well prior to the pressure jump, dP triggers did not occur. Part II (Figure 13.4) provides statistics showing the relative arrival time of pressure and wind speed disturbances.

The value of temperature sensors relative to pressure or wind sensors is best treated by the O'Hare airport 1977 experiment, which recorded data from six towers with collocated temperature, pressure, and wind sensors. On the basis of observations made thus far, surface temperature sensors, although valuable for scientific studies of thunderstorm density currents, frequently show little or no response to the passage of a leading portion of a thunderstorm outflow. Therefore, although they respond to the cold air in the downflow region itself and in some cases respond well to a thin, slowly moving flow of cold air with strong surface interaction, temperature sensors are not well suited for use as part of a warning system. Statistics pertinent to these questions appear in Part II of this report.

7.2 A Comparison Between Anemometers and Pressure Sensors.

Bedard and Hooke (1977) summarize the advantages and disadvantages of anemometers and pressure jump detectors as part of an airport warning system. A comparison indicates that the sensors can complement each other. Pressure sensors promise to detect downbursts and currents that do not reach the surface, whereas wind sensors can detect outflows of limited depth or of warmer air. Both sensor types should be capable of responding reliably to the most energetic events. Part II of this report provides statistical bases for some of these conclusions.

8. INSTRUMENTATION PROBLEM AREAS AND THEIR SOLUTIONS

8.1 dP Detector Temperature Sensitivity

A temperature response (arising from the fact that temperature changes in the sensor reference volume in-turn cause pressure changes) results in two areas of concern:

- a. The detector threshold characteristics are a function of time-of-day.
- b. The possibility exists that local temperature variability could cause sensor mis-match within an array.

Although a design change will reduce this variation in sensitivity, this present design has not prevented the evaluation of the concept or the detection of most events. This problem was identified with the dP sensors using the Dulles array and not while using installations at O'Hare airport or near the National Severe Storms Laboratory (NSSL) tower. Analysis of both the O'Hare and NSSL data sets indicated reliable detection of pressure jumps above the design pressure/rise time threshold with no detections of disturbances below the threshold. Subsequent tests in Boulder documented the fact that the detection threshold is modulated by diurnal temperature changes (Figure 8.1).

The "standard" dP detector threshold varies between .5 and 1 mb, while the modified design shows negligible variability (typically less than .05 mb). The modified design involves increasing the thermal time constant so that the pressure changes induced by temperature changes are slow enough to be suppressed by the dP sensor high-pass filter. This is accomplished by using a larger (2000 cc) and better insulated reference volume, placing this volume in an insulated container, and increasing the internal thermal mass. Inserting a cylinder (7 3/4 inches high, 4 cm in diameter with 2 cm wall thickness) packed with stainless steel wool inside the reference volume provides the thermal mass increase.

This new design is recommended for future installations. The systems at O'Hare, NSSL, and Dulles operated satisfactorily in spite of this problem

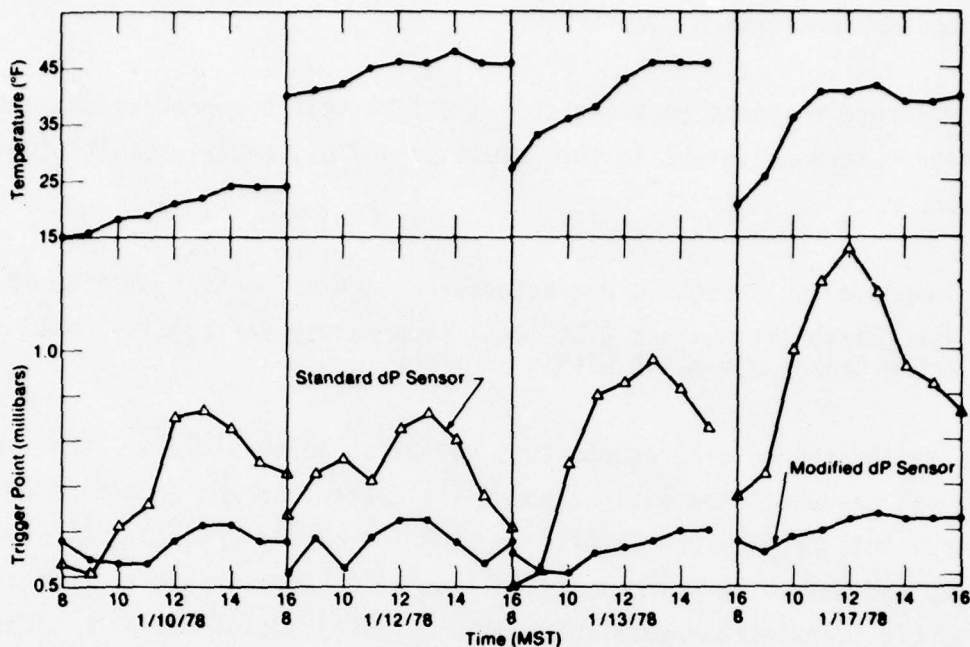


Figure 8.1. dP detector threshold variation with temperature.

because the sensors are well-matched and thunderstorms tend to occur at times (late afternoon or early evening) or under conditions when the standard sensor characteristics best meet design criteria of 0.5 mb trigger level.

8.2 Noise on Telephone Lines

Several leased phone lines encountered a sporadic, broad-band noise problem. The noise would increase in level (particularly after rains) and cause some dP tone discriminators to signal false alarms. This did not confuse signal analysis since sensors showing this problem can be easily isolated from the data logger or identified as anomalous. For a typical problem site, an increase of line noise would cause false triggers on one of the dP decoders. A false trigger occurring every few seconds also activated

the local display indicator which usually permitted a maintenance man to switch that site out until the noise problem was fixed. (Each decoder output passed through a switch panel permitting any dP detector to be switched in or out as well as triggers to be simulated.) Sporadic triggers from one or two sites occurring over periods of hours were entirely different from the progressive triggering of large numbers of sites during an event. This noise problem did not complicate analysis. However, on some nights the noise would increase on one line causing false alarms and excess use of magnetic tape. The dP signal tones were quite low on some data lines because of higher-than-anticipated losses. This fact required setting the tone decoders for low level input signals, making them more susceptible to noise. One solution was to re-design the oscillator, increasing the output level from about 5 to 25 volts peak-to-peak. Such high-output oscillators installed on the longer lines reduced this difficulty. One area of uncertainty exists concerning false triggers due to line noise induced by thunderstorms. For systems designed to respond to initial dP triggers of long (>1 sec) duration this should not present a problem.

8.3 Absolute Pressure Sensor Problems

There was no known failure from any of the Po sensors once installed and operating in the field. This comment applies for 1 unit at NSSL, 5 units at O'Hare airport and 12 units at Dulles. Two Po sensors required external mechanical adjustment after shipment. Experience with these sensors has been quite good. In June 1977 modification of the FM discriminators that were used to decode Po data reduced the carrier level appearing at the discriminator outputs. Although data could be processed in spite of high carrier levels, the residual carrier caused additional, unnecessary noise on the digital recordings. Increasing the value of a low pass filter capacitor in the discriminator output stage, dropped the carrier level to less than 10 mv peak-to-peak. The Po data is used as a reference for evaluation of the dP array operation and for meteorological studies. Since the dP detectors are quite effective for the detection of pressure jumps, absolute pressure sensors

are not required for operational warning systems (unless scientific data collection or other goals — e.g., gravity-shear wave detection — exist).

8.4 Plugged Inlets

Each dP and Po sensor was equipped with a porous cylinder covering the inlet to the atmosphere. Made of hydrophobic material, this cylinder reduces local wind noise and prevents dust and insects from entering the sensor. This inlet is made of sub-millimeter size hydrophobic balls which are fused together in the manufacturing process. They have a low flow resistance and reduce flow noise by integrating the total pressure field over the surface of the cylinder (the cylinder is approximately 2 inches high, 3/4 inch in diameter with 1/8 inch walls). The pressures induced by a gust front or downflow appear coherently at all points on the cylinder surface. These inlet covers were found missing from three dP sensors and mud wasps had made a nest in each plugging the inlet. In addition one dP sensor at O'Hare had this problem. In the current field design the inlet covers are pressed in place over the inlet and must be removed for calibration. A new inlet design permits the inlet cover to be secured with a screw. Also designed is a calibration adaptor which slides over the inlet cover, eliminating the necessity for its removal (apparently several inlet covers were not replaced after calibration).

8.5 Vandalism

There were no instances of vandalism for the O'Hare system, although one sensor was badly damaged by a truck. At the NSSL tower, someone chopped up a data cable. The Dulles area is quite rural, which would explain why 28 dP sensors were damaged by firearms (the problem was greatest in deer season).

Fortunately only one sensor had to be replaced because of this problem. Most local people were curious about the sensors and tended to be slightly protective of them. Several people had to be assured that the sensors were not eavesdropping devices. For any future installations the placement of articles in local papers explaining the purposes of the installation should help assist site surveys and probably reduce vandalism.

8.6 Lightning Damage

Lightning caused the greatest number of sensor problems. At Dulles grounds were not provided for about half of the dP sensor installations. Although surge protection for the dP oscillators was provided the surge protectors do not work without system ground. This resulted in 10 oscillators damaged at unprotected sites. No lightning problems were experienced for the O'Hare system dP sensors during two years of operation.

Damage to telephone lines caused segments of the array (each segment consisting of from 3 to 7 sensors per phone line) to be down for periods of time. Most of these outages were of short duration. However, a lightning strike necessitated replacement of an underground cable, resulting in an outage for southeast segments of the array that lasted over 3 weeks.

8.7 Anemometer Problems

A great deal of trouble was experienced in keeping the anemometer array in operation (Figure 1.5). One of the problems occurred partly because a vent-valve was not installed by the manufacturer. Water would be found in the bottoms of the cases and frequently this would cause the chart paper to stick and jam. A representative installed the valves, but water problems continued. Apparently the seatings for "O"-ring seals were not made properly for some cases. The addition of a 5-watt bulb to reduce humidity and improvement of the "O"-ring seating on cases

showing leaks should solve this problem. An improvised solution (which helped) was to run a strip of tape across the outside seam.

There were a variety of electronic problems. Some problems obviously resulted from lightning strikes, since the locations that are well suited for wind measurements are on exposed hills and are thus susceptible to lightning strikes (Figure 8.2). The units were repaired and re-calibrated by the manufacturer, but still encountered failures. With an active maintenance program good wind speed and direction data during the key portions of the 1977 thunderstorm season were obtained. A large stock of spares for anemometers and a quick response maintenance agreement with the manufacturer would help to reduce storm damage outages.

8.8 Power Failures

Power failures accounted for the greatest number of outages during the thunderstorm season. The Doppler sounder was particularly susceptible and was down for key months, from early July through early September. The Doppler sounder was also out for short periods as a result of surges on the power lines caused by distant thunderstorms; thus required improved surge protection. Power outages also caused the Doppler sounder to miss gust front events.

The dP sensors are well suited for operation during thunderstorms. Their internal batteries make them immune from regional power failures and the multiple phone lines give added reliability to the total system (since it is unlikely that several phone lines will be down simultaneously). The anemometers were modified to provide battery back-up in the event of local power outages.

The original system at the central recording station (CRS) had a battery back-up built into it to handle local power failures. It was intended to provide a separate back-up system for the Po digital recorder but when this proved unreliable the load of the absolute pressure sensor



Figure 8.2. Typical anemometer location.

recorder was added to the rest of the system. The fact that the chargers could only handle the normal system load and not the excess load after a local power failure, did not interfere with the recording of events and the entire system operated for over one hour during a power failure. During 1977 the system would usually have to be brought back to normal operation manually after power failures of long duration. Subsequently chargers with larger capacities were installed.

8.9 System Stability

There were no observed long-term changes in sensor characteristics for either the dP or Po sensors. This comment also applies to the CRS instrumentation. Followup testing should include measurement of the sensor trigger threshold as a function of temperature, checking the

repeatability and stability relative to the initial laboratory tests. Also the long-term integrity of system seals should be insured. Two oscillators changed their center frequencies, but subsequent design changes insured greater stability. However, these seemed to be isolated cases, possibly related to lightning surges, and no wholesale replacement of dP oscillators is recommended.

One mechanical problem exists with hinges on some dP and Po cases showing evidence of rust. The solution seems to apply oil to the existing cases and to specify proper hinges in any future case procurement.

8.10 Recording Station Problems

The problems encountered with the central recording station (CRS) were minimal. The dP data logger operated for over one year without a malfunction. It finally failed (December 1977). The Kennedy tape deck failed once during the test interval, because of a burned out bulb in the marker sensing system. The Po digital recorder malfunctioned several times due to multiplexer chip failures. These were apparently caused by power line surges. There were no failures since the recorder was connected to the main system power source (the batteries providing surge protection). The Po digital recorder initially had no battery back-up.

9. SYSTEM MAINTENANCE

9.1 Calibration

Bedard (1977) describes the pressure calibrator. Because of the magnitude of the task of calibrating the complete system, frequent calibration, which would be desirable based upon technical reasons, would be impractical. Calibration prior to, during, and after local thunderstorm seasons is recommended. More modest arrays could be calibrated monthly. For dP sensors, calibration consists in applying positive pressure of steadily increasing magnitude to determine the trigger threshold. Applying a step function of pressure of 1 millibar and measuring the duration of the resulting trigger indicates

the sensor time constant. Changes in the sensor time constant can occur because of leaks in the reference volume or connecting tubing as well as because of changes in the flow resistor. For the Po sensors, a positive 1 millibar pressure applied for 2 minutes checks the system calibration through the recording and processing systems. Other checks are the battery voltages, tone levels, center frequencies and alignments at the time of calibration. The calibrations should not be performed during periods of high winds or large pressure changes (e.g., gravity-shear waves or frontal passages). With the standard dP detector, calibrations can be performed on an overcast day with stable temperature, despite the temperature sensitivity problem.

9.2 Alternate Calibration Methods

An internal calibrator, capable of being remotely activated, would greatly ease the logistics of operating large arrays. Field experience indicated that most problems occurred with the oscillator or data lines. The pressure sensor is quite simple and promises very high reliability. A remotely activated test of only the tone oscillator would be a great help operationally. This could be done, for example, by passing a d-c current through the data lines and activating a relay (which is in parallel with the pressure switch).

For dP sensors operated in the vicinity of runways in dense arrays, one calibration possibility is to use the pressure field beneath low-flying aircraft (Section 4.1.6) to test the system.

9.3 Tests After Bad Weather

In retrospect it seems that most of the phone line and instrumentation problems resulted from lightning. After severe thunderstorms, measuring the Po tones is one method of verifying that a large portion of the system is operating. Measuring line-loop resistances for these lines handling only dP data will detect most data line problems. Anemometers should be checked physically (because of our past experience) on a weekly or bi-monthly basis. An operational system hardened with surge protectors,

battery back-ups and additional grounds should operate reliably during thunderstorms. In fact the Dulles system (once sufficient standby power was available) operated through numerous thunderstorms and local power failures with no loss of data.

10. OUTLOOK FOR THE FUTURE AND CONCLUDING REMARKS

The Dulles system proved valuable for two reasons. First, it provided a basis for evaluating the instrumentation and techniques under a variety of field conditions. Several modifications both of the equipment and the analysis procedures (e.g., requiring dP triggers to occur for several seconds) resulted from this experiment. The bases were developed for knowledgeably applying these sensors in systems deployed under a variety of conditions.

Second, we obtained data concerning thunderstorm outflows. A wealth of data far exceeding our expectations was obtained. The data presented here as case studies represent only the first step in analysis. The analysis of Fujita (1978), working with data from a single day, emphasizes the great value of these data, not only for providing more scientific insight into the processes involved, but also for providing operationally needed information (quantitative deductions of the hazard statistically and in three-dimensions). Part II of this report concentrates on developing statistics from the entire data set and will present conclusions based upon that viewpoint.

Evidence is mounting for the dual nature of the problem (the thunderstorm gust front and down flow region both representing hazards), and the spatial scales outlined in Section 6.1 suggest two configurations for detection systems, each with a complementary goal. Figure 10.1 shows a possible array configuration for the detection of large-scale, coherent events (typical of thunderstorm gust fronts). This would provide warning times of from 5 to 10 minutes. Present indications are that configurations like the one shown in Figure 10.1 will represent a reasonable compromise between reliability for detection and practicality in implementation.

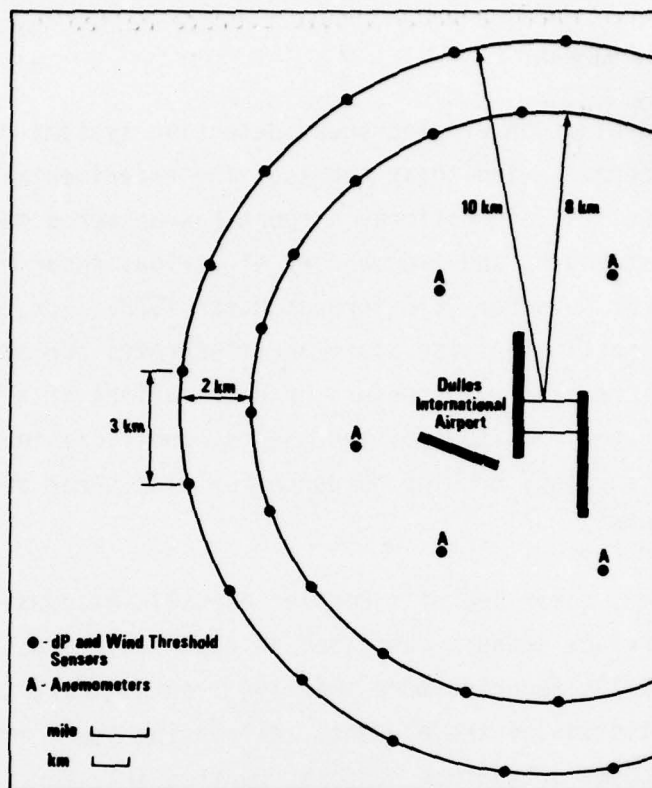


Figure 10.1. Possible array configuration for the detection of large-scale coherent events.

The description of a detection concept for the thunderstorm down flow region is not included in this report.

Although such systems should provide practical and reliable methods of providing thunderstorm-wind-shear warnings, in the long term future advances in remote sensing methods could eventually provide alternative solutions to this aircraft safety problem. However long-term surface sensor use is anticipated, not only because of the simplicity, low-cost, and expected reliability of surface arrays, but also because their outputs should complement 3-dimensional views provided by remote sensing techniques (Filling in information obscured by obstructions, range or resolution problems).

PART II STATISTICAL RESULTS

11. INTRODUCTION AND SUMMARY

The design and evaluation of wind-shear detection systems require statistical data concerning wind-shear events. The experimental wind-shear measuring system at Dulles International Airport has answered much of this need, recording the strengths and frequencies of various shear events over an 18-month period from November 1976 through March 1978. For this location it is now possible to estimate false alarm and miss-rates for surface arrays of temperature, pressure, and wind sensors or combinations of these. Furthermore, data concerning the magnitude of the shears, their origin, and relationship to the local meteorology provide guidance for wind-shear detection and avoidance (Bedard, 1978).

The Dulles system, comprised of a Doppler acoustic-microwave radar and a dense network of surface sensors described in papers by Hardesty et al. (1977), and Bedard et al. (1977), recorded more than 160 events. Part II of this report reviews the statistics of these events, discussing their implications for the design of systems of surface sensors, particularly for the detection of thunderstorm outflows. Eighty-two percent of 113 significant events occurred in conjunction with thunderstorms, squall-lines, or frontal passages. The chief source of false alarms for anemometers was boundary layer disturbances representing 10% of the 113 significant events, while gravity shear waves related to the 500-mb winds caused most false alarms for pressure sensors (4% of the 113 significant events). By using complementary arrays of wind and pressure sensors total system false alarms can be greatly reduced.

These data demonstrate the importance of stable surface layers in determining the representativeness of surface temperature and wind measurements of flow at higher levels (stable surface layers causing underestimates of system severity). Wind vector measurements, providing more information than point temperature measurements, offer operational advantages for detection systems. Conversely, pressure sensors will not reliably detect thin outflows (100-200 m) occurring at a distance from downflows having small dimensions. Again the wind and pressure sensors combine to provide a total system offering high reliability for detection of outflows. The data set

offers wide possibilities for further exploitation including case study comparisons with numerical models case study comparisons with weather radar data, and summaries of shear data and Doppler sounder profiles for computations of aircraft response and design of remote sensing systems.

The observations range from large wind surges, pressure jumps, and temperature drops caused by strong thunderstorm gust fronts to weak wind surges caused by mixing beneath ground-based inversions. A complete mesoanalysis was not possible for each event (for example, Fujita, 1978). Thus, the categorization of events must remain tentative. Nevertheless the source mechanism for most disturbances was clear and only a small percentage of events seemed difficult to identify. Also, some measurements placed in one category (for example a pre-frontal squall-line) show evidence of other effects as well — a boundary layer break up, gravity waves and downflows could also accompany the flow discontinuity. Moreover, the definition of an event and comparisons between the various sensors is a circular process since each element of the system is itself being evaluated.

One further point of caution is in order before presenting the data, one has to be careful in designing detection systems based upon short-term (1 year) observations, since it is usually extreme deviations from the norm that cause disasters in terms of lives and property. In spite of these qualifications these data represent great value in terms of being able to relate γ -scale array (~ 1 km spacings) observations to vertical remote sensor data, permitting documentation of the structure, source and detectability of a variety of wind-shear events. The accumulated information is valuable for the design of detection systems. Table 11.1 is a summary of key conclusions.

The definitions appearing below will provide background for understanding the sections presenting the statistical data.

WIND SHEAR - The local variation of the wind vector, or any of its components in a given direction (Glossary of Meteorology, 1959).

VERTICAL WIND SHEAR - The variation in the vector wind velocity with changing height (Greene et al., 1977).

AD-A075 922

NATIONAL OCEANIC AND ATMOSPHERIC ADMINISTRATION BOUL--ETC F/G 1/5
A THUNDERSTORM GUST-FRONT DETECTION SYSTEM, PART I. SYSTEM OPER--ETC(I
AUG 79 A J BEDARD, F H MERREM, D SIMMS DOT-FA76WAI-622
FAA-RD-79-55 NL

UNCLASSIFIED

2 OF 2

AD
A075922



END
DATE
FILMED
11-79
DDC

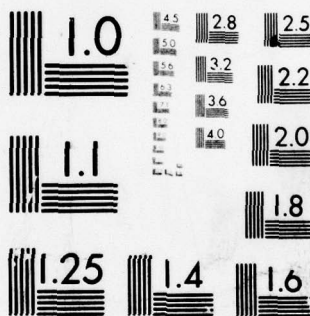


TABLE 11.1

SUMMARY OF KEY CONCLUSIONS

- a) Combinations of wind sensors and pressure sensors can reliably detect outflow systems (particularly thunderstorm gust fronts) with low false alarm rates.
- b) Evidence indicates that it is difficult to infer reliably the vertical wind shear (dU/dZ) from surface measurements (Figs. 13.10a and 13.10b).
- c) Boundary layer disturbances (Fig. 12.2) are the chief source of false alarms for wind sensing systems and gravity-shear waves aloft (Fig. 12.3) for pressure sensing systems.
- d) The problem of outflow interaction with stable layers (Figs. 13.7a and 13.7b) represents the chief limitation to the use of temperature sensors for surface detection of outflow systems. This problem also can prevent surface wind vectors from reliably indicating the magnitude of the flow aloft (frequently causing underestimates in excess of factors of 2).
- e) Surface temperature sensors are not well suited for use in outflow detection systems in comparison with wind or pressure sensors.
- f) There is no clear relation between the vertical shear (dU/dZ) prior to the outflow disturbance and the vertical shear associated with the disturbance (Fig. 13.10b).
- g) More statistics are required concerning the severity, frequency of occurrence, dimensions and time scales for downbursts.
- h) The data set contains individual cases and shear profile information valuable for comparison studies with numerical models, aircraft response modeling and the design of future remote sensing systems.
- i) Pressure sensors frequently provide a warning in excess of 1 minute compared with wind sensors (Fig. 13.4).
- j) Gravity waves can induce shears comparable with thunderstorm gust fronts (Fig. 16.1).

HORIZONTAL WIND SHEAR - The variation in the vector wind velocity with horizontal distance (Greene et al., 1977).

INCREASING (DECREASING) PERFORMANCE WIND SHEAR - A method of describing a given wind shear in terms that define the resulting response of an aircraft (e.g., increasing performance wind shear indicates increased relative air-speed and increasing lift with the aircraft rising above its intended path). This definition was suggested at an airline pilot's association, air safety workshop in 1977.

SIGNIFICANT EVENT - An observation that could have triggered warning systems based upon surface wind vector changes, upper level flow changes, or pressure jumps.

FALSE ALARM - Conditions meeting criteria for significance measured without an accompanying increase in low-level shear.

MISS - Failure to observe an event producing a large enough wind-shear change to present a hazard to aircraft operations. (Richwien and McLeod, 1978, suggest 5 knots/30 M over a 100 M depth as a definition of operationally significant shear). More work needs to be done in defining dangerous shear for a variety of aircraft and conditions.

BOUNDARY LAYER DISTURBANCE - Abrupt increase in surface winds caused by the sudden appearance of a higher level (e.g., 100 to 300 M) flow at lower altitudes. A propagating wind shear increase may not occur for these events. Conversely, in the case of the sudden erosion of a surface-based inversion, a reduction in vertical wind shear ($\frac{dU}{dz}$) may result.

12. HISTOGRAMS SHOWING FREQUENCY OF VARIOUS TYPES OF EVENTS AS A FUNCTION OF MONTH-OF-YEAR

12.1 Thunderstorms, Squall-lines and Fronts (Figure 12.1)

Figure 12.1 shows that most of these disturbances occur during the summer months. The solid bars indicate the portion of these disturbances that were significant (because of the magnitude of the

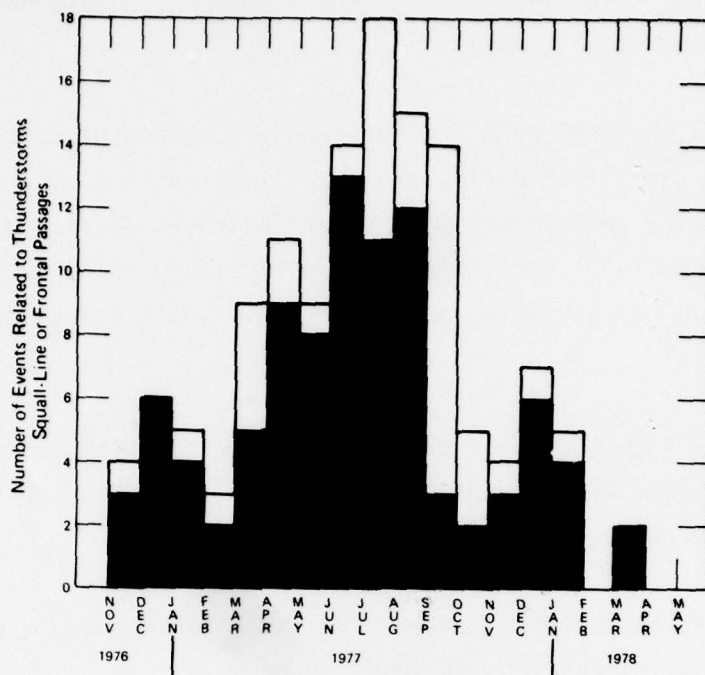


Figure 12.1 Histogram showing the number of events related to thunderstorms, squall-lines or frontal passages as a function of month-of-the-year.

accompanying wind surge or pressure jump). Of the 131 events related to thunderstorms, squall-lines and fronts, 93 were characterized as significant because they could have triggered warning systems based upon surface wind vector changes, upper level flow changes or pressure jumps. This category accounted for 82% of all of the "significant" events. This breakdown agrees with the percentage obtained (82%) by Bedard and Cairns (1977) for the Chicago O'Hare airport area. The exact agreement is probably coincidental.

12.2 Boundary Layer Effects (Figure 12.2)

The next most frequent class of disturbances is caused by "boundary layer effects" resulting from a jet aloft mixing down to the surface through a surface-based inversion. The 18 events in this category accounted for 11 or about 10% of the total number

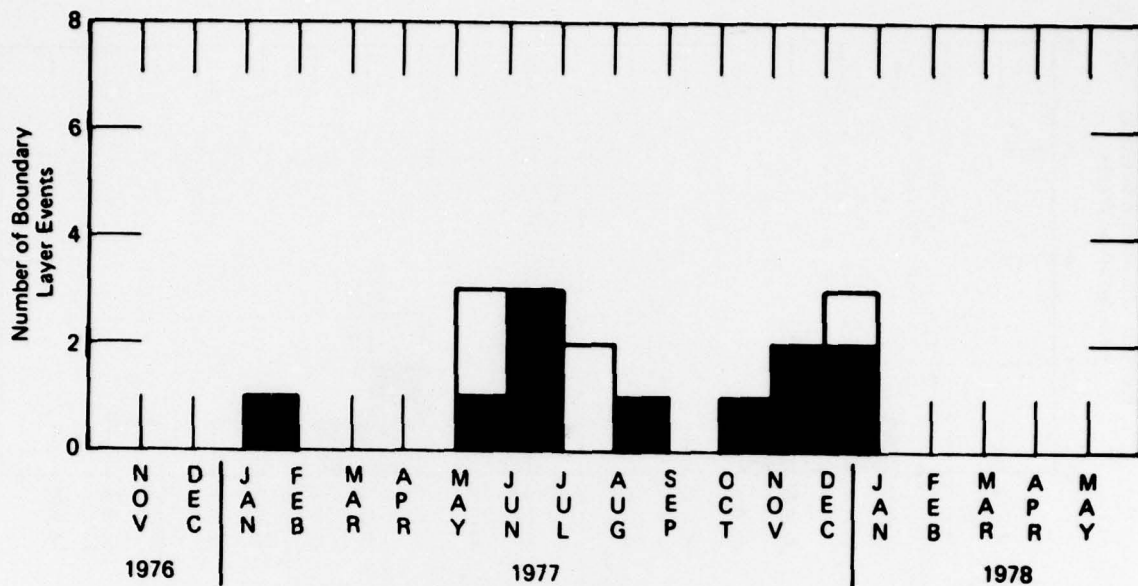


Figure 12.2. Histogram showing the number of events related to boundary layer effects as a function of month-of-the-year.

of significant disturbances due to all causes. This class of disturbance is a chief source of false alarms for wind detectors. Pressure jumps large enough to trigger dP detectors accompanied 3 of the surface wind surges. Paradoxically, the existence of a wind surge at the surface can signify the breakup of a surface inversion and the end of a dangerous vertical shear (dU/dZ) situation.

12.3 Gravity-Shear Waves (Figure 12.3)

Whereas boundary layer effects can cause false alarms for wind sensor systems, gravity-shear waves aloft can account for most false alarms on pressure sensor systems. The 8 events detected occurred during the fall and winter months accounting for 5 or about 4% of the total number of significant events, detected. Only very minor wind speed disturbances occurred at the times of these pressure waves.

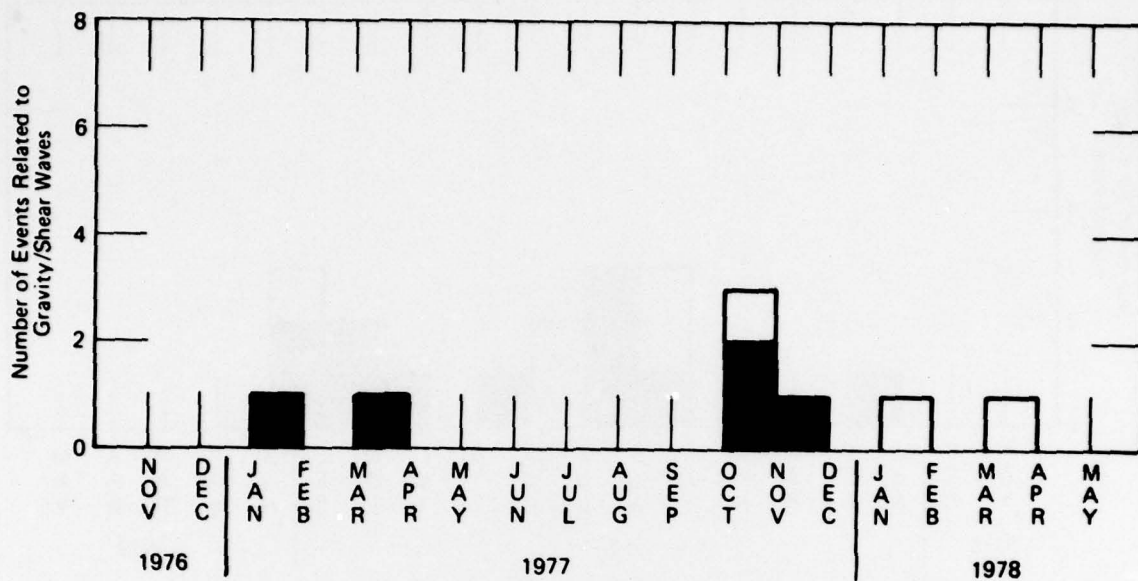


Figure 12.3. Histogram showing the number of events related to gravity/shear waves and the 500 mb winds as a function of month-of-the-year.

12.4 Gravity Waves (Figure 12.4)

Although wind shear may often be a factor in the production and propagation of these waves, the term gravity wave is used to emphasize their frequent relation to ground-based inversions. A paper by Chimonas and Bedard (1978) indicates that such coherent waves can increase the danger of already hazardous wind-shear situations. One of the four waves measured involved both pressure and surface wind changes large enough to cause detection by a system of surface sensors and could have been important to aircraft operations.

12.5 High Winds (Figure 12.5)

High, gusty winds can cause local pressure fluctuations large enough to cause false alarms. Three notable cases occurred

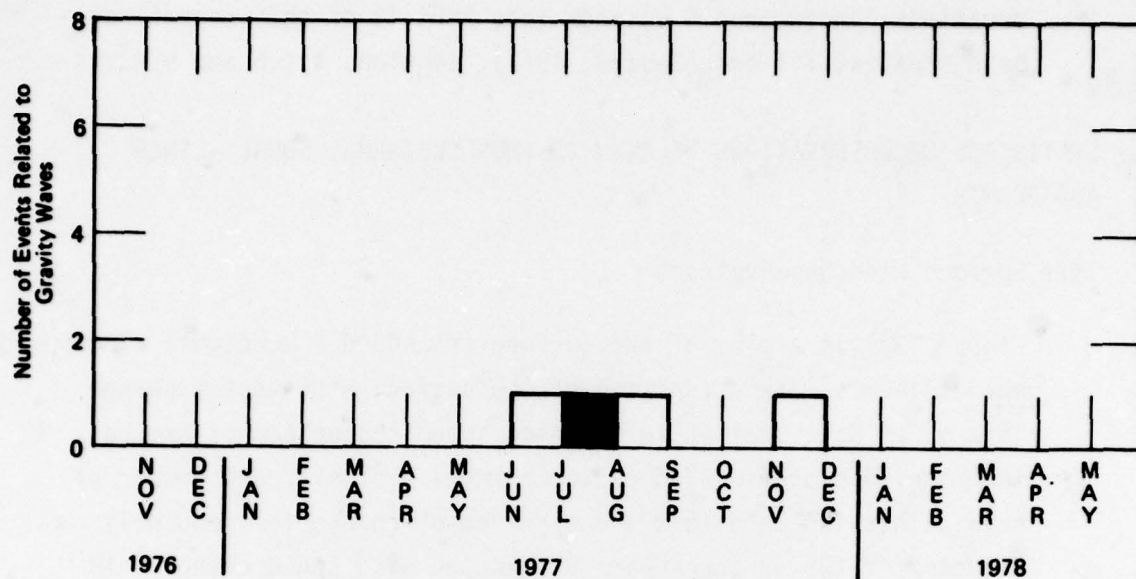


Figure 12.4. Histogram showing the number of events related to gravity waves as a function of month-of-the-year.

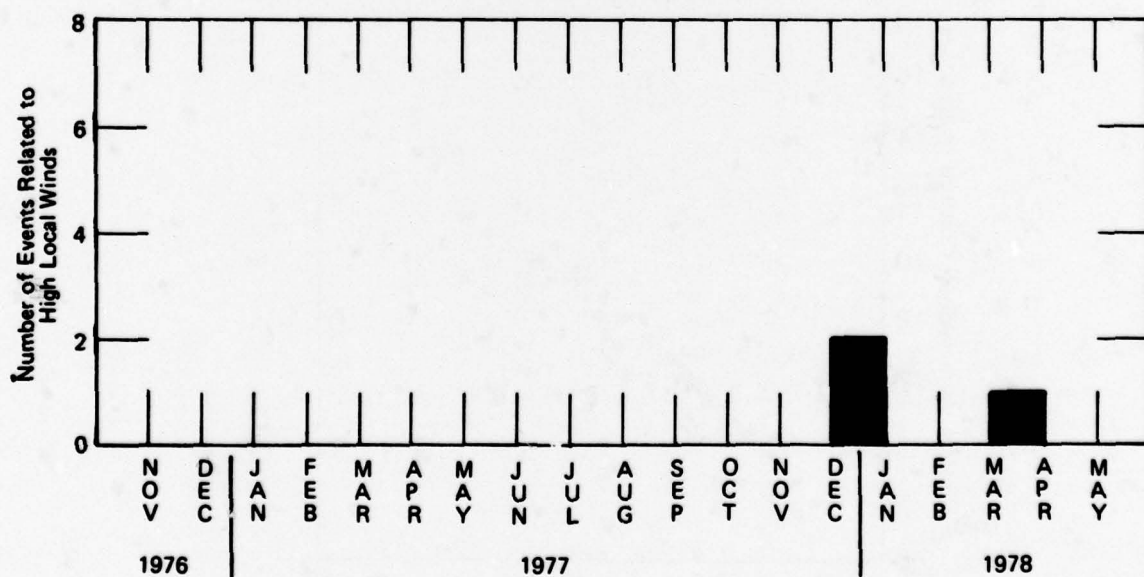


Figure 12.5. Histogram showing the number of events related to high winds as a function of month-of-the-year.

during the winter months. Fortunately these fluctuations are of short duration (usually less than 4 seconds) and may be eliminated by requiring significant pressure triggers to have durations longer than 4 seconds (see Part IV of this report) or using spatial filters (Bedard, 1977), sections 4.1.5 and 5.2.

13. STATISTICS OF OBSERVATIONS RELATED TO THUNDERSTORMS, SQUALL-LINES AND FRONTS

13.1 Surface Wind Observations

Figure 13.1 is a plot of the surface (standard 7 m height) wind speed change in m s^{-1} as a function of the surface wind vector change in m s^{-1} . Note that while the wind speed change cannot exceed the magnitude of the wind vector change, a significant number of data points indicate that the wind vector change is frequently a factor of two or three larger than the wind speed change. In fact three points show no wind speed change accompanying wind vector shifts. These data indicate the value in making measurements of wind vector differences.

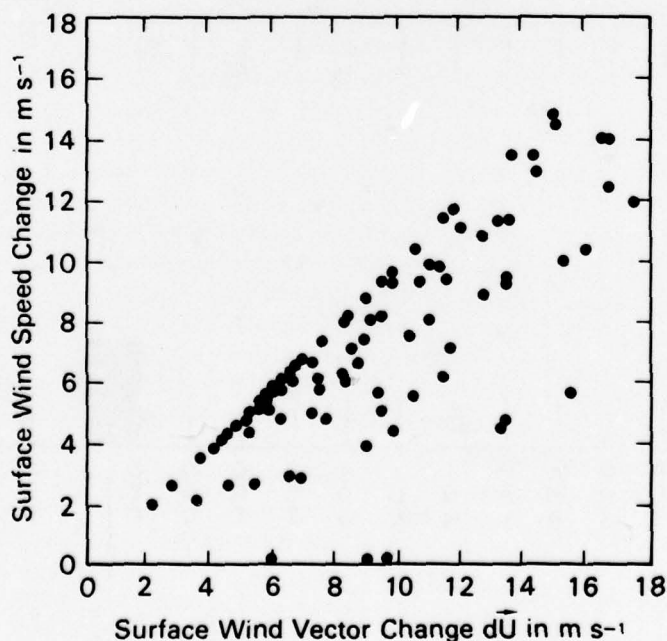


Figure 13.1. Plot of surface wind speed change as a function of surface wind vector change.

Figure 13.2 is a plot of the peak wind speed as a function of vector difference. Although the wind speed surge can be much smaller than the vector change, a wind speed threshold detector (Bedard and Fujita, 1978) with a trigger point at say 20 knots would detect most disturbances having vector shifts in excess of 10 m s^{-1} . In fact figures 13.1 and 13.2 show that the probability of such detection is greater the more severe the vector shift. In these plots where spatial variability occurs with a number of anemometers, the data point represents the average value.

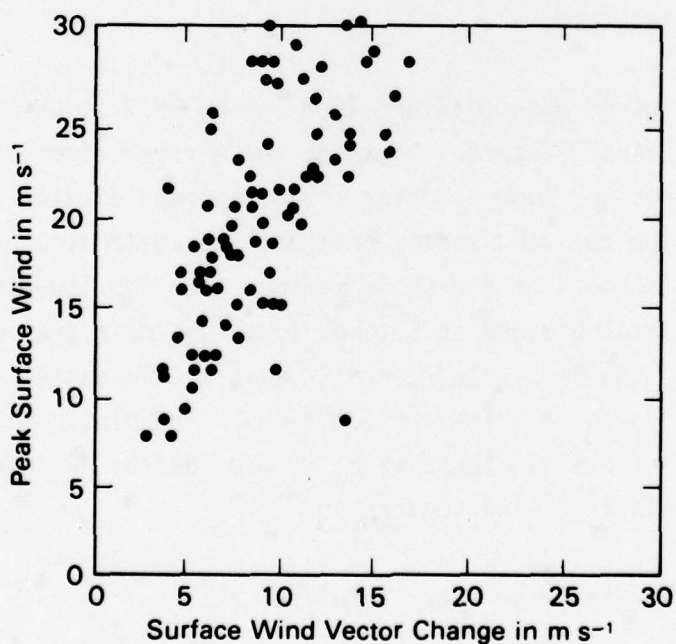


Figure 13.2. Plot of peak surface wind as a function of surface wind vector change.

13.2 Surface Pressure Observations

Figure 13.3a is a plot of the maximum pressure in mb as a function of the rise time (τ) in seconds for all events for which accurate pressure data were available. Figure 13.3b is a plot of the maximum pressure change as a function of the rise time τ for events showing a surface wind vector change of at least 7 m s^{-1} . The straight lines on figures 13.3a and 13.3b indicate the approximate threshold of a pressure jump sensor designed for wind-shear detection. Data from the less accurate station barograph added to figure 13.3b plot were the only pressure data source for the first 5 months of operation. This group of data points shown at 900 sec (15 minute) periods represents a maximum rise-time estimate for these events. Note that most of the events having large amplitudes and short rise times (< 600 seconds) occur with the larger wind vector surges. As with the anemometer data, where spatial variability occurs with a number of pressure sensors, the data point plotted represents average values of pressure and rise time.

Figure 13.4 is based upon data obtained during 1977 at Chicago's O'Hare International Airport. It shows the arrival times of the start of the pressure jump detector triggers compared with either the time at which the wind vector change for a co-located anemometer exceeded 15 knots or the surge maximum time for low-wind cases. These data obtained at 6 tower locations near the ends of runways, use the same data recording system eliminating any ambiguity concerning relative arrival times. The plots indicate that a warning of over 1 minute is often provided by dP detectors relative to co-located wind sensors.

13.3 Doppler Acoustic-Microwave Radar Observations

The Doppler acoustic-microwave radar described by Hardesty et al., (1977) provided wind speed and wind direction profiles for comparison with the array of surface sensors. These profiles represent

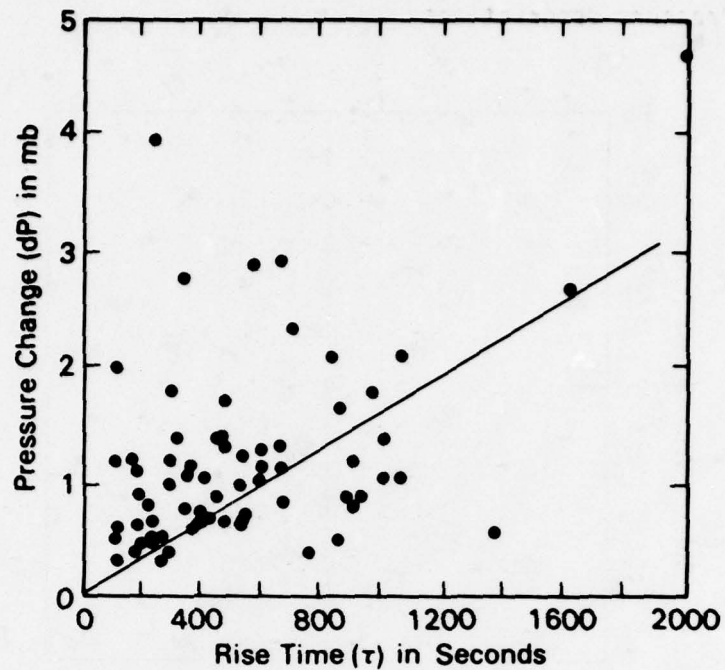


Figure 13.3a. Pressure change (dP) as a function of rise time (τ) for all events.

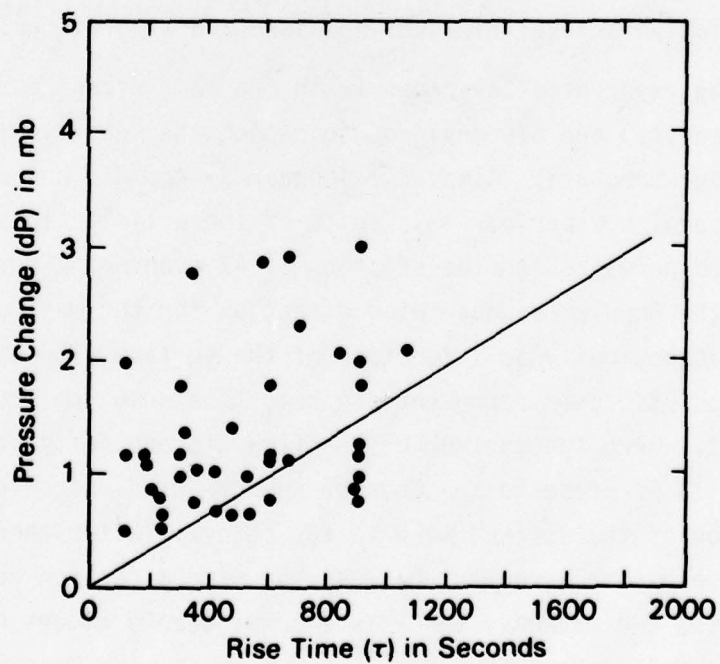


Figure 13.3b. Pressure change (dP) as a function of rise time (τ) for events showing a surface wind vector change exceeding 15 knots.

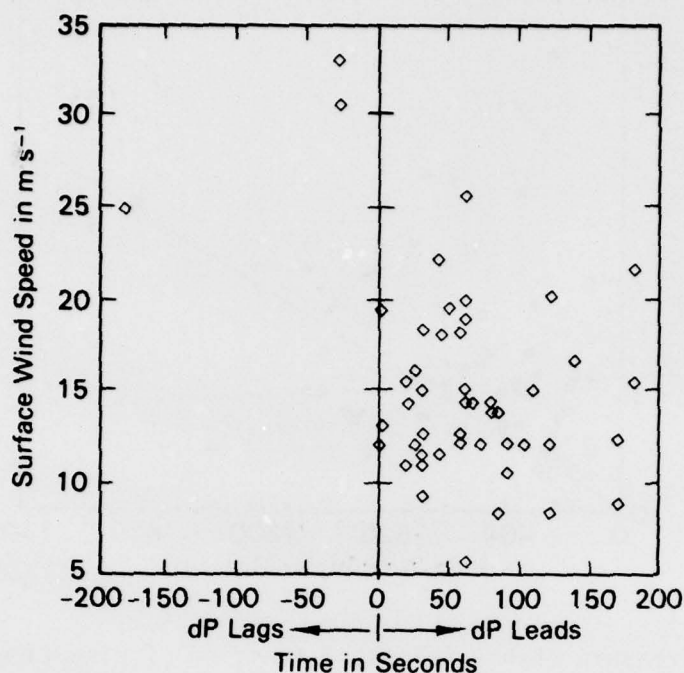


Figure 13.4. Relative arrival times of pressure and wind disturbances.

6 minute exponential averages (with the most recent data weighted most heavily) and are designed to depict the mean flows rather than the fine structure. Also, the sounder system did not operate for several key periods. In spite of these limitations, the profiles obtained permitted the description of 47 events. Figure 13.5a shows the Doppler sounder wind direction for the maximum of the flow discontinuity as a function of the surface wind direction. These points could represent any height between the ground to about 1500 ft, where the maximum of the flow discontinuity occurred. Figure 13.5b presents the Doppler sounder wind vector change as a function of the surface wind vector change. While there is relatively good agreement between the wind direction estimates using the two methods, there is a considerable amount of scatter in the wind vector comparison. Low surface wind measurements could result from stable layers near the surface; while low sounder estimates could result from failures to detect vertical components or from the averaging time used.

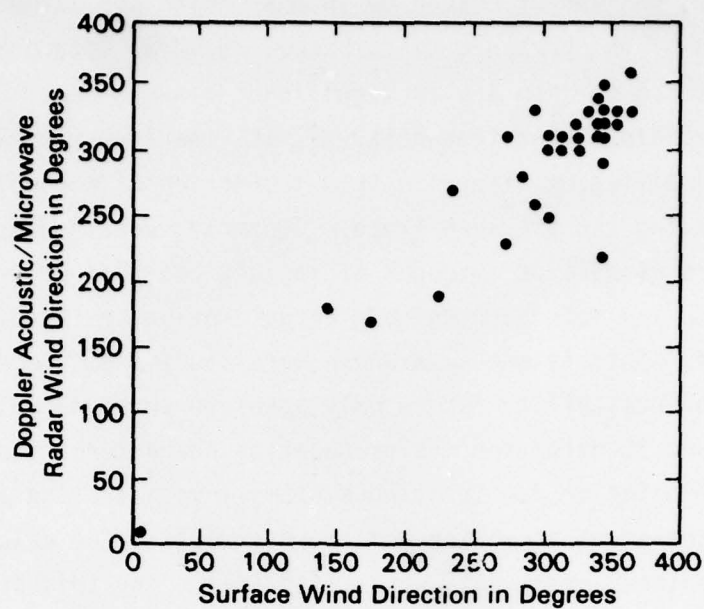


Figure 13.5a. Doppler acoustic/microwave radar wind direction in degrees as a function of surface wind direction in degrees.

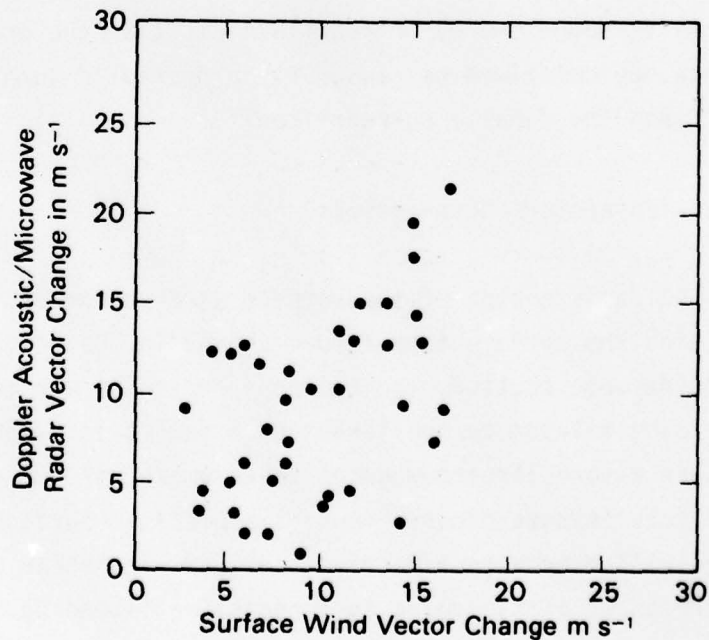


Figure 13.5b. Doppler acoustic/microwave radar vector change in m s⁻¹ as a function of surface wind vector change.

Figures 13.6a and 13.6b compare the Doppler sounder azimuth in degrees and vector change $d\vec{U}$ in m s^{-1} with the azimuth and speed of motion of the pressure disturbance. Several data points in the azimuth comparison are in significant disagreement. Two possibilities can explain such differences. First, the lower level flow could be from a different direction than the motion of a downflow system dominating the pressure trace. Secondly, veering surface wind vectors as well as averages of rapidly changing upper level flow vectors may not represent the actual motion of the discontinuity itself. This is one area where more study seems necessary. A further possibility (where only absolute pressure calculations are used to determine the propagation characteristics) is that accelerating or decelerating systems invalidate the assumption of constant speed of motion and cause errors in the calculations. The dense dP array data was not influenced by this problem.

Figure 13.6b shows that the pressure disturbance propagation speed tends to be greater than the Doppler sounder wind vector change. For transient events, the sounder averaging time could make the profiles presented not representative of the flow maxima. Another possibility suggested by Charba (1974) is that the pressure disturbance may sometimes be caused by an hydraulic jump propagating faster than the density current itself.

13.4 Surface Temperature Observations

Figure 13.7a is a plot of the surface wind vector change in m s^{-1} as a function the surface temperature change in $^{\circ}\text{C}$. Although there is considerable scatter, the tendency for the lower temperature drops to be related to the larger gust surges is evident. However there are also a large number of cases where zero or even positive temperature changes occur. Thus it seems that surface temperature sensors will not be an effective tool for wind shear warning systems and perhaps of little value in forecasting impending shear associated with thunderstorm outflows.

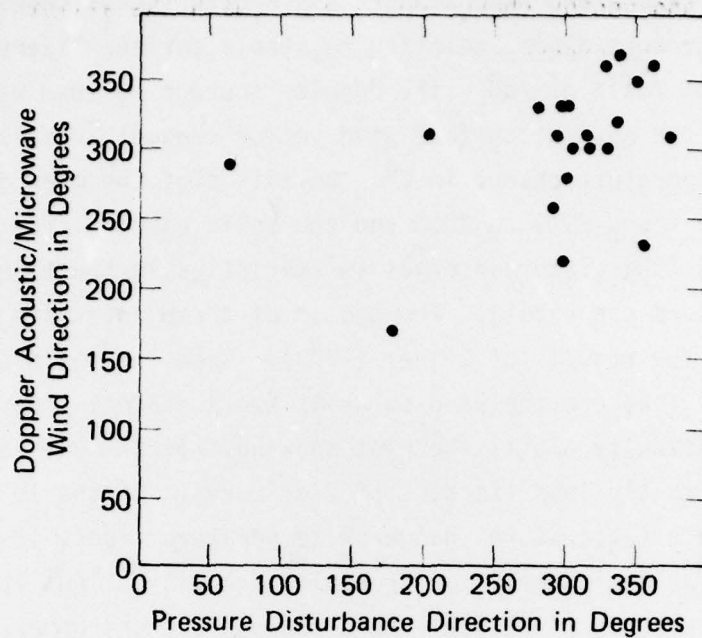


Figure 13.6a. Doppler acoustic/microwave wind direction in degrees as a function of pressure disturbance direction in degrees.

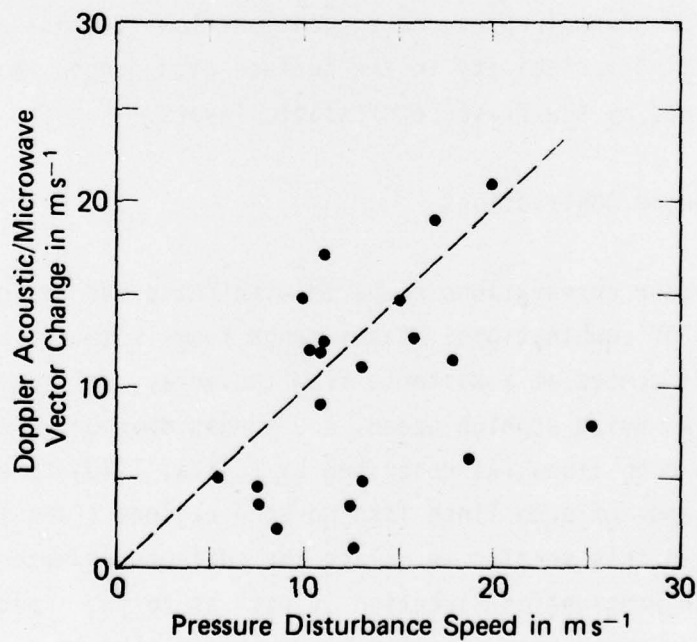


Figure 13.6b. Doppler acoustic/microwave vector change in m s^{-1} as a function of pressure disturbance speed.

Figure 13.7b is an important figure because it illustrates that both temperature and wind sensors can underestimate the severity of density currents aloft, pointing to stable surface layers as the cause. The ratio $d\vec{U}_d/d\vec{U}_s$ (the Doppler sounder maximum wind vector change to the maximum surface wind vector change) appears as a function of the temperature change in $^{\circ}\text{C}$. On this plot the open diamonds occur during the hours 0900 to 2000 and the solid circles from 2000 to 0900 local time (this later interval is statistically the time during which stable layers can exist). The choice of these intervals was guided by the results of Geiger (1973). When the ratio $d\vec{U}_d/d\vec{U}_s$ is greater than one the wind surge at the surface is less than the discontinuity aloft; the plot showing that in many cases it is significantly less (factors of 2 or more). Of the 19 cases showing zero temperature change or temperature rises, 13 or 68% occurred during intervals of probable stability. Thus it appears that the presence of stable layers can prevent the upper level flow from being represented at lower levels.

Thunderstorm outflows following previous thunderstorms will encounter such stable layers because of the cool air present from the previous storm. For several cases, subsequent outflows demonstrated large spatial variability in the surface wind surges that could be explained by the presence of stable layers.

13.5 Weather Radar Observations

Weather radar observations compared with these events indicate a variety of combinations. Cases range from isolated, small stationary echoes at a distance from the array, well-defined echo lines moving at high speed, and surges developing from bulges in echo lines (as described by Fujita, 1978) to extensions from the ends of echo lines into no-echo regions (Part I, section 3.1.1). In this section we relate the surface parameters to the echo bearing or propagation direction as well as to the speed of motion of the echo. Events also occurred within broad echo regions and are not

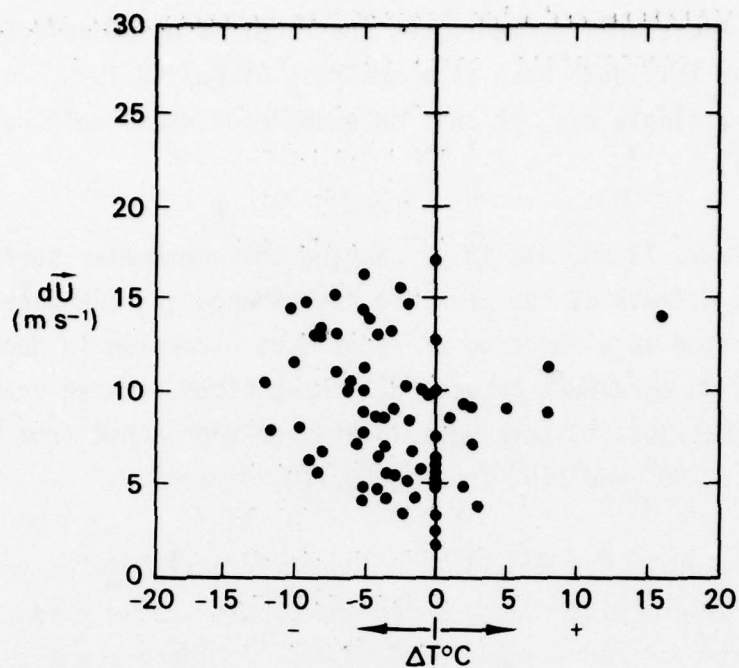


Figure 13.7a. Surface wind vector change as a function of surface temperature change.

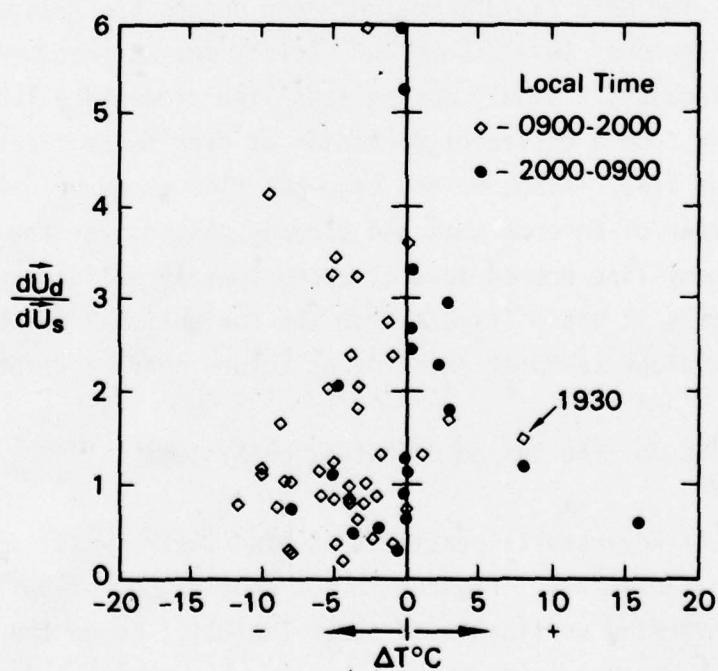


Figure 13.7b. Plot of the ratio of the Doppler sounder wind vector change $d\vec{U}_d$ to the surface wind vector change $d\vec{U}$ as a function of the surface temperature change.

treated in this section; several of these showed evidence of downflow effects. Additional mesoanalyses are required using selected events from this data base (the analysis of Fujita 1978, using only data from a single day, is only an example of what could be done with these data).

Figures 13.8a, 13.8b, and 13.8c compare the anemometer surface wind direction, azimuth of the pressure disturbance and the Doppler radar wind direction as a function of radar echo direction in degrees. There is quite good agreement between all these plots. These graphs also indicate that most systems were located or approached from between azimuths of 250° and 360° from the Dulles array.

Figures 13.9a, 13.9b, and 13.9c compare the surface wind vector change, pressure disturbance speed and Doppler radar wind vector change as a function of radar echo speed in m s^{-1} . There seems to be a tendency for the surface wind vector to be less than the radar echo speed while the pressure disturbances tend to be greater. However, there is a considerable amount of scatter in the data points. It seems that the more rapidly moving radar echoes are related to the more intense lower level flows and rapidly moving pressure changes. In several cases, a slowly moving echo line produced a lobing echo moving from a different direction at over twice the speed of the echo line. Also, in one case the flow surge originated from the rear of an echo that had already passed over the array. Although many line echoes move at approximately uniform speeds in some cases it was difficult from the conventional weather radar data alone to infer existing or future surface effects.

13.6 Implications for the Design of Detection Systems

A summary of key results pertinent to wind-shear system designs appears in Table 13.1. Figures 13.10a and 13.10b, emphasize several points concerning vertical wind shear (dU/dZ). Using the Doppler

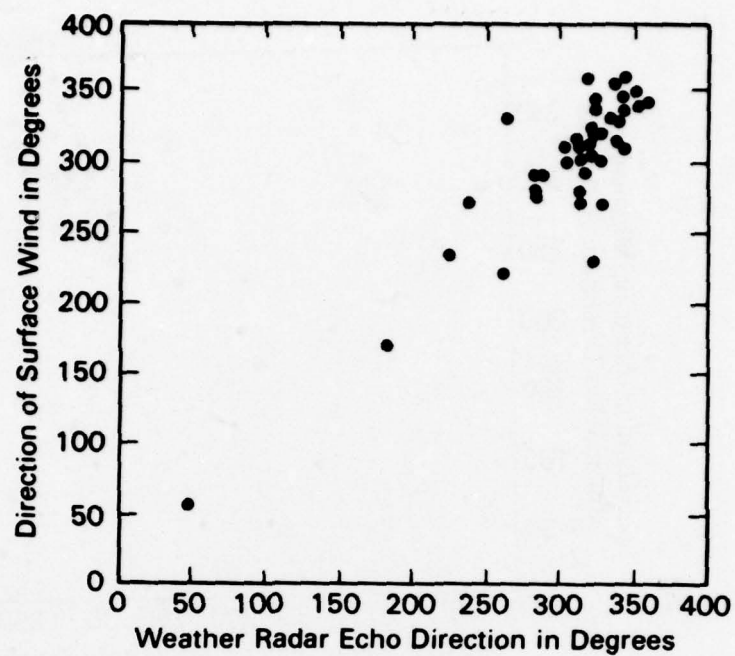


Figure 13.8a. Direction of surface wind as a function of weather radar echo direction in degrees.

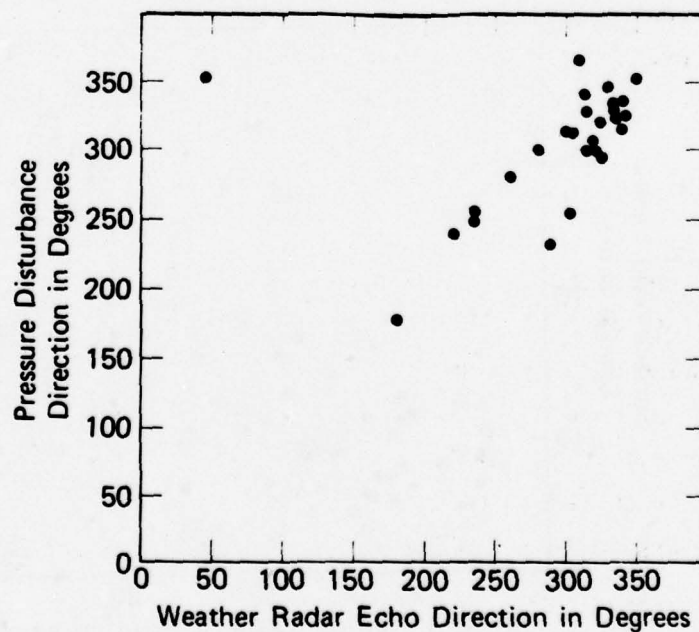


Figure 13.8b. Direction of pressure disturbances as a function of weather radar echo in degrees.

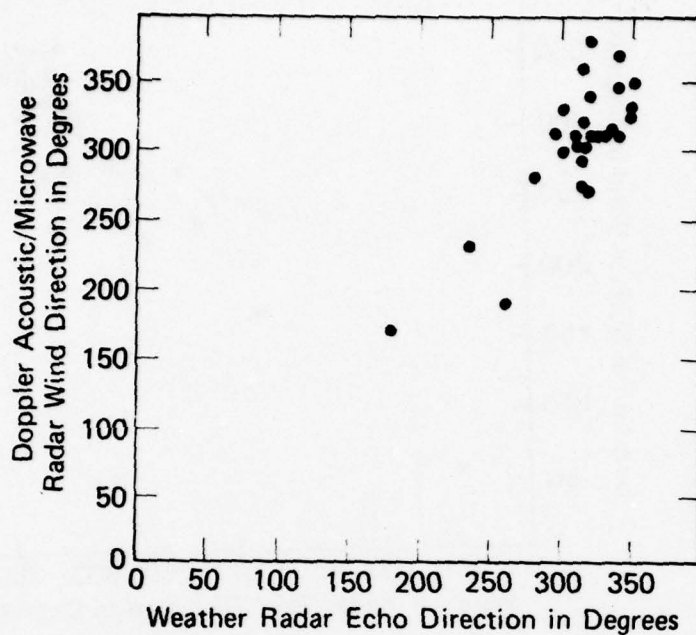


Figure 13.8c. Direction of Doppler acoustic/microwave radar wind as a function of weather radar echo in degrees.

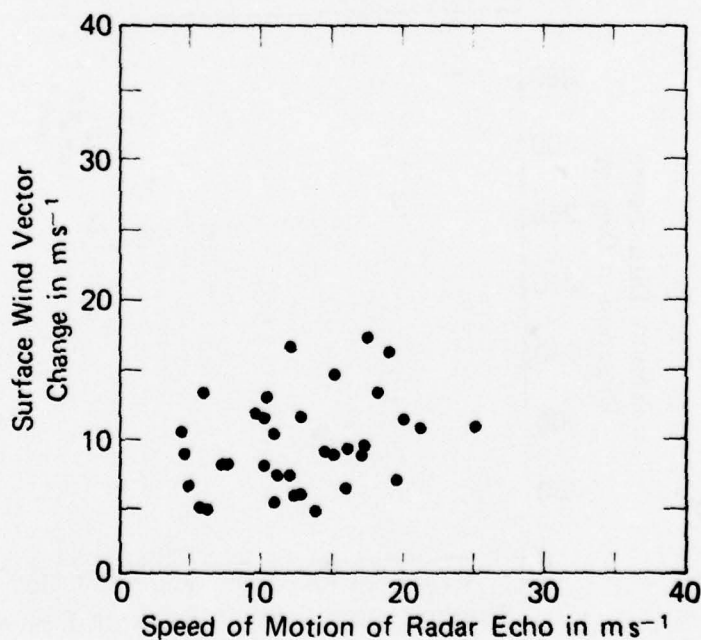


Figure 13.9a. Surface wind vector change as a function of speed of motion of radar echo in m s^{-1}

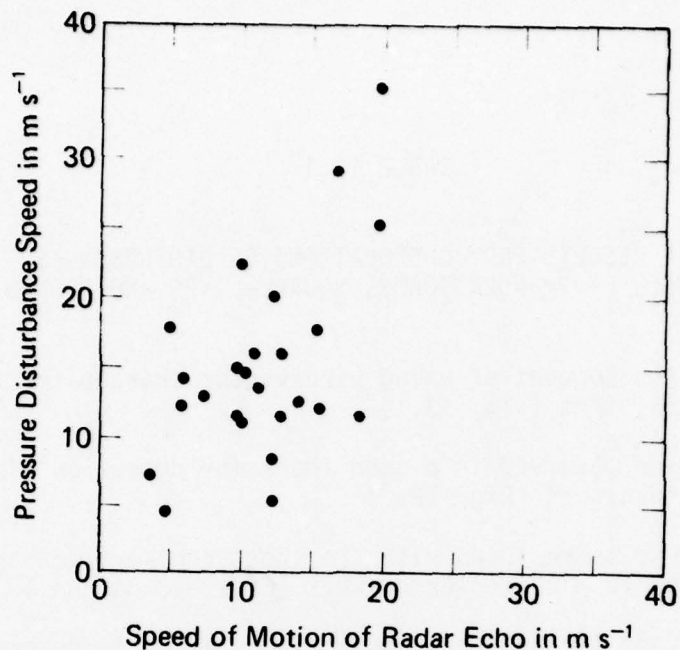


Figure 13.9b. Speed of pressure disturbance as a function of speed of motion of radar echo in m s^{-1} .

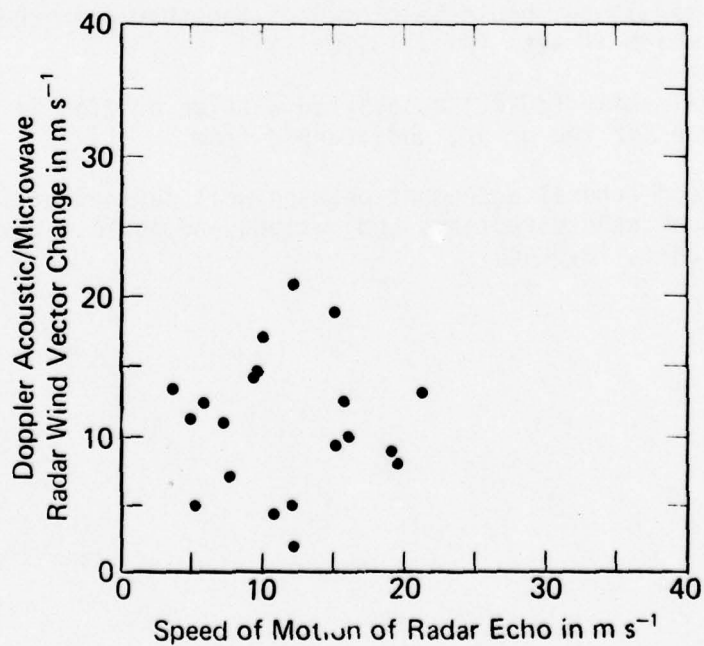


Figure 13.9c. Doppler acoustic/microwave radar wind vector change as a function of speed of motion of radar echo in m s^{-1} .

TABLE 13.1

KEY RESULTS FROM OBSERVATIONS OF DISTURBANCES
CAUSED BY THUNDERSTORMS, SQUALL-LINES AND FRONTS

- a) Validated the concept of using wind vector changes for the detection of outflow systems (Fig. 13.1).
- b) The peak wind observed is a good index for detection of the more severe disturbances (Fig. 13.2).
- c) The larger pressure jumps with the shorter rise times are related to the more severe wind vector changes (Figs. 13.3a and 13.3b).
- d) Stable surface layers are a controlling factor in determining the "representativeness" by surface wind vector changes of the flow aloft (Figs. 13.7a and 13.7b).
- e) It is difficult to infer reliably the vertical wind shear (dU/dZ) from surface measurements (Fig. 13.10b).
- f) The shear magnitude should be presented together with the layer thickness over which it acts (Fig. 13.10a).
- g) The vertical shear (dU/dZ) associated with an outflow is frequently smaller than for the prior, undisturbed flow.
- h) There is good general agreement between well defined or isolated weather radar echo directions and motions and surface measurements (Figs. 13.8a-c, 13.9a-c).

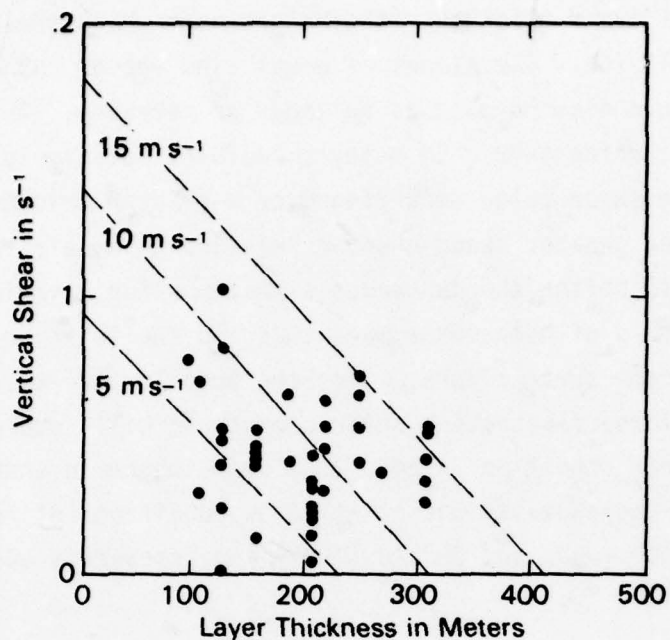


Figure 13.10a. Vertical shear in s^{-1} determined from Doppler acoustic/microwave radar as a function of layer thickness in meters for thunderstorm squall-line and frontal-related events.

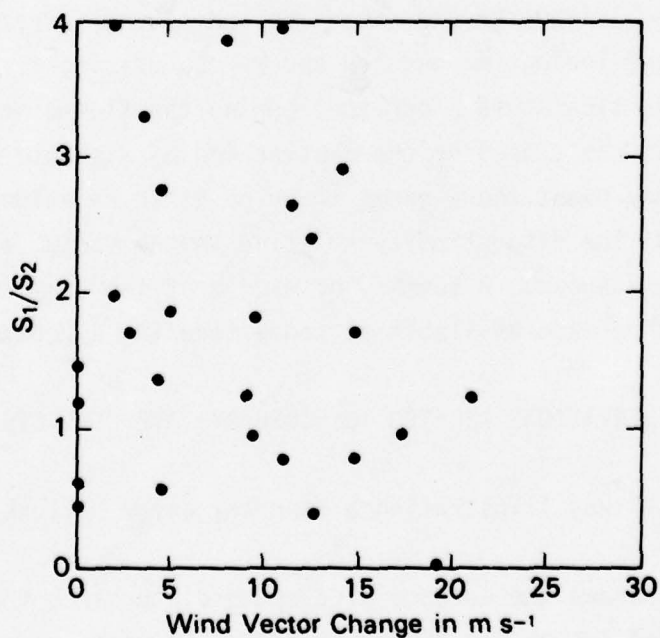


Figure 13.10b. The ratio of vertical shear S_1 associated with the discontinuity to the vertical shear S_2 prior to the discontinuity as a function of the horizontal wind vector change.

profiles maximum shear values were computed and appear as a function of layer thickness (the height over which they occurred) in figure 13.10a. The slopes of equal wind vector change on this figure should also be used as an index of severity. Thus, a shear of 0.08 occurring over a 50 m layer could be relatively safe compared to the same shear value occurring over a greater thickness and hence representing greater speed changes relative to an air foil. There is a need to define the dangerous situations for a variety of aircraft in terms of both shear magnitude and the layer or length over which the shear occurs. Also the profiles are averaged so that certainly large fluctuating shear components will accompany some average shear condition. There is a need to obtain statistics concerning these deviations relative to conditions of mean shear. A paper by Chimonas and Bedard (1979) addresses this question in more detail.

Figure 13.10b is a plot of the vertical shear (S_1), dU/dZ , associated with the flow discontinuity divided by the vertical shear (S_2) prior to the arrival of the discontinuity as a function of the vector change. When there is no change in the shear magnitude the ratio is one; values greater than one indicating increased shear and less than one indicating reduced shear. Surprisingly, for 6 of the cases the vertical shear decreased behind the flow discontinuity. Perhaps this was caused by the destruction of a stable surface layer. In any event there seems to be no clear relationship between the speed of the discontinuity relative to the medium and the associated vertical wind shear. A summary of wind profiles from these data sets should be made available to those modeling aircraft response.

14. STATISTICS OF OBSERVATIONS RELATED TO BOUNDARY LAYER EFFECTS

14.1 Sample Case Study Illustrating a Boundary Layer Disturbance

Figure 14.1 shows the surface wind speed disturbance together with vertical profiles at two different times. Also a pressure jump and small temperature disturbance accompanied the wind surge.

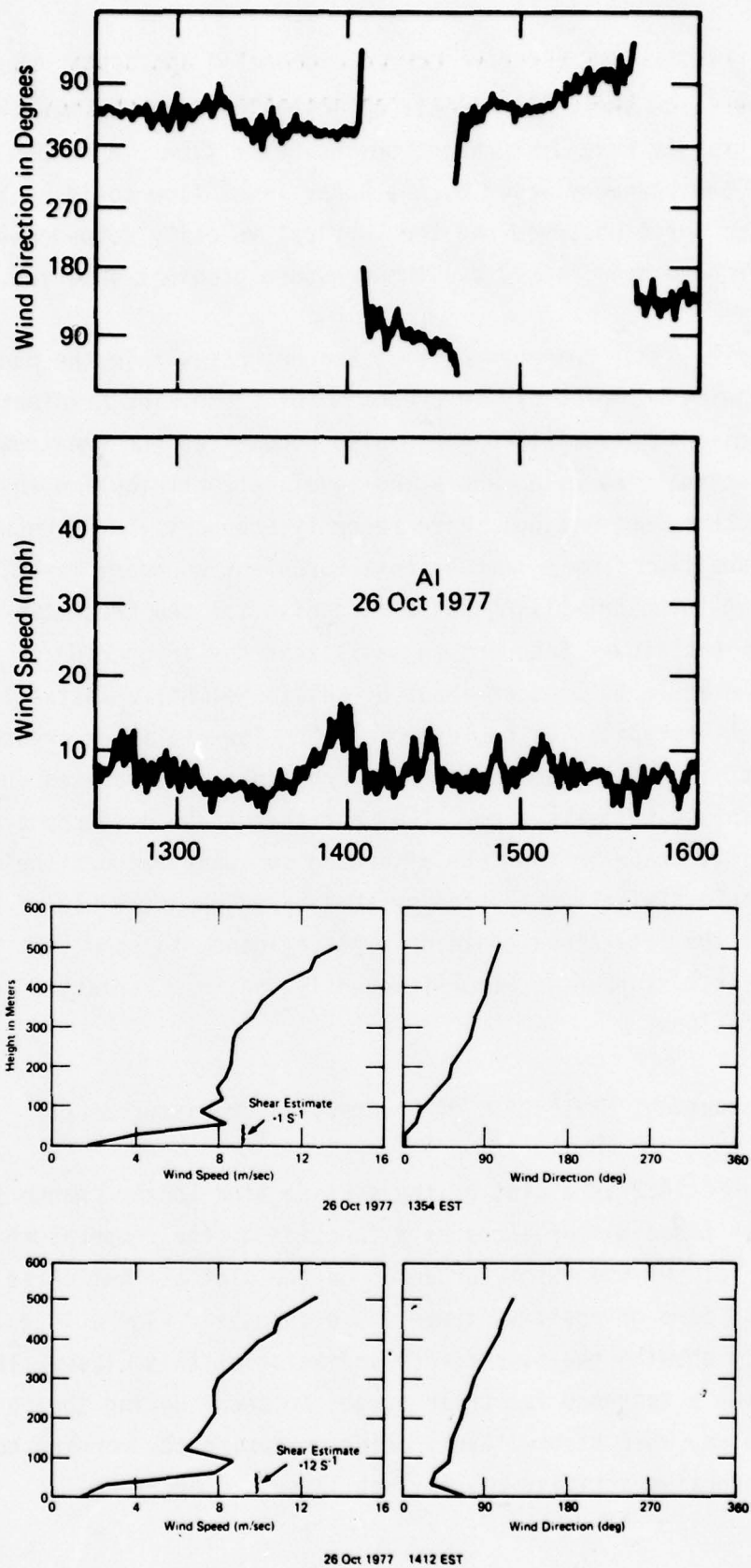


Figure 14.1. Sample case study illustrating a boundary layer disturbance.

The large shear that exists at lower levels could have resulted in a gravity wave disturbance on the basic flow. A sudden penetration of the boundary layer by the upper level flow could explain the wind surge observed and the vertical velocity components caused (or have been caused by) the pressure gradient observed.

Durst (1933) compared data at two heights within the boundary layer showing examples of the breakdown of steep wind gradients in inversions. Izumi (1964) has also documented the breakdown of a nocturnal inversion and a low-level jet, attributing the breakdown to turbulent mixing. More recently Schubert (1977) documented the transition from a laminar to a turbulent boundary layer, showing that turbulent mixing was a mechanism for the breakdown of the laminar flow. Schubert suggests that the triggering of the breakdown could be brought about by Kelvin-Helmholtz instabilities. Such instabilities could explain the low-amplitude pressure changes that frequently accompany boundary layer disturbances observed with the Dulles system. The fact that these disturbances tend not to occur in the late afternoon somewhat reduces their impact upon gust front detection systems based upon the use of anemometers. But the literature contains ample evidence to show that such boundary layer disturbances occur frequently and in a variety of geographical locations.

14.2 Measurement Statistics of Boundary Layer Disturbances

Figure 14.2 is a plot of the surface wind vector change associated with these disturbances as a function of the temperature change in $^{\circ}\text{C}$. Of the 19 disturbances on the plot all but three occurred with zero or positive temperature changes. Figure 14.3 is a histogram showing the time-of-day variation of this class. There seems a tendency for these surges to occur during the hours of the day when stable layers occur or during the morning hours when convective activity causes such layers to break up.

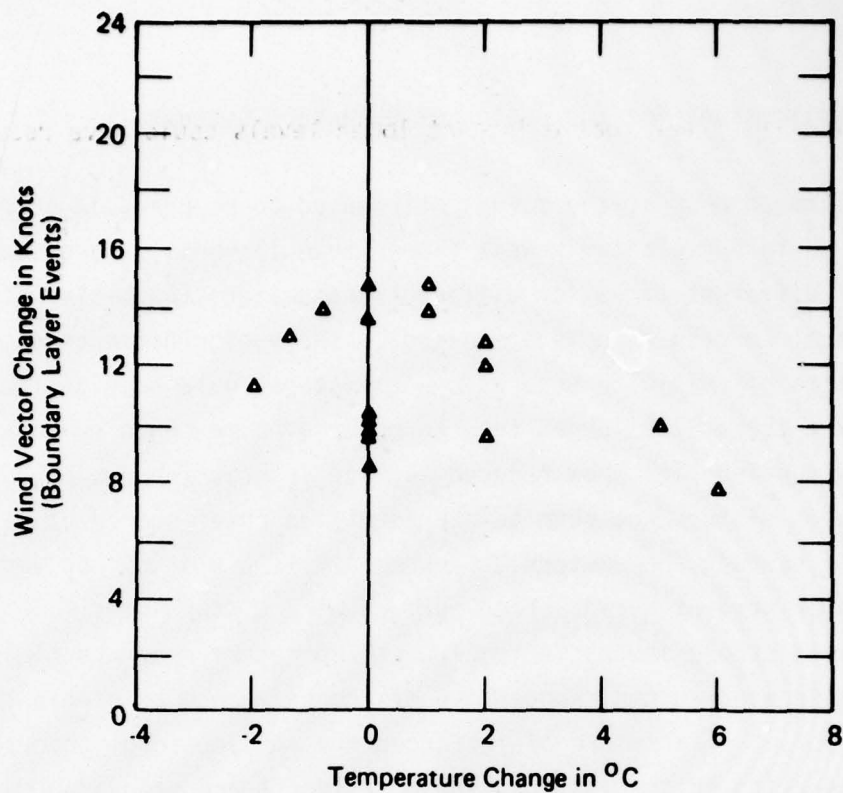


Figure 14.2. Surface wind vector change in kts as a function of surface temperature change in °C.

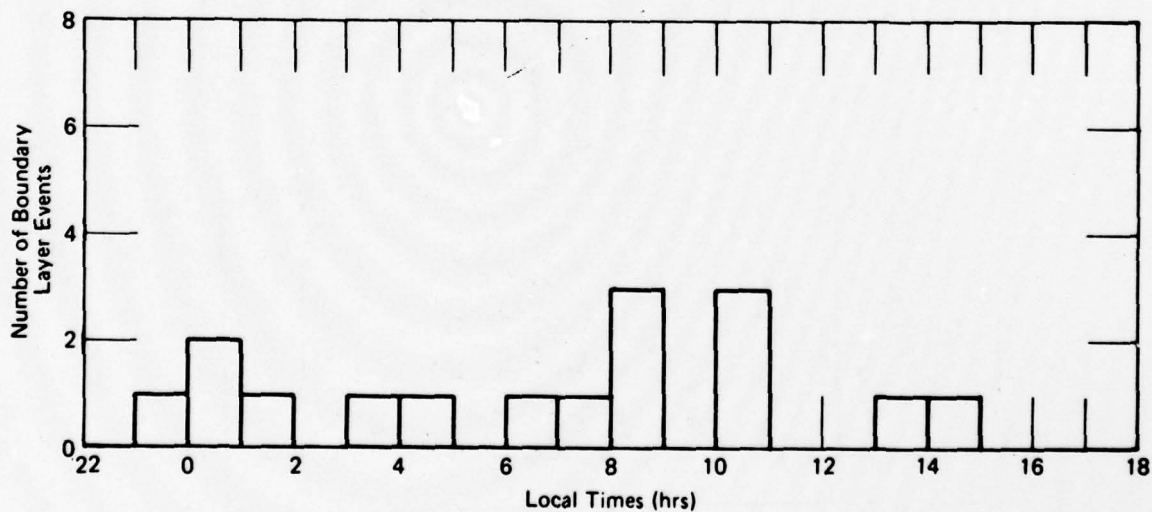


Figure 14.3. Histogram showing the number of boundary layer disturbances as a function of time of day.

14.3 Implications for the Design of Detection Systems

Although most of the surges attributed to boundary layer disturbance tend to be relatively weak (lower than 15 knots), such surges occurred at different times for different anemometers (probably because local terrain effects dominated). The vector differences between pairs of spatially separated anemometers could be significant. Also these wind surges tend to occur at times when propagating flow discontinuities show reduced surface interaction. Such boundary layer disturbance seem to represent the chief source of false alarms for surface anemometers. Figure 14.4 is a plot of the vertical shear present during these surface wind disturbances. This plot shows strong shears in the lowest 200 meters near the times of these wind surges, suggestive of the existence of stable surface layers. In a number of instances the surface surge coincided with a reduction in the vertical shear. Also, there is evidence (Hill, 1976) that in different geographical locations much larger wind surges could occur.

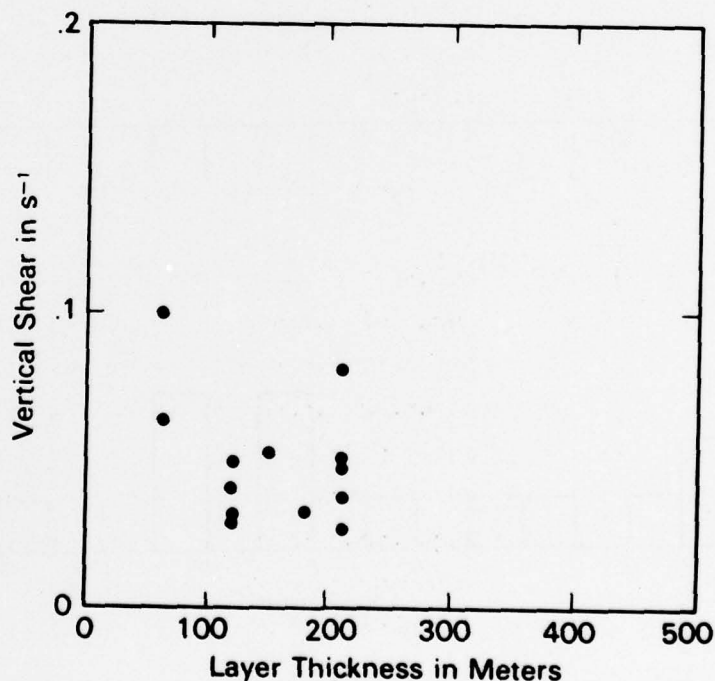


Figure 14.4. Vertical shear in s^{-1} determined from Doppler acoustic/microwave radar as a function of layer thickness in meters for events related to boundary-layer disturbances.

15. STATISTICS OF OBSERVATIONS RELATED TO GRAVITY-SHEAR WAVES

15.1 Sample Case-Study Illustrating a Gravity-Shear Wave Disturbance

Figure 15.1 shows a gravity-shear-wave-related pressure disturbance, the corresponding anemometer trace, and 500-mb weather map near the time of the disturbance. Bedard and Cairns (1977) review past observations of gravity-shear waves which indicate good correlation with the direction and speed of upper level jet streams. Chimonas and Bedard (1979) review more recent observations.

15.2 Measurement Statistics for Gravity-Shear Wave Disturbances

Figure 15.2 compares the horizontal trace speed in m s^{-1} of the pressure waves with the 500-mb wind speed above the Dulles location. Note that the speeds of the pressure waves (usually $> 30 \text{ m s}^{-1}$) are higher than normally measured with thunderstorms or squall-lines (Figure 13.6b). Figure 15.3 compares the azimuth of the pressure waves with the 500-mb wind direction above the Dulles location. These observations are consistent with past observations and the percentage (4%) of the total number of significant events consistent with the estimates of Bedard and Cairns (1977) for the Chicago O'Hare airport area.

15.3 Implications for the Design of Detection Systems

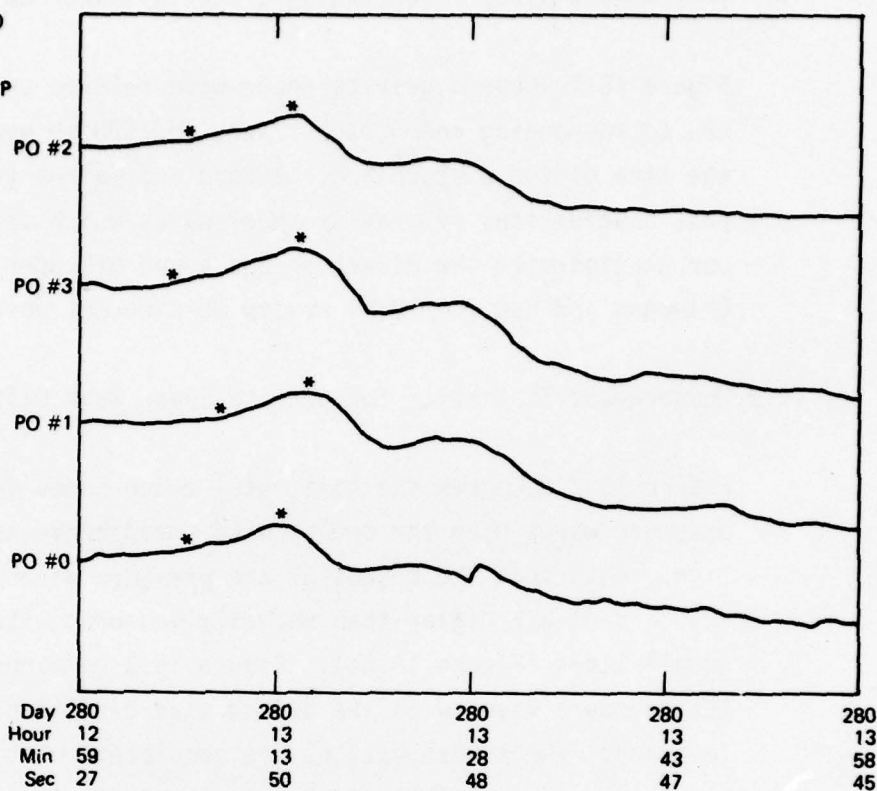
Gravity-shear waves related to upper level jet streams represent the most important source of false alarms for pressure sensor systems. The fact that only minor wind speed and direction disturbances near the surface accompany these events and the fact that they frequently occur in the absence of adverse weather conditions help to prevent these false alarms from presenting a major problem. Although these waves do constitute false alarms (insofar as a low-level wind shear hazard does not exist), instances of severe clear air turbulence aloft could be caused by gravity-shear wave activity (Chimonas and Bedard 1979).

For Specified PO
Please Indicate
Minimum, Then
Maximum Delta P
Points on Graph

PO#0
PO#1
PO#3
PO#2

a)

2.5 mb



NW-PO# 0 Time 0 Sec
NE-PO# 1 Time 122 Sec
SE-PO# 8 Time 81 Sec
SW-PO# 2 Time 40 Sec

Scan (0 1 2): az 255.83 Vel 49.32
Scan (0 1 8): az 261.24 Vel 48.63
Scan (0 8 2): az 267.61 Vel 61.30
Scan (1 8 2): az 262.09 Vel 44.73

Average: az 261.69 Vel 50.31

b) Rise Time—Min to Max:
PO# 0 428 seconds
PO# 1 405 seconds
PO# 8 578 seconds
PO# 2 450 seconds

Change in Pressure:
PO# 0 0.49 Millibar
PO# 1 0.51 Millibar
PO# 8 0.67 Millibar
PO# 2 0.47 Millibar

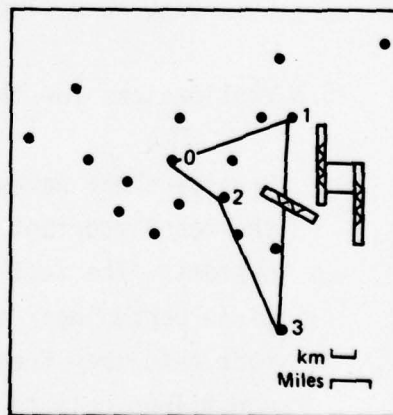


Figure 15.1. Case study illustrating a gravity-shear wave disturbance.

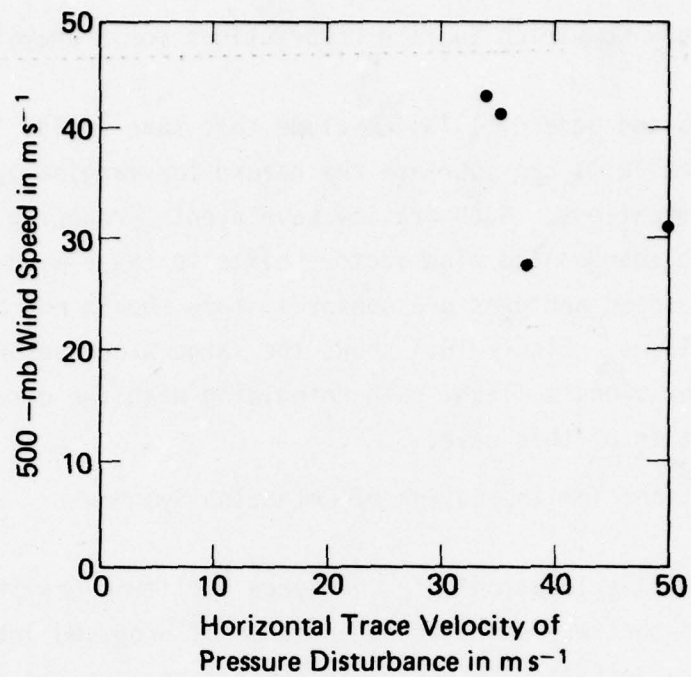


Figure 15.2. Horizontal trace velocity of pressure disturbance as a function of 500-mb wind speed.

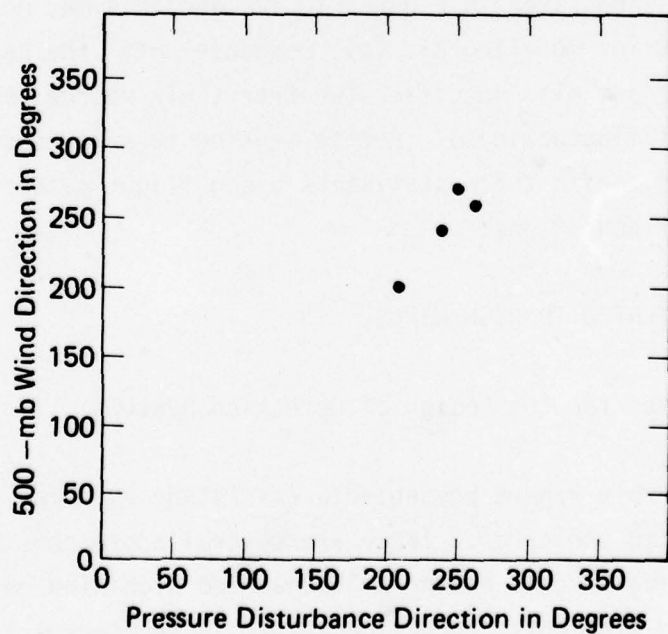


Figure 15.3. Azimuth of pressure disturbance as a function of 500-mb wind direction.

16. OBSERVATIONS RELATED TO GRAVITY WAVES

16.1 Case Study Comparing Surface Observations for a Gravity-Wave Event

Chimonas and Bedard (1979) conclude that wave fields (such as shown in Figure 16.1) can increase the hazard for marginally dangerous shear situations. Such gravity wave events producing large enough pressure changes and wind vector shifts to cause wind-shear alerts on wind speed and pressure sensor systems should not be considered false alarms. Figure 16.1 shows the large wind vector changes that can occur along a flight path coinciding with the direction of propagation of this wave.

16.2 Implications for the Design of Detection Systems

At the Dulles location only one large amplitude gravity wave occurred that was significant in terms of proposed detection systems. Such large waves could constitute a hazard in their own right. The paper by Chimonas and Bedard (1979) points out that smaller amplitude waves may excite aircraft response resonances and hence be important for aircraft operations. In fact, the shear statistics indicated in Figures 13.10a and 14.4 may not be sufficient for modeling air foil response until the perturbation statistics are also specified (whether their source be waves or incoherent fluctuations). Remote sensing techniques should be applied to obtain these statistics along flight paths under a variety of conditions.

17. OBSERVATIONS RELATED TO HIGH WINDS

17.1 Implications for the Design of Detection Systems

Part I of this report presented a case study relating to high-wind-induced pressures. There are several approaches possible for reducing or eliminating such unwanted high-wind responses. Methods in wind-noise reduction appear in sections 4.1.5 and 5.2.

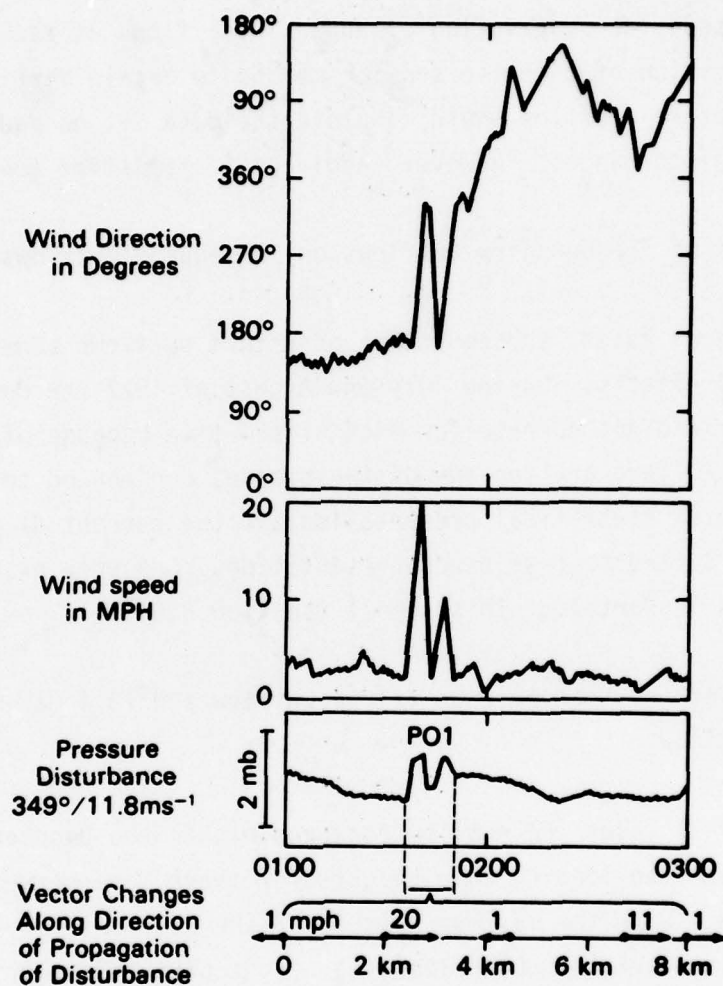


Figure 16.1. Case study illustrating a gravity wave disturbance.

18. SPECIAL TOPICS

18.1 Comparisons Between Daytime and Nighttime Events

The available data suggests that nighttime surface inversions can impede the observation of upper level flows at the surface. The addition of a remote sensing method to obtain vertical temperature profiles would complete the data set needed to study these disturbances. However, additional statistics are required.

18.2 Effects of Thunderstorm Outflows on Subsequent Outflows

In several cases, subsequent thunderstorm outflows showed complex spatial effects. During July and August of 1977 the Doppler sounder did not operate for much of the time because of lightning damage. There are too few of these cases documented to permit a meaningful statistical presentation and the current data set is better suited to case study presentations. One such example appears in Part I of this report (section 3.5).

18.3 Height of the Leading Edge of the Outflow and 18.4 Maximum Height of the Outflow

In only 11 cases the outflow occurred within the Doppler sounder profile. The leading edge heights for these were between 120 and 350 m with the maximum heights of the outflows varying from 250 m to above the 600 m limiting height of the Doppler sounder. Again these data are more suited to detailed case study presentations including comparisons with monostatic acoustic sounder results. There were many events where the flow maxima occurred above the height at which reliable Doppler profiles were obtained. The high surface winds associated with gust front passages were often the cause of a loss in reliability for higher level (> 300 m) returns.

However, using the pressure data the height of density currents can be estimated since the temperature change across many of the observed gust fronts is known. Using the hydrostatic equation, heights were computed for those events showing little evidence of dynamic pressure effects (e.g., a pressure "nose") and also showing strong surface interaction (surface measurements of temperature representing the temperature of the flow aloft). Nevertheless, these two factors (dynamic pressure effects and underestimates of the temperature drop) can both cause overestimates of the height of the current of cold air. Good agreement was found (usually within 100 m) for cases where the gust-front height could be estimated using the acoustic/microwave Doppler radar or the acoustic monostatic radar.

Figure 18.1 is a histogram showing the percentage of the 47 cases at various heights. For just over 50% of the cases, heights less than 1-km are estimated, with events in the 400 to 600 m height range appearing most frequently (25%).

The heights of gust fronts have been compared with other variables such as propagation speed and the temperature drop. The equation for a simple gravity current (e.g., Charba, 1974) is:

$$C = F \left\{ gh \frac{\Delta T}{T} \right\}^{1/2} . \quad (18.1)$$

Where C is the propagation speed, F is an internal Froude number (interpreted as the ratio of the inertia force to the buoyancy force of the current), g is local gravity, ΔT is the temperature difference across the front, and T is the local temperature.

Figure 18.2 is a plot of gust-front height in kilometers as a function of propagation speed. The plot shows much scatter with some tendency for the larger propagation speeds to occur with the larger gust front heights as might be expected from equation 18.1.

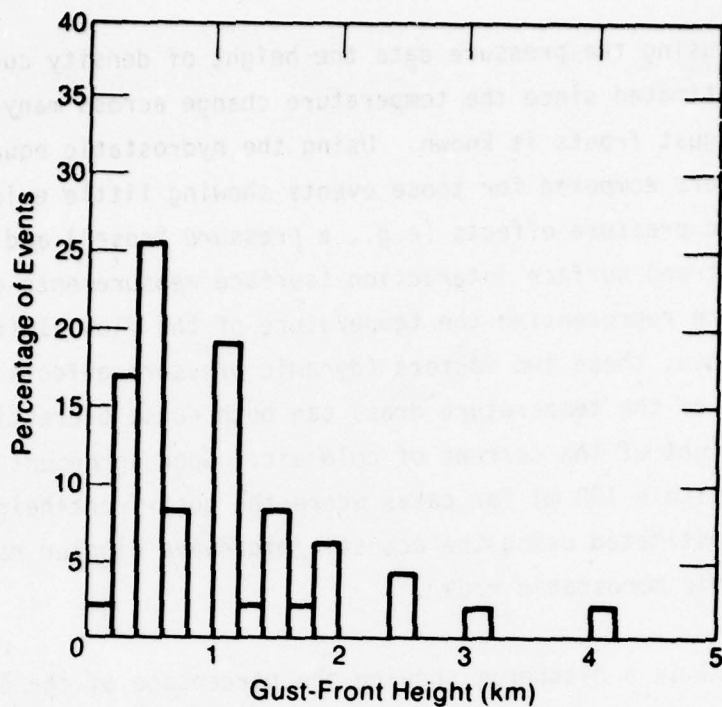


Figure 18.1. Histogram showing the percentage of gust-fronts as a function of height.

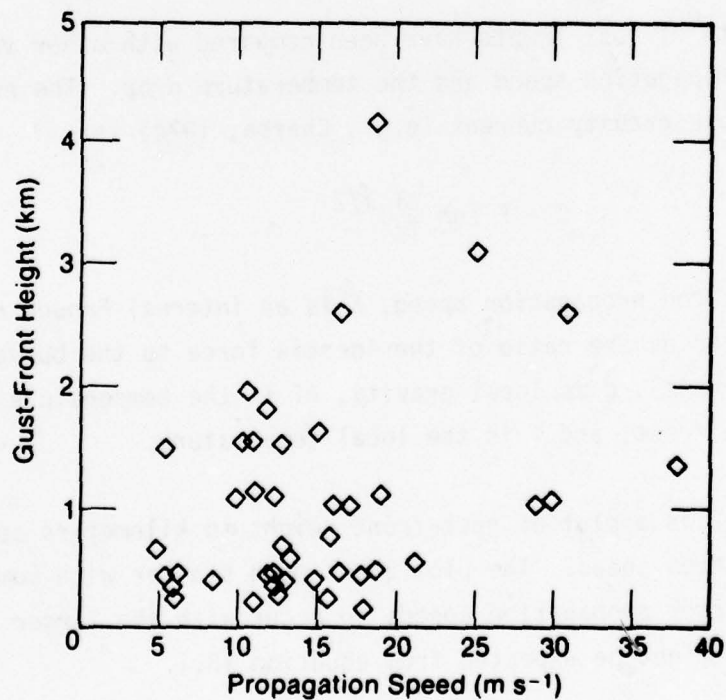


Figure 18.2. Gust front height in kilometers as a function of propagation speed.

Figure 18.3 is a plot of gust-front height as a function of temperature difference across the front. Most of the large height estimates (> 1 km) occur with the smaller temperature drops.

There are two possible explanations for larger gust-front heights occurring with the smaller temperature drops. One explanation is that the lower temperature drops tend to be less representative of the flow aloft, having weaker interaction with the surface. The other explanation is that the smaller negative buoyancy forces occurring with smaller temperature drops within downflows permit more divergence to occur at higher altitudes.

18.5 The Widths of Transition Regions at the Leading Edges of Gust-Fronts

The width of the transition region between the cold air of a gust-front and the undisturbed medium is another parameter important in determining aircraft response. Caracena and Kuhn (1978) used the temperature field in estimating the distribution of gust-front "thermal widths", finding an average width of 3 km with a most probable width of about 2.5 km using observations taken in Oklahoma.

The rise time of the pressure field is used to estimate the widths of transition regions as described in section 3.11 with figure 3.26 of Part I of this report indicating that the air accelerated upward by the approaching gust-front also contributes to the pressure field. Thus, estimates of widths using pressure data will include this region of upward accelerated air and tend to be wider than thermal widths.

In some cases, the pressure field continued to rise over 10's of minutes, possibly because of multiple downflows behind the gust front. This could explain some of the estimates of transition regions of 10's of kilometers. Figure 18.4, a histogram of the widths of transition regions deduced from pressure data indicates widths in the range 3.5 to 5 km occurring most frequently.

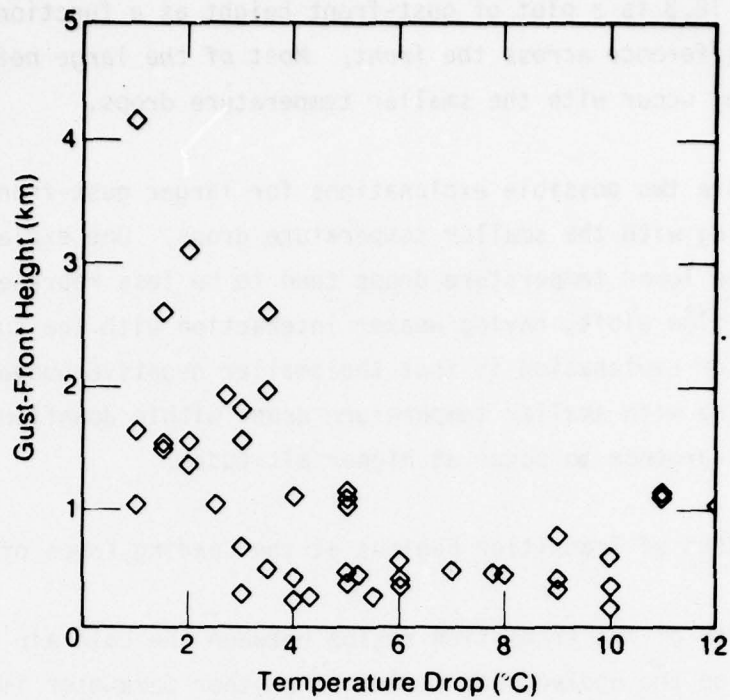


Figure 18.3. Gust front height in kilometers as a function of temperature drop across the front in $^{\circ}\text{C}$.

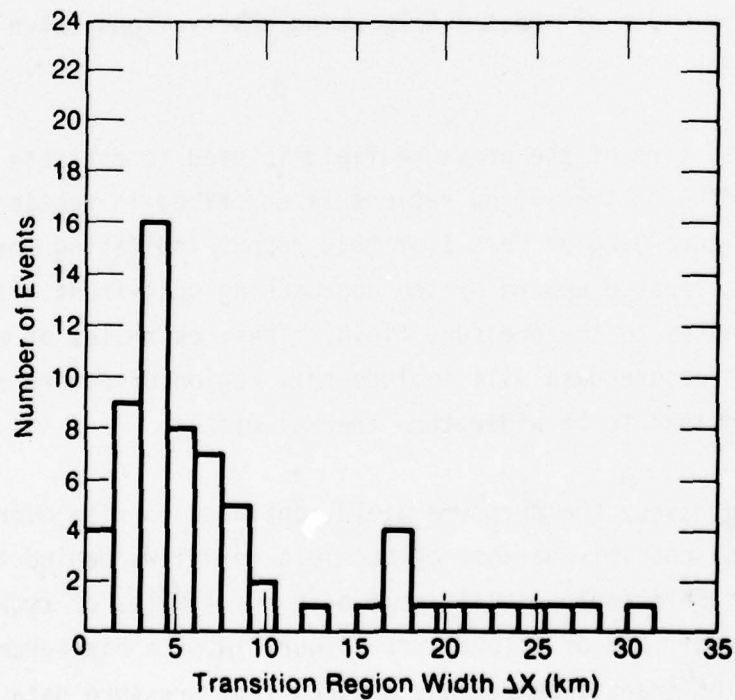


Figure 18.4. Histogram of the widths of gust-front transition regions.

A plot of "pressure widths" as a function of the propagation speed of the discontinuity is shown in figure 18.5. There appears to be a weak relation between the speed of the disturbance and the width of the transition region (with some of the faster moving lines of discontinuity tending to have wider transition regions — as might be expected from the greater shear and momentum transfer that can occur).

An aircraft landing at 100 ms^{-1} would pass through a region 3.5 km wide in 35 seconds, suggesting that a pilot might easily correct for the variations in relative air speed. However, these transition zones can have complex circulations present within them as well as waves and turbulence along the shear and density layers. Compounding the problem of distinguishing sporadic air speed fluctuations from the mean changes is the low altitude of the aircraft (possibly less than 100 m) when the zone is traversed.

18.6 Froude Number and Reynolds Number Determinations for Gust Fronts

As indicated in section 18.4 the internal Froude number, F , is an estimate of the ratio of the inertial force to the buoyancy force of gust fronts and thus can be a measure of their relative importance. Figure 18.6 is a histogram of Froude number values calculated from equation 18.1. These determinations were made for 41 cases, with a large distribution in values ranging over an order of magnitude from .49 to 4.9.

Charba (1974) reviewed measurements of Froude number obtaining a value of 1.25 for some of his data. Also, Charba (based upon a limited number of observations) found evidence that the Froude number is proportional to the propagation speed of the air mass. Charba suggested that the contributions of the source region (down flow momentum) could explain why the Froude number was larger for thunderstorm gust fronts than large-scale atmospheric cold surges, laboratory experiments (Middleton, 1966), or sea breeze fronts (Simpson et al., 1977).

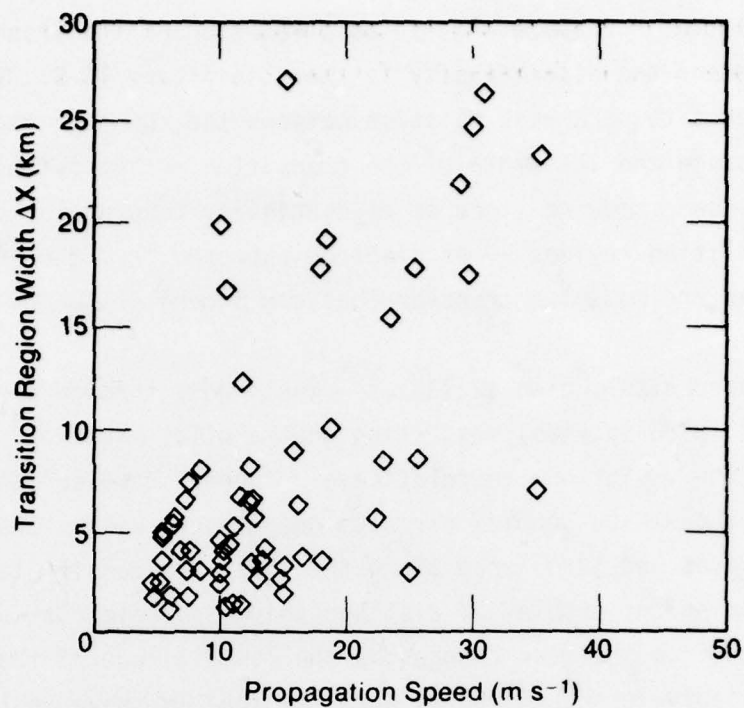


Figure 18.5. Transition region width as a function of propagation speed.

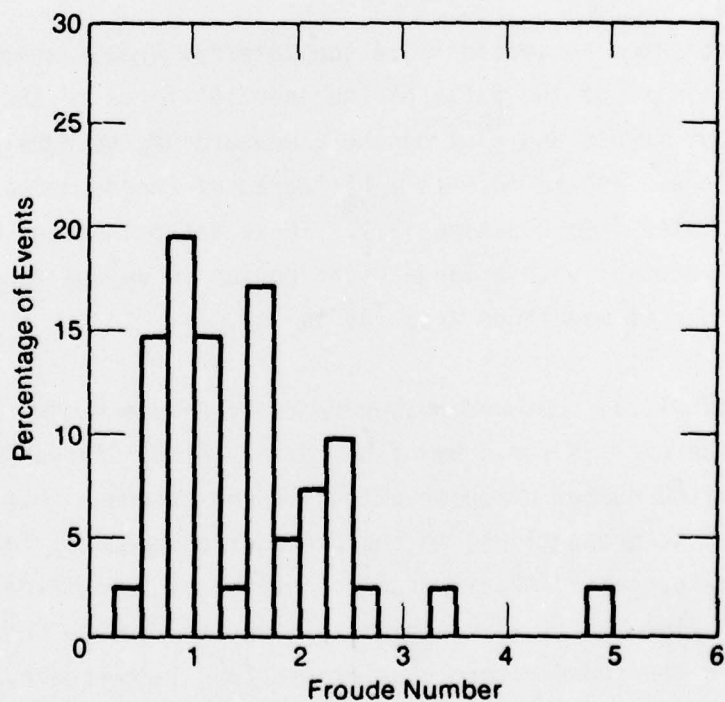


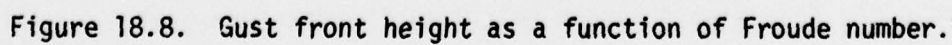
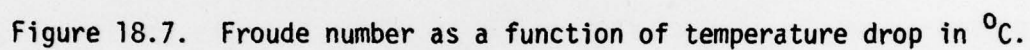
Figure 18.6. Histogram of the Froude number for gust-fronts.

Figure 18.7 shows the Froude number as a function of the temperature drop in degrees C. Figure 18.8 is a plot of gust front height as a function of Froude number. Neither figure 18.7 or 18.8 for the Dulles Airport data set show evidence of a relationship.

On the other hand if the Froude number is plotted as a function of the observed propagation speed (figure 18.9), there is evidence supporting the suggestion of Charba (1974) that the Froude number is directly proportional to the propagation speed. These data represent an additional argument for the importance of downflow momentum, particularly for the more severe systems showing high propagation speeds. For the most severe thunderstorm gust fronts, the downflow source region must be detected in addition to the resulting gust front in order to provide reliable warnings. Calculations suggest it will be possible to detect the dynamic pressure beneath a downdraft over 100 seconds before the development of the near-surface gust front. Developing a better knowledge of the downflow — surface interaction is another area requiring more work.

Simpson (1969) compared laboratory and atmospheric density currents, noting that for tank experiments the Froude number does not depend upon Re (Reynolds number) for $Re > 10^3$, F being about .75 for Re equal to 10^8 . Figure 18.10 from the Dulles airport data set is a plot of Froude number as a function of Reynolds number and shows some evidence for F to be proportional to Re (particularly for the lower limits of F). Figure 18.10 can be interpreted as a further indication of the importance of downflow momentum to the dynamics of gust-front systems.

The ratio of the height of the gust-front nose to the total height as a function of Re , shows no clear relationship. This suggests that surface based stable layers and not frictional effects often determine the nose height of thunderstorm gust fronts.



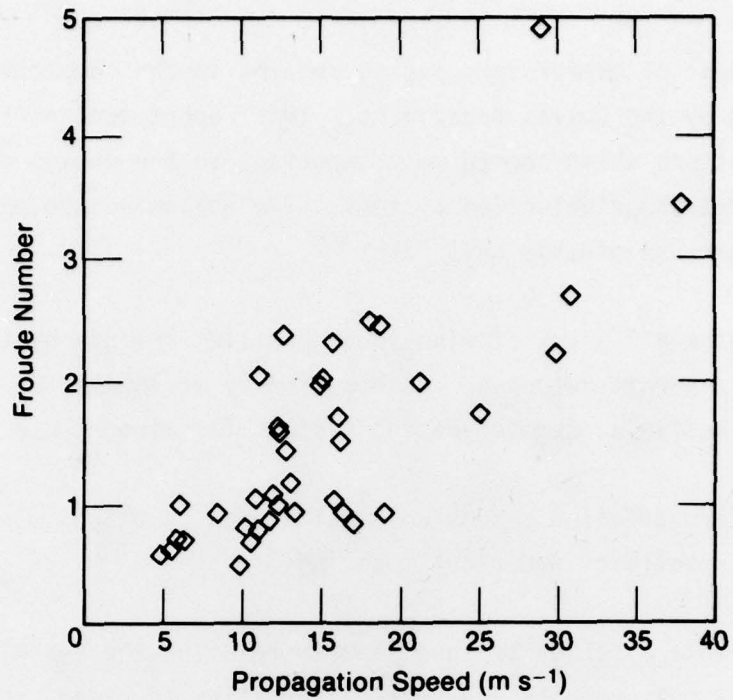


Figure 18.9. Froude number as a function of propagation speed.

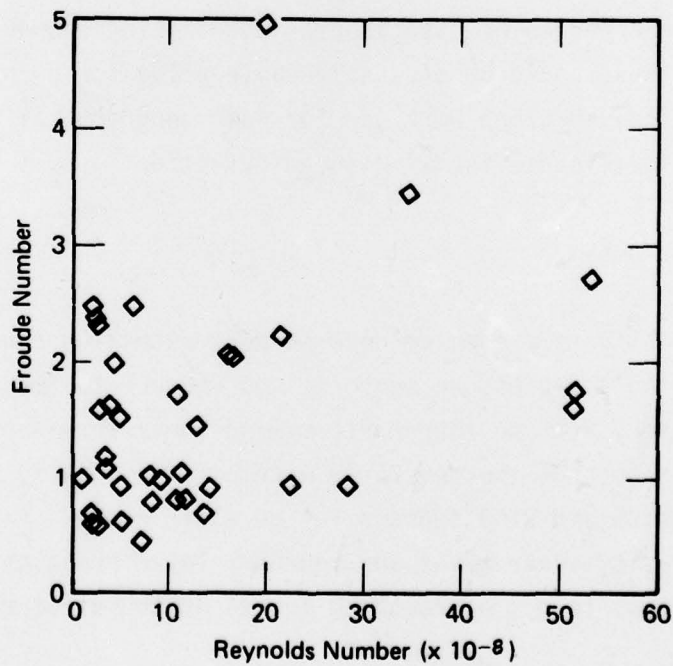


Figure 18.10. Froude number as a function of Reynolds number.

19. POSSIBILITIES FOR ADDITIONAL USE OF THESE DATA SETS

A great deal of useful information remains in the complete data base generated by the Dulles experiment. This report concentrated on those portions which seemed most important to the design of surface sensor wind-shear detection systems. The following are possibilities for further use of this data base:

- a) Provide a library of wind-shear profiles for use by those modeling aircraft response. Such a library would also be valuable for designing remote sensing systems for airport use.
- b) Perform detailed case studies of events selected to compare with the results of numerical modeling.
- c) Assemble a series of case studies relating the γ -scale Dulles array measurements and vertical profiles to radar echoes. This could provide additional insights for interpretation of weather radar echoes.
- d) Assemble a series of case studies documenting boundary layer breakdown. These could be of considerable value for comparison with theoretical modeling work and for some geographical areas be of great significance for wind shear detection.

20. CONCLUDING REMARKS

The statistical data presented here support detection concepts requiring combinations of wind and pressure sensors, and suggest two modes of operation for operational use. With no thunderstorm wind-shear threat present (e.g., no weather radar echoes of thunderstorms within 100 km), a system using both pressure sensors and wind sensors for an alert reduces false alarms caused by both gravity-shear waves and boundary layer breakups. With severe local weather present (e.g., approaching fronts or thunderstorms) using

either pressure or wind sensors for an alert reduces the possibility of missing events because of stable layers limiting flow near the surface or thin layers from small, distant downflows. Bedard and Hooke (1978) suggest a configuration of pressure sensors, anemometers, and wind speed threshold sensors (Bedard and Fujita (1978)) for thunderstorm wind-shear detection near airports (Part I, section 10).

Some localities seem susceptible to shears of different origin requiring specifically tailored detection techniques. For example Hill (1976) identifies a chief source of dangerous shear for Reno, Nevada, as downslope winds above a ground-based inversion. A vertically profiling remote sensor (e.g., Hardesty et al., 1977) offers protection in such situations. Although several detected events were interpreted as downbursts (Fujita and Carecena, 1977) the means of independently measuring the magnitude of the vertical speeds involved were not available. However, closely spaced arrays of pressure and wind threshold sensors (200-m intervals) along runways can detect transient and spatially concentrated downbursts.

As more complete data concerning wind shear become available from different geographical regions, and wind-shear detection systems are developed, proper consideration should be given to the multi-faceted nature of the total wind shear problem. There is a need to increase the cooperative work between those developing wind shear data sets, those estimating and measuring aircraft response, and those developing advanced remote sensors. The production of algorithms defining significant shear for remote sensing systems depends upon definitions of the precise limits of dangerous shear for a variety of aircraft which in turn depend upon the availability of realistic data from case studies of atmospheric shear events, including the fluctuating components.

APPENDIX I

Analysis Software

1. Dulles absolute pressure and temperature software.
 - 1.1 Program for listing digital tapes.
 - a. Printout of data.
 - b. Rough plot of data.
 - 1.2 Programs for placing absolute pressure and temperature data in form for analysis by graphics system.
 - a. Version that averages data and eliminates bad data points.
 - b. Version that processes non-averaged data.
 - 1.3 Graphics system analysis programs for absolute pressure and temperature data.
 - a. Plot routine for up to 15 pressure sensors.
 - b. Plot routine for temperature data.
 - c. Program that plots pressure data and automatically computes the azimuth, speed of motion, pressure amplitude and rise time when the start of the pressure rise and the pressure peak are identified with a cursor.
 - d. Program that provides information on site location and sensor details. Data is taken from original data tapes and placed on cartridges for off-line analysis. These programs are interactive permitting e.g., choice of scales, time intervals and sensors.
2. Dulles dP software.
 - 2.1 Programs for listing digital tapes.
 - a. Printout of data.
 - b. Rough plot of sensor status as a function of time.
 - c. Rough x-y plot of sensor position and status.
 - d. A variety of alarm options with selective listing.

- 2.2 Programs for placing dP data in a form for analysis by graphics system.
 - a. Version that places all data in form for transfer to graphics system data cartridge.
 - b. Version that permits interactive editing of dP tapes (e.g., separation of overlapping events) prior to transfer.

- 2.3 Graphics system analysis programs for dP data.
 - a. Plot routine showing the sensor array and the sequence of dP triggers as a function of time.
 - b. Program permitting estimates of the form of a discontinuity to be made. Vectors are drawn showing the direction of propagation.
 - c. Program that provides information concerning site location and sensor details (programs are interactive).

3. Dulles anemometer software.

- 3.1 Plot routine which draws vectors from the location of each anemometer depicting the wind speed and direction before and after the arrival of a discontinuity.
- 3.2 Program that provides information concerning site location and sensor details.

4. Dulles dP site library routine.

This permits information for up to 300 sensors to be logged and the information dumped in a variety of ways. This also has recently been made interactive so that site changes and calibration information can be made easily.

REFERENCES

- Bedard, A. J., Jr. (1977). The d-c pressure summator: Theoretical operation, experimental tests and possible practical uses. *Fluidics Quarterly*, 9, No. 1, 26-51.
- Bedard, A. J., Jr. and R. K. Cook (1968). Transfer of aircraft weight to the surface of the earth. 75th Meeting of the Acoustical Society of America, (ABSTRACT).
- Bedard, A. J., Jr. and D. W. Beran (1977). Detection of gust fronts using surface sensors. NOAA Tech. Memo. ERL WPL-20, 15 pp.
- Bedard A. J., Jr. and M. M. Cairns (1977). Atmospheric pressure jumps measured with arrays of sensitive pressure sensors in the vicinity of Chicago's O'Hare International Airport. NOAA Tech. Memo. ERL WPL-28, 29 pp.
- Bedard, A. J., Jr., W. H. Hooke and D. W. Beran (1977). The Dulles airport pressure jump detector array for gust front detection. *Bull. Amer. Meteor. Soc.*, 58, No. 9, 920-926.
- Bedard, A. J., Jr. and H. B. Meade (1977). The design and use of sensitive pressure-jump sensors to detect thunderstorm gust fronts. Part I: Pressure-jump detector design. *J. Appl. Meteor.* 16, No. 10, 1049-1055.
- Bedard, A. J., Jr. and T. T. Fujita (1978). An omnidirectional, tilt insensitive, wind speed threshold detector. *Proc. 4th Symposium on Meteorological Observations and Instrumentation*, April 10-14, Denver, Colorado. *Amer. Meteor. Soc. Boston, Mass.* 83-86.
- Bedard, A. J., Jr. and W. H. Hooke (1978). The Dulles airport pressure-sensor array for gust-front detection...system design and preliminary results. *Proc. 4th Symposium on Meteorological Observations and Instrumentation*, April 10-14, Denver, Colorado. *Amer. Meteor. Soc., Boston, Mass.* 115-124.

Bedard, A. J., Jr. and M. J. Sanders Jr. (1978). Thunderstorm-related wind shear detected at Dulles International Airport using a Doppler acoustic/microwave radar, a monostatic sounder and arrays of surface sensors. Conference on Weather Forecasting and Analysis and Aviation Meteorology, October 16-19, Silver Spring, Md. Amer. Meteor. Soc., Boston, Mass. 347-352.

Bedard, A. J., Jr. (1978). The Dulles International Airport wind-shear detection system — statistical results. Conference on Atmospheric Environment of Aerospace Systems and Applied Meteorology, November 14-16, New York, N.Y. Amer. Meteor. Soc. Boston, Mass. 57-66.

Beran, D. W., W. H. Hooke, and S. F. Clifford (1973). Acoustic echo-sounding techniques and their application to gravity-wave, turbulence, and stability studies, Boundary Layer Meteorology, 4, 133-153.

Beran, D. W., P. A. Mandics, A. J. Bedard, Jr. and R. G. Strauch (1976). A wind shear and gust front warning system. Preprints, Seventh Conference on Aerospace and Aeronautical Meteorology and Symposium on Remote Sensing from Satellites, Amer. Meteor. Soc., Nov. 16-17, Melbourne, Fla. p. 167-174.

Caracena, F. (1978). A comparison of two downbursts of different mesoscales. Conference on Weather Forecasting and Analysis and Aviation Meteorology, October 16-19, Silver Spring, Md. Amer. Meteor. Soc., Boston, Mass. 293-300.

Caracena, F. and P. M. Kuhn (1978). Remote sensing thunderstorm outflow severity with an airborne IR sensor. Conference on Weather Forecasting and Analysis and Aviation Meteorology, October 16-19, Silver Spring, Md. Amer. Meteor. Soc., Boston, Mass. 287-292.

Charba, J. (1974). Application of gravity current model to analysis of squall-line gust front. Mon. Weather Rev., 102, 140-156.

Chimonas, G. and A. J. Bedard Jr. (1979). Atmospheric gravity waves and aircraft disturbances. (In editorial process.)

- Durst, C. S. (1933). Breakdown of steep wind gradients in inversions. Quart. J. R. Met. Soc., 59, 131-136.
- Faust, H. (1947). Untersuchungen von Forstschaden hinsichtlich der windstruktur bei einer Bö. Meteor. Rundschau., 1, 290-297.
- Fujita, T. T. (1977). Project Nimrod (First Report), University of Chicago, 12.
- Fujita, T. T. (1978). Manual of downburst identification for project Nimrod. SMRP Res. Pap. 156, Univ. of Chicago, Chicago, Ill. 92 pp.
- Fujita, T. T. and H. R. Byers (1977). Spearhead echo and downburst in the crash of an airliner. Mon. Wea. Rev., 105, 129-146.
- Fujita, T. T. and F. Caracena (1977). An analysis of three weather-related aircraft accidents. Bull. Amer. Meteor. Soc., 58, 1165-1181.
- Fujita, T. T. (1978). Wind Shear at Dulles airport on 18 May 1977. SMRP Res. Pap. 159, University of Chicago, Chicago, Ill. 19 pp.
- Geiger, R. (1973). The climate near the ground. Harvard University Press, 611 pp.
- Glossary of Meteorology (1959). Amer. Meteor. Soc. Boston, Mass., 638 pp.
- Goff, R. C. (1976). Vertical structure of thunderstorm outflows. Mon. Wea. Rev., 104, No. 11, 1429-1440.
- Gossard, E. E. and W. H. Hooke (1975). Waves in the Atmosphere, Elsevier Press, 456 pp.
- Gossard, E. E. and W. H. Munk (1954). On gravity waves in the atmosphere. J. Meteor., 11, 259-269.
- Greene, G. E., H. W. Frank, A. J. Bedard, Jr., J. A. Korrell, M. M. Cairns and P. A. Mandics (1977). Wind shear characterization. Final report to the Federal Aviation Administration, prepared by the Wave Propagation Laboratory, NOAA, 120 pp.

- Hallock, J. N. (1972). Pressure measurements of wake vortices near the ground. *J. of Aircraft*, 9, No. 4, 311-312.
- Hardesty, R. M., P. A. Mandics, D. W. Beran and R. G. Strauch (1977). The Dulles airport acoustic/microwave radar wind and wind-shear measuring system. *Bull. Amer. Meteor. Soc.*, 58, No. 9, 910-918.
- Hill, C. D. (1976). Other kinds of wind shear. NOAA Tech. Memo. NWS WR-108, 17 p.
- Hooke, W. H., J. M. Young and D. W. Beran (1972). Atmospheric waves observed in the planetary boundary layer using an acoustic sounder and micro-barograph array. *Boundary-Layer Meteor.*, 2, 371-380.
- Izumi, Y. (1964). The evolution of temperature and velocity profiles during breakdown of a nocturnal inversion and a low-level jet. *J. Appl. Meteor.*, 3, 70-82.
- Kjelaas, A. G., E. E. Gossard, J. M. Young and W. R. Moninger (1975). Dispersion and spectra of gravity waves probably generated by a convective storm. *Tellus*, 27, No. 1, 25-33.
- Middleton, G. V. (1966). Experiments on density and turbidity currents, I. Motion of the head. *Canadian J. Earth Sci.*, 3, 523-546.
- Parry, H. D. and M. J. Sanders, Jr. (1972). The design and operation of an acoustic radar. *IEEE Transactions on Geoscience Electronics* GE-10, No. 1, 54-64.
- Prandtl, L. and O. G. Tietjens (1934). *Applied hydro-and aerodynamics*. New York: Dover Publications, 185-188.
- Richwein, B. and R. Mcleod (1978). Low-level frontal wind shear forecast test. Final report to the Federal Aviation Administration. Prepared by the Weather Service Forecast Office, National Weather Service, NOAA, 24 pp.

- Schubert, J. F. (1977). Acoustic detection of momentum transfer during the abrupt transition from a laminar to a turbulent boundary layer. *J. Appl. Meteor.*, 16, 1292-1297.
- Simpson, J. E. (1969). A comparison between laboratory and atmospheric density currents. *Quart. J. R. Meteor. Soc.*, 95, 758-765.
- Simpson, J. E., D. A. Mansfield, and J. R. Milford (1977). Inland penetration of sea-breeze fronts. *Quart. J. R. Meteor. Soc.*, 103, 47-76.
- Teske, M. E. and W. S. Lewellen (1978). The prediction of turbulence and wind shear associated with thunderstorm gust fronts. Conference on Atmospheric Environment of Aerospace Systems and Applied Meteorology, November 14-16 New York, N.Y. Amer. Meteor. Soc. Boston, Mass.